

**DEVELOPMENT AND NUMERICAL IMPLEMENTATION OF NONLINEAR  
VISCOELASTIC-VISCOPLASTIC MODEL FOR ASPHALT MATERIALS**

A Dissertation

by

CHIEN-WEI HUANG

Submitted to the Office of Graduate Studies of  
Texas A&M University  
in partial fulfillment of the requirements for the degree of

DOCTOR OF PHILOSOPHY

December 2008

Major Subject: Civil Engineering

**DEVELOPMENT AND NUMERICAL IMPLEMENTATION OF NONLINEAR  
VISCOELASTIC-VISCOPLASTIC MODEL FOR ASPHALT MATERIALS**

A Dissertation

by

CHIEN-WEI HUANG

Submitted to the Office of Graduate Studies of  
Texas A&M University  
in partial fulfillment of the requirements for the degree of

DOCTOR OF PHILOSOPHY

Approved by:

Chair of Committee,	Eyad Masad
Committee Members,	Robert Lytton
	Rashid Abu Al-Rub
	Anastasia Muliana
	Gordon Airey
Head of Department,	David Rosowsky

December 2008

Major Subject: Civil Engineering

**ABSTRACT**

Development and Numerical Implementation of Nonlinear Viscoelastic-Viscoplastic  
Model for Asphalt Materials (December 2008)

Chien-Wei Huang, B.S., I-Shou University;

M.S., National Cheng-Kung University

Chair of Advisory Committee: Dr. Eyad Masad

Hot mix asphalt (HMA) is a composite material which consists of aggregates, air voids and asphalt materials. The HMA response is typically described to be viscoelastic-viscoplastic, and its response is a function of temperature, stress/strain rate, and stress/strain level. Many researches have shown that the viscoelastic response of asphalt mixtures can be nonlinear once the stress/strain value exceeds a certain threshold level. This study presents a nonlinear viscoelastic-viscoplastic model for describing the behavior of asphalt materials under various conditions. A new method is developed in this study for separating the viscoelastic response from the viscoplastic response.

The first part of this study focuses on the implementation of Schapery nonlinear viscoelastic model in finite element (FE) using a user-defined material subroutine (UMAT) within the ABAQUS commercial software. The FE implementation employs the recursive-iterative integration algorithm, which can improve the convergence and save the calculating time. The verification of the nonlinear viscoelastic model is achieved by analyzing (1) the response of asphalt mixtures tested in the Simple Shear

Test (SST) at several temperatures and stress levels, (2) the response of unaged and aged asphalt binders tested in the Dynamic Shear Rheometer (DSR), and (3) the response of asphalt binders in the multiple stress creep recovery test (MSCR).

In the second part of this study, the nonlinear viscoelastic-viscoplastic constitutive relationship is implemented using UMAT. The viscoplastic component of the model employs Perzyna's theory with Extended Drucker-Prager yield surface which is modified to account for the difference in material response under compression and extension stress states. The study includes parametric analysis to illustrate the effect of nonlinear viscoelastic parameters and viscoplastic parameters on the asphalt mix response. The capability of the model in describing the fatigue and permanent deformation distresses of asphalt pavements is illustrated using finite element simulations.

The constitutive model developed in this study can describe the behavior of asphalt materials (asphalt binder, asphalt mastic and mixtures) under various testing conditions. This study also achieved the FE implementation of a nonlinear viscoelastic-viscoplastic constitutive model that can simulate the fatigue and permanent deformation distresses of asphalt pavement structures.

## **DEDICATION**

This dissertation is dedicated to my family for providing me with the necessary help and support that I needed to finish this work.

## ACKNOWLEDGMENTS

I would like to take this opportunity to thank Dr. Masad for his support, knowledge, encouragement, and patience. Dr. Masad is a great teacher and a close friend. He helped me with my research and also my life. I am so lucky and proud to be one of his students.

I would like to acknowledge the help of Dr. Muliana with the nonlinear viscoelastic response of materials and the finite element implementation of nonlinear viscoelasticity theory. The help of Dr. Abu Al-Rub in the numerical implementation of the viscoelastic-viscoplastic model presented in Chapter V is highly appreciated. I also would like to thank Dr. Hussain Bahia from the University of Wisconsin-Madison for sharing the experimental measurements presented in Chapter II. I acknowledge the fruitful discussions with Dr. Gordon Airey from the University of Nottingham on the nonlinear response of asphalt binders. I also acknowledge his support in providing the experimental measurements presented in Chapter III and his insightful comments on the analysis of this data. The multiple creep and recovery test data was provided by Dr. John D'Angelo of the Federal Highway Administration. I thank them for their support of this study.

Special thanks to Dr. Robert Lytton and Dr. Dallas Little for their help and support. Also, I want to acknowledge my friends Enad Mahmoud, Veronica Castelo Branco, Emad Kassem, Dr. Shadi Saadeh, and Dr. Samer Dessouky for their help.

## TABLE OF CONTENTS

		Page
ABSTRACT .....		iii
DEDICATION .....		v
ACKNOWLEDGMENTS.....		vi
TABLE OF CONTENTS .....		vii
LIST OF FIGURES.....		x
LIST OF TABLES .....		xv
CHAPTER		
I	INTRODUCTION.....	1
	Background .....	1
	Problem Statement .....	4
	Objective .....	5
	Organization of the Dissertation .....	6
II	NONLINEAR VISCOELASTIC ANALYSIS OF ASPHALT MIXES SUBJECTED TO SHEAR LOADING .....	8
	Overview .....	8
	Introduction .....	9
	Numerical Implementation of the Schapery Nonlinear Viscoelastic Material Model.....	11
	Experimental Measurements .....	20
	Data Analysis .....	22
	Model Verification.....	28
	Summary of Findings.....	36
III	NONLINEAR VISCOELASTIC ANALYSIS OF UNAGED AND AGED ASPHALT BINDERS.....	38
	Overview .....	38
	Introduction .....	39

CHAPTER	Page
Objectives and Scope of the Study.....	40
The Schapery's Nonlinear Viscoelastic Model.....	42
Experimental Measurements and Data Analysis.....	43
Time-Temperature Shift.....	49
Nonlinearity Stress Shift.....	51
Aging Shift.....	54
Finite Element Analysis of Binder Response.....	57
Conclusions.....	61
IV CHARACTERIZATION OF ASPHALT BINDER RESISTANCE TO PERMANENT DEFORMATION BASED ON NONLINEAR VISCOELASTIC ANALYSIS OF MULTIPLE STRESS CREEP RECOVERY (MSCR) TEST.....	63
Overview.....	63
Introduction.....	64
Objectives and Tasks.....	66
Experimental Measurements.....	67
Nonlinear Plasto-Viscoelastic Analysis Procedure.....	68
Analysis of Results.....	77
Nonlinear Viscoelastic Parameters.....	77
Validity of Using a Linear Model for Describing Permanent Strain.....	82
Nonlinearity in ALF Binders.....	84
Analysis of ALF Binder Permanent Deformation.....	88
Conclusions.....	92
V NUMERICAL IMPLEMENTATION OF NONLINEAR VISCOELASTIC-VISCOPLASTIC MODEL.....	94
Overview.....	94
Introduction.....	95
Objectives and Tasks.....	97
Development of Nonlinear Viscoelastic-Viscoplastic Model.....	97
Nonlinear Viscoelastic Model.....	98
Viscoplastic Model.....	99
Yield Surface Function.....	100
Viscoplastic Potential Energy Function.....	103
Hardening Function.....	104
The Numerical Algorithm of Nonlinear Viscoelastic-Viscoplastic Model.....	107
Verification of Finite Element Implementation.....	115



CHAPTER	Page
Parametric Analysis.....	120
Finite Element Simulation.....	127
Conclusions .....	142
VI SUMMARY AND CONCLUSIONS.....	143
Summary and Main Conclusions .....	143
Recommendations .....	147
REFERENCES .....	148
VITA .....	156

## LIST OF FIGURES

FIGURE	Page
2.1 The Flowchart of the Recursive-Iterative Algorithm.....	19
2.2 A Photograph of the Testing Chamber.....	21
2.3 The Relationship Between Time-Temperature Shift Factor and Temperature for the Fine HMA Mix .....	24
2.4 The Relationship Between Time-Temperature Shift Factor and Temperature for the Coarse HMA Mix .....	24
2.5 The Relationship Between Nonlinear Parameter and Strain Level for the Fine HMA Mix.....	26
2.6 The Relationship Between Nonlinear Parameter and Strain Level for the Coarse HMA Mix.....	26
2.7 Diagram of Two-Step Loading .....	29
2.8 Diagram of One-Step Loading.....	29
2.9 Model Verification Using Two-Step Loading Shown in Figure 2.7.....	30
2.10 Model Verification Using One-Step Loading Shown in Figure 2.8 .....	31
2.11 The Verification of Strain Level 0.01% for Fine HMA Mixes .....	32
2.12 The Verification of Strain Level 0.04% for Fine HMA Mixes.....	33
2.13 The Verification of Strain Level 0.07% for Fine HMA Mixes.....	33
2.14 The Verification of Strain Level 0.1% for Fine HMA Mixes.....	34
2.15 The Verification of Strain Level 0.01% for Coarse HMA Mixes.....	34
2.16 The Verification of Strain Level 0.04% for Coarse HMA Mixes.....	35
2.17 The Verification of Strain Level 0.07% for Coarse HMA Mixes.....	35

FIGURE	Page
2.18 The Verification of Strain Level 0.1% for Coarse HMA Mixes .....	36
3.1 The Stress Sweep Test Data of Unaged Asphalt Binder .....	45
3.2 The Stress Sweep Test Data of Aged Asphalt Binder .....	46
3.3 The Relationship Between $N G^* / G_{ini}^* $ and Stress .....	47
3.4 The Stress Sweep Test Data of Unaged Asphalt Binder After Normalizing by the Ultimate Stress .....	48
3.5 The Stress Sweep Test Data of Aged Asphalt Binder After Normalizing by the Ultimate Stress .....	49
3.6 The Relationship Between Temperature Shift Factor ( $a_T$ ) and Temperature .....	50
3.7 The Relationship Between Nonlinear Parameter and Normalized Stress Level .....	52
3.8 The Master Curve After Stress Vertical Shifting .....	53
3.9 The Master Curve After Stress Horizontal Shifting .....	53
3.10 Data Before and After Applying the Aging Shift Factor .....	56
3.11 Verification of the Finite Element Analysis at a Temperature of 20 °C.....	58
3.12 Viscoelastic Properties ( $J'$ and $J''$ ) for Unaged Binder at 30 °C and Linear Stress Level (Normalized Stress of 0.01) .....	59
3.13 Viscoelastic Properties ( $J'$ and $J''$ ) for Unaged Binder at 30 °C and Nonlinear Stress Level (Normalized Stress of 1) .....	60
4.1 The Effect of Nonlinear Parameter $g_0$ .....	69
4.2 The Effect of Nonlinear Parameter $g_1$ .....	70
4.3 The Effect of Nonlinear Parameter $g_2$ .....	70

FIGURE	Page
4.4 A Schematic Diagram of Creep and Recovery Loading and Strain Response.....	75
4.5 A Flowchart of the Procedure for the Analysis of Strain Components.....	76
4.6 The Strain Components of PG 70-22 at 58 °C .....	79
4.7 Comparisons of Irrecoverable Strain for Different Binders at Different Temperatures .....	80
4.8 The Nonlinear Parameters of Binder PG 70-22 at 58 °C .....	81
4.9 The Nonlinear Parameters of PG 70-28 Binder at 64 °C .....	81
4.10 The Comparison of Experimental Measurements of Permanent Strain and Linear Dashpot Analysis Results for Stress Levels 1 to 6 .....	83
4.11 The Comparison of Experimental Measurements of Permanent Strain and Linear Dashpot Analysis Results for Stress Levels 7 to 9 .....	83
4.12 The Comparison of Irrecoverable Strain Using the New Method and the Dashpot Approach.....	84
4.13 The Results of Nonlinear Parameters for the Air Blown Binder .....	85
4.14 The Results of Nonlinear Parameters for the SBS-Modified Binder .....	86
4.15 The Results of Nonlinear Parameters for the ELVALOY-Modified Binder .....	86
4.16 The Results of Nonlinear Parameters for the Control Binder .....	87
4.17 The Results of Nonlinear Parameters for the SBSLG-Modified Binder....	87
4.18 The Relationship between Stress and $J_{nr}$ .....	90
4.19 The Comparison of $J_{nr}$ without Separation and ALF Rutting .....	91
4.20 The Comparison of $J_{nr}$ with Separation and ALF Rutting.....	91
5.1 The Extended Drucker-Prager Yield Surface.....	102

FIGURE	Page
5.2 The Influence of Stress Path on the $I_1 - \sqrt{J_2}$ Plane .....	102
5.3 The Flowchart of Nonlinear Viscoelastic-Viscoplastic Implementation ...	113
5.4 The Flowchart of Newton-Raphson Method for Viscoplastic Strain Increments .....	114
5.5 The Schematic Diagram of Loading .....	118
5.6 The Total Strain Comparison Between FE Solution and Calculated Results .....	119
5.7 The Error of Total Strain Between FE Solution and Calculated Results ...	119
5.8 The Effect of Yield Surface Parameter $\alpha$ .....	122
5.9 The Effect of Yield Surface Parameter $d$ .....	123
5.10 The Effect of Viscoplastic Potential Energy Parameter $\beta$ .....	124
5.11 The Effect of Flow Function Parameter $\Gamma$ .....	124
5.12 The Effect of Flow Function Parameter $N$ .....	125
5.13 The Effect of Hardening Function Parameters $\kappa_0$ .....	125
5.14 The Effect of Hardening Function Parameters $\kappa_1$ .....	126
5.15 The Effect of Hardening Function Parameters $\kappa_2$ .....	126
5.16 The Sketch of Pavement Section.....	129
5.17 Three Different Meshes for Conducting Sensitivity of FE Size .....	130
5.18 The Strain Comparison of Three Different Meshes .....	131
5.19 The Von Mises Stress Comparison of Three Different Meshes.....	131
5.20 The Viscoelastic and Viscoplastic Strain Comparison at 15 <sup>th</sup> Loading Cycle .....	136

FIGURE	Page
5.21 The Nonlinear Parameters Comparison at 15 <sup>th</sup> Loading Cycle.....	137
5.22 The Viscoelastic and Viscoplastic Strain Comparison at 25 <sup>th</sup> Loading Cycle .....	138
5.23 The Nonlinear Parameters Comparison at 25 <sup>th</sup> Loading Cycle.....	139
5.24 The Comparison of Total Strain Between High and Intermediate Temperature .....	140
5.25 The Comparison of Nonlinear Viscoelastic Strain Between High and Intermediate Temperature .....	140
5.26 The Viscoplastic Strain Under Intermediate and High Temperature .....	141

## LIST OF TABLES

TABLE	Page
2.1 The Temperature Shift Factors.....	23
2.2 The Nonlinear Parameters $g_1, g_2$ at Different Strain Levels.....	25
2.3 Linear Viscoelastic Material Coefficients.....	27
2.4 Percent Difference Between Model Results and Experimental Measurements.....	32
3.1 The Temperature Shift Factor for Each Temperature .....	50
3.2 The Nonlinear Parameters and Stress Shift Factors at Different Stress Levels.....	51
3.3 Linear Viscoelastic Coefficients of the Prony Series.....	52
3.4 The Aging Shift Factor for Each Combination of Temperature and Normalized Stress Levels .....	55
4.1 The Ultimate Stress for Each Binder.....	89
4.2 The Results of $J_{nr}$ and the Ranking.....	90
5.1 Viscoelastic Material Parameters (Lai and Bakker, 1996).....	117
5.2 Viscoplastic Material Parameters.....	118
5.3 The Element Size, Total FE Number and Calculating Time.....	128
5.4 The Coefficients of Nonlinear Parameter for Intermediate and High Temperature .....	135
5.5 The Viscoplastic Parameters for Intermediate and High Temperature .....	135

## CHAPTER I

### INTRODUCTION

#### BACKGROUND

There has been emphasis in recent years in developing a mechanistic model for predicting the performance of asphalt mixtures. The primary challenge in developing such a mechanistic model has been in formulating a constitutive relationship that accounts for the dependency of asphalt mixture response on temperature, loading rate, stress/strain levels and stress state (Perl et al., 1983, Sides et al., 1985, Collop et al., 2003, and Masad et al., 2002).

Several studies have focused on developing constitutive relationships for asphalt mixtures. However, most of these relationships focused on predicting a certain pavement distress (permanent deformation, fatigue, low temperature cracking) that is associated with certain ranges of temperatures and loading rates. Sides et al. (1985) proposed a one-dimensional mathematical relationship to describe the elastic, viscoelastic, plastic, and viscoplastic components of asphalt mix response submitted to uniaxial loading. These relationships were empirical and could not be extended to the three-dimensional case that is necessary for numerical implementation and performance prediction. Chehab et al. (2003) developed what was referred to as an elasto-viscoplastic continuum model to characterize asphalt mixes subjected to uniaxial loading. The viscoelastic behavior was modeled using Schapery's theory, while an empirical strain hardening model was used to characterize the viscoplastic behavior.

---

This dissertation follows the style of *Journal of Engineering Mechanics* (ASCE).



Sousa et al. (1993) developed a nonlinear elastic, viscous model with damage to predict permanent deformation of HMA. This model employed nine parameters  $C_1 \sim C_9$  to represent the nonlinear elastic response. This study conducted a Simple Shear Test, an Uniaxial Strain Test, and a Volumetric Test to obtain the nonlinear elastic parameters; the viscous component was modeled by several sets of Maxwell model with spring and dashpot. The damage effect was accounted for in changing the viscous or dashpot parameter as a function of shear strain. Sousa and Weissman (1994) improved the nonlinear elastic, viscous model by incorporating an elastoplastic component to account for yielding and development of permanent strain. The model employed the Von Mises yield surface with kinematic hardening. However, the irrecoverable component is time-independent in this model. Seibi et al. (2001) developed the elasto-viscoplastic constitutive model for HMA that was implemented in the finite element package ABAQUS. The model used the Perzyna's theory of viscoplasticity with the Drucker-Prager yield surface. The isotropic hardening and associate flow rule were used to describe the material response once the material reached the yield surface. However, this model considered the recoverable component as elastic. Collop et al. (2003) developed a three-dimensional, elasto-viscoplastic constitutive model with damage that includes elastic, delayed elastic and viscoplastic components. This model used the power law function of stress to model the viscoplastic strain rate. Lu and Wright (1998) proposed a visco-elastoplastic model in which Hooke's law was used to model the elastic strain component, a power law function of stress and time was used to present the viscoelastic strain component. The viscoplastic strain component was modeled using

Perzyna's theory of viscoplasticity. Oeser and Moller (2004) developed a three-dimensional constitutive model that uses a Hook-Kelvin-Newton element to present the elastic, viscoelastic, and viscoplastic components, respectively. The Von Mises yield surface function was used in the tension zone, while the Drucker-Prager function was employed in the compression zone. The model also considered the temperature effect, healing and damage effect. Erkens et al. (2002) developed a three-dimensional constitutive model to account for the strain rate sensitive, temperature-, and loading history-dependent on HMA. This model used Desai et al. (1986) flow surface to represent the plastic behavior of the mixture. Nevertheless, these models do not include the nonassociated behavior in material constitutive model and do not consider the nonlinearity of recoverable component.

At Texas A&M University, Tashman (2003) developed a nonassociated elasto-viscoplastic model for HMA. This model considered the anisotropy, damage effects and work hardening. Tashman (2003) considered the recoverable response to be elastic. Dessouky (2005) extended the work by Tashman (2003) by modifying the yield surface in order to account for the difference in the mixture response under extension and compression stress states. Dessouky (2005) also considered the recoverable response to be time-independent. Saadeh (2005) conducted extensive experiments in order to characterize recoverable and irrecoverable responses of the mixture. Saadeh (2005) found that the recoverable response is nonlinear and it experiences damage at the test temperatures (59°C). He developed an experimental method for separating the nonlinear recoverable and irrecoverable components.

## **PROBLEM STATEMENT**

The behavior of asphalt materials (binders, mastics and full mixtures) is complex and it is influenced by temperature, stress/strain level, and stress/strain rate. Furthermore, the total response of asphalt materials subjected to an applied stress contains recoverable (viscoelastic) and irrecoverable (viscoplastic) strain components that could occur simultaneously. The viscoelastic component of the response becomes more dominant as temperature decreases and loading rate increases.

The relationship between stress and the recoverable strain component can be nonlinear depending on the applied stress/strain limits and temperature. Damage can be manifested in changes in the mixture recoverable response. The viscoplastic response is also complex and it becomes more dominant as temperature increases and the rate of loading decreases.

It is necessary to separate the recoverable and irrecoverable strain in order to develop the constitutive relationships for describing these components and determine the model's parameters associated with each component. Consequently, there is a need to develop a mechanistic model that incorporates both the viscoelastic and viscoplastic components of mixture response. The mechanistic model needs to be implemented in finite element in order to predict performance under realistic boundary conditions representing the laboratory and the field.

## **OBJECTIVE**

This primary objective of this study is to develop a mechanistic model for asphalt materials that accounts for both the nonlinear viscoelastic and viscoplastic components of the response of asphalt mixtures. This objective is achieved through the following tasks:

1. Implement the Schapery nonlinear viscoelastic model in finite element.
2. Verify the suitability of the nonlinear viscoelastic model in describing the behavior of asphalt material by analyzing:
  - a. the results of testing asphalt mixtures using the Simple Shear Test (SST) at several temperatures and stress levels,
  - b. the response of unaged and aged asphalt binders tested in the Dynamic Shear Rheometer (DSR), and
  - c. the response of asphalt binders in the multiple stress creep recovery test (MSCR).
3. Develop a method for separating the nonlinear viscoelastic and viscoplastic components of asphalt mixture response.
4. Implement the nonlinear viscoelastic-viscoplastic model in finite element and conduct parametric analysis in order to demonstrate the capabilities of the model in describing mixture performance at various loading conditions.

## **ORGANIZATION OF THE DISSERTATION**

This dissertation is organized following the research paper format. Chapters II, III, IV, and V are research papers that have been or will be submitted as refereed journal papers.

Chapter I includes the introduction which contains background on modeling asphalt mixture response and performance, problem statement, objectives and the outline of this dissertation.

Chapter II is the paper from the *Journal of Time Dependent Materials*. This chapter includes the finite element implementation of Schapery nonlinear viscoelastic model in finite element and the use of this model in describing the behavior of asphalt mixtures subjected to shear loading at different temperatures, loading frequencies and strain levels.

Chapter III is a paper that was published in the *Journal of the Construction and Building Materials*. This chapter includes the nonlinear viscoelastic analysis of aged and unaged asphalt binders. It demonstrates the capability of the model in accounting for the effect of aging on asphalt response.

Chapter IV is a paper that utilizes the nonlinear viscoelastic model to describe the response of asphalt binders subjected to multiple creep and recovery loading cycles. In this chapter, a method is developed for separating the nonlinear viscoelastic response from the plastic response. Consequently, the plastic strain is used to derive a parameter for characterizing the resistance of asphalt binders to permanent deformation.

Chapter V is a paper that includes the nonlinear viscoelastic-viscoplastic model and numerical implementation. In this chapter, the parametric analysis was conducted to illustrate the effect of viscoplastic parameters, and a FE model was developed to simulate a pavement section under intermediate and high temperature.

Chapter VI is conclusions that combine the results from all chapters.

## CHAPTER II

### NONLINEAR VISCOELASTIC ANALYSIS OF ASPHALT MIXES SUBJECTED TO SHEAR LOADING\*

#### OVERVIEW

This study presents the characterization of the nonlinear viscoelastic behavior of hot mix asphalt (HMA) at different temperatures and strain levels using the Schapery nonlinear viscoelastic model. A recursive-iterative numerical algorithm is generated for the nonlinear viscoelastic response and implemented in a displacement-based finite element (FE) code. Then, this model is employed to describe experimental frequency sweep measurements of two asphalt mixes with fine and coarse gradations under several combined temperatures and shear strain levels. The frequency sweep measurements are converted to creep responses in the time domain using a phenomenological model (Prony series). The master curve is created for each strain level using the time temperature superposition principle (TTSP) with a reference temperature of 40°C. The linear time-dependent parameters of the Prony series are first determined by fitting a master curve created at the lowest strain level, which in this case is 0.01%. The measurements at strain levels higher than 0.01% are analyzed and used to determine the nonlinear viscoelastic parameters. These parameters are shown to increase with increasing strain levels, while the time-temperature shift function is found to be

---

\* Full text reprinted with permission from “Nonlinear viscoelastic analysis of asphalt mixes subjected to shear loading” by Chien-Wei Huang, Eyad Masad, Anastasia H. Muliana and Hussain Bahia, 2007. *Mechanics of Time Dependent Materials*, Vol. 11, pp. 91-110, Copyright [2008] by Springer Science + Business Media.

independent of strain levels. The FE model with the calibrated time-dependent and nonlinear material parameters is used to simulate the creep experimental tests, and reasonable predictions are shown.

## **INTRODUCTION**

Hot mix asphalt (HMA) is a composite material that consists of aggregates, asphalt binder, and air voids. HMA exhibits time-dependent behavior, which can be linear or nonlinear depending on the combination of stress or strain level, temperature, and loading rate. The linear behavior indicates that the material properties are functions of time and temperature, and the response obeys the homogeneity and superposition principles (Ferry, 1961).

The nonlinear behavior of HMA can be caused by the rotation and slippage of aggregates and the localized high strains in the binder phase (Kose et al., 2000). Experimental studies by Collop et al. (2002) and Airey et al. (2004) established stress and strain limits after which the nonlinear behavior of asphalt binders become evident. Masad and Somadevan (2002) used the Dynamic Shear Rheometer to measure the linear and nonlinear viscoelastic properties of asphalt binders and mixtures at different temperatures, frequencies, and strain levels. They also used finite element (FE) analysis and image correlation techniques to determine the strain distribution within the HMA microstructure. The results showed that the strain in some part of the binder phase of the mixture is high enough to induce nonlinear response. Abbas (2004) and Abbas et al.



(2004) developed an incremental viscoelastic model to simulate the nonlinear behavior of asphalt binders within the asphalt mix microstructure using FE analysis.

In spite of the overwhelming experimental evidence showing the nonlinear response of asphalt mixes, there has not been a systematic approach to model this response. The Schapery single integral model is one of the most popular models and has been applied to characterize the influence of stress and strain level on the nonlinear constitutive behavior of engineering materials (Christensen, 1968; Schapery, 1969; Schapery, 2000). Lou and Schapery (1971) simulated the glass fiber–epoxy nonlinear time-dependent behavior, while Shields et al. (1998) used the Schapery theory to analyze the nonlinear behavior of asphalt mixtures. The Schapery single integral model is relatively easy to implement in a numerical scheme. Touati and Cederbaum (1997) presented a numerical scheme of the Schapery theory to predict the nonlinear stress relaxation via the Runge-Kutta method. They transferred the nonlinear convolution integral into a set of first-order nonlinear equations, which are solved to predict nonlinear stress relaxation response. In the follow-up study, Touati and Cederbaum (1998) extended this method to analyze the orthotropic laminated plane. Haj-Ali and Muliana (2004) developed a recursive-iterative integration algorithm to analyze the three-dimensional nonlinear viscoelastic behavior of polymeric materials. Sadd et al. (2004) developed a recursive scheme of the Schapery theory and implemented it in ABAQUS finite element package to represent the micromechanical model of asphalt mixes.

The main objectives of this study are to implement a numerical representation of the Schapery nonlinear viscoelastic model and to analyze the nonlinear behavior of asphalt mixtures at different temperatures and strain levels. This study employs the recursive-iterative integration numerical algorithm in the implementation of the Schapery nonlinear viscoelastic model. This algorithm improves convergence since it uses the predictor-corrector method at both the material and structure levels.

Model verification was achieved by comparing the model results with shear test measurements at different combinations of strain levels, temperatures, and time. The master curves of the experimental data and the time-temperature shift coefficients were first determined for each strain level. The linear viscoelastic Prony coefficients were calculated at the lowest strain level used in these tests. Then, the nonlinear parameters were obtained by shifting the master curves vertically. In order to obtain the long-term viscoelastic behavior, the temperature-strain master curve was formed by shifting the respective temperature master curve at higher strain levels to the temperature master curve at the lowest strain level.

## **NUMERICAL IMPLEMENTATION OF THE SCHAPERY NONLINEAR VISCOELASTIC MATERIAL MODEL**

Consider the Schapery (1969) strain response due to a stress  $\sigma^\tau$ , which is expressed as:

$$\varepsilon(t) = g_0 D_0 \sigma^t + g_1 \int_0^t \Delta D (\psi^t - \psi^\tau) \frac{d(g_2 \sigma^\tau)}{d\tau} d\tau \quad (2-1)$$

where  $D_0$  is the instantaneous elastic compliance,  $\Delta D$  is the transient compliance, and  $\psi^t$  is the reduced time. It is given by:

$$\psi^t = \int_0^t \frac{d\xi}{a_T a_s} \quad (2-2)$$

$g_0$ ,  $g_1$ , and  $g_2$  are the nonlinear parameters related to stress or strain status,  $a_T$  is the temperature shift factor, and  $a_s$  is the strain or stress shift factor. The parameter  $g_0$  is related to the nonlinear instantaneous compliance,  $g_1$  is associated with the nonlinear transient compliance, and  $g_2$  is related to the loading rate effect on nonlinear response. Eq. (2-1) reduces to the Boltzmann superposition integral for linear materials, with  $g_0$ ,  $g_1$ , and  $g_2$  being equal to unity. The Prony series is used to represent the transient compliance  $\Delta D$  as follows:

$$\Delta D^{\psi^t} = \sum_{n=1}^N D_n \left( 1 - \exp(-\lambda_n \psi^t) \right) \quad (2-3)$$

where  $D_n$  is the  $n^{\text{th}}$  coefficient of the Prony series and  $\lambda_n$  is the  $n^{\text{th}}$  retardation time.

Numerical analyses give approximations of the exact solutions. A recursive method is used to solve the nonlinear viscoelastic integral equations with a finite number of incremental time steps, e.g., Lai and Bakker (1996), and Poon and Ahmad (1999). Lai and Bakker (1996) presented an integration algorithm for a nonlinear stress-based viscoelastic model assuming that the nonlinear parameters are constant over the time increment. However, this is not the case, and an iterative scheme should be included in order to minimize this error, especially when the nonlinear viscoelastic integral is used

to express the strains in terms of stress-based variables. Poon and Ahmad (1999) proposed an integration scheme for stress relaxation with strain-based nonlinear functions that is compatible with a displacement-based FE method. The choice of the state variables resulted in conversion of the hereditary integral to a set of linear differential equations. The iterations for stress correction were not required due to the use of strain-based nonlinear parameters. Though iterative stress correction can be avoided by use of strain-based parameters, it is often more difficult to conduct experimental tests for characterizing the strain-based material parameters.

In a nonlinear analysis, using a very tight incremental time is computationally expensive and often leads to divergence after a certain number of steps. The divergence is due to the accumulated residual errors. To overcome this problem, an iterative method is added within each incremental time step at the material level. This method uses the recurrence formula that does not require storing entire strain histories at the material level. The linear strain formulation is used within the recursive approach to give the trial solutions, and then the stress corrector scheme is added at the material level to minimize errors arising from the linearization and to consequently enhance convergence. Haj-Ali and Muliana (2004) and Muliana and Kim (2007) demonstrated that neglecting the iteration at the material level could result in more than 50% strain errors. In this study, the recursive-iterative integration approach developed by Haj-Ali and Muliana (2004) is used to implement the Schapery nonlinear viscoelastic model.

The strain response for isotropic materials can be decoupled into deviatoric and volumetric parts. It can be presented as:

$$\varepsilon_{ij} = \frac{1}{2G} S_{ij} + \frac{\sigma_{kk}}{9K} \delta_{ij} = \frac{1}{2} J S_{ij} + \frac{1}{3} B \sigma_{kk} \delta_{ij} \quad (2-4)$$

where  $G$  and  $K$  are shear modulus and bulk modulus, respectively.  $J$  and  $B$  are shear compliance and bulk compliance, respectively.  $S_{ij}$  is the deviatoric stress, and  $\sigma_{kk}$  is the volumetric stress. Applying the Schapery integral constitutive model, the deviatoric and volumetric strain can be expressed as:

$$e_{ij}^t = \frac{1}{2} g_0^t J_0 S_{ij}^t + \frac{1}{2} g_1^t \int_0^t \Delta J^{(\psi^t - \psi^\tau)} \frac{d(g_2^\tau S_{ij}^\tau)}{d\tau} d\tau \quad (2-5)$$

$$\varepsilon_{kk}^t = \frac{1}{3} g_0^t B_0 \sigma_{kk}^t + \frac{1}{3} g_1^t \int_0^t \Delta B^{(\psi^t - \psi^\tau)} \frac{d(g_2^\tau \sigma_{kk}^\tau)}{d\tau} d\tau \quad (2-6)$$

where  $e_{ij}$  is the deviatoric strain and  $\varepsilon_{kk}$  is the volumetric strain.  $J_0$  and  $B_0$  are instantaneous elastic shear compliance and instantaneous elastic bulk compliance, respectively.  $\Delta J$  and  $\Delta B$  are transient shear compliance and transient bulk compliance, respectively.

Motivated by experimental measurements showing the Poisson's ratio  $\nu$  to vary only slightly for wide ranges of temperatures and loading rates (ASTM, 1995; Benedetto et al., 2007),  $\nu$  is assumed to be time-independent leading to the following expression of the compliances:

$$\begin{aligned} J_0 &= 2(1 + \nu)D_0 & B_0 &= 3(1 - 2\nu)D_0 \\ \Delta J(\psi) &= 2(1 + \nu)\Delta D(\psi) & \Delta B(\psi) &= 3(1 - 2\nu)\Delta D(\psi) \end{aligned} \quad (2-7)$$

After substituting Eqs. (2-3) and (2-7) into (2-5) and (2-6), the deviatoric and volumetric can be written in terms of hereditary integral formulation and as follows:

$$e_{ij}^t = \frac{1}{2} \left[ g_0^t J_0 + g_1^t g_2^t \sum_{n=1}^N J_n - g_1^t g_2^t \sum_{n=1}^N J_n \frac{1 - \exp(-\lambda_n \Delta \psi^t)}{\lambda_n \Delta \psi^t} \right] S_{ij}^t - \frac{1}{2} g_1^t \sum_{n=1}^N J_n \left[ \exp(-\lambda_n \Delta \psi^t) q_{ij,n}^{t-\Delta t} - g_2^{t-\Delta t} \frac{(1 - \exp(-\lambda_n \Delta \psi^t))}{\lambda_n \Delta \psi^t} S_{ij}^{t-\Delta t} \right] \quad (2-8)$$

$$\varepsilon_{kk}^t = \frac{1}{3} \left[ g_0^t B_0 + g_1^t g_2^t \sum_{n=1}^N B_n - g_1^t g_2^t \sum_{n=1}^N B_n \frac{1 - \exp(-\lambda_n \Delta \psi^t)}{\lambda_n \Delta \psi^t} \right] \sigma_{kk}^t - \frac{1}{3} g_1^t \sum_{n=1}^N B_n \left[ \exp(-\lambda_n \Delta \psi^t) q_{kk,n}^{t-\Delta t} - g_2^{t-\Delta t} \frac{(1 - \exp(-\lambda_n \Delta \psi^t))}{\lambda_n \Delta \psi^t} \sigma_{kk}^{t-\Delta t} \right] \quad (2-9)$$

For implementation in the finite element method, the incremental shear and bulk strains are derived and shown as:

$$\begin{aligned} \Delta e_{ij}^t &= e_{ij}^t - e_{ij}^{t-\Delta t} \\ &= \bar{J}^t S_{ij}^t - \bar{J}^{t-\Delta t} S_{ij}^{t-\Delta t} - \frac{1}{2} \sum_{n=1}^N J_n \left[ g_1^t \exp(-\lambda_n \Delta \psi^t) - g_1^{t-\Delta t} \right] q_{ij,n}^{t-\Delta t} - \\ &\quad \frac{1}{2} g_2^{t-\Delta t} \sum_{n=1}^N J_n \left\{ g_1^{t-\Delta t} \left[ \frac{1 - \exp(-\lambda_n \Delta \psi^{t-\Delta t})}{\lambda_n \Delta \psi^{t-\Delta t}} \right] - g_1^t \left[ \frac{1 - \exp(-\lambda_n \Delta \psi^t)}{\lambda_n \Delta \psi^t} \right] \right\} S_{ij}^{t-\Delta t} \end{aligned} \quad (2-10)$$

$$\begin{aligned} \Delta \varepsilon_{kk}^t &= \varepsilon_{kk}^t - \varepsilon_{kk}^{t-\Delta t} \\ &= \bar{B}^t \sigma_{kk}^t - \bar{B}^{t-\Delta t} \sigma_{kk}^{t-\Delta t} - \frac{1}{3} \sum_{n=1}^N B_n \left[ g_1^t \exp(-\lambda_n \Delta \psi^t) - g_1^{t-\Delta t} \right] q_{kk,n}^{t-\Delta t} - \\ &\quad \frac{1}{3} g_2^{t-\Delta t} \sum_{n=1}^N B_n \left\{ g_1^{t-\Delta t} \left[ \frac{1 - \exp(-\lambda_n \Delta \psi^{t-\Delta t})}{\lambda_n \Delta \psi^{t-\Delta t}} \right] - g_1^t \left[ \frac{1 - \exp(-\lambda_n \Delta \psi^t)}{\lambda_n \Delta \psi^t} \right] \right\} \sigma_{kk}^{t-\Delta t} \end{aligned} \quad (2-11)$$

where  $\bar{J}^t$  and  $\bar{B}^t$  can be expressed as:

$$\bar{J}^t = \frac{1}{2} \left[ g_0^t J_0 + g_1^t g_2^t \sum_{n=1}^N J_n - g_1^t g_2^t \sum_{n=1}^N J_n \frac{1 - \exp(-\lambda_n \Delta \psi^t)}{\lambda_n \Delta \psi^t} \right] \quad (2-12)$$

$$\bar{B}^t = \frac{1}{3} \left[ g_0^t B_0 + g_1^t g_2^t \sum_{n=1}^N B_n - g_1^t g_2^t \sum_{n=1}^N B_n \frac{1 - \exp(-\lambda_n \Delta \psi^t)}{\lambda_n \Delta \psi^t} \right] \quad (2-13)$$

The variables  $q_{ij,n}^{t-\Delta t}$  and  $q_{kk,n}^{t-\Delta t}$  are the shear and volumetric hereditary integrals, respectively, for every Prony series term  $n$  at previous time  $t - \Delta t$ . The hereditary integrals are updated at the end of every converged time increment, which will be used for the next time increment. The formulation of shear and volumetric hereditary integrals are:

$$q_{ij,n}^t = \exp(-\lambda_n \Delta \psi^t) q_{ij,n}^{t-\Delta t} + (g_2^t S_{ij}^t - g_2^{t-\Delta t} S_{ij}^{t-\Delta t}) \frac{1 - \exp(-\lambda_n \Delta \psi^t)}{\lambda_n \Delta \psi^t} \quad (2-14)$$

$$q_{kk,n}^t = \exp(-\lambda_n \Delta \psi^t) q_{kk,n}^{t-\Delta t} + (g_2^t \sigma_{kk}^t - g_2^{t-\Delta t} \sigma_{kk}^{t-\Delta t}) \frac{1 - \exp(-\lambda_n \Delta \psi^t)}{\lambda_n \Delta \psi^t} \quad (2-15)$$

The shear and volumetric strain increments can be determined from Eqs. (2-10) and (2-11) provided that the stresses are given. This algorithm will be implemented in the displacement-based FE framework, in which strains are the given variables. The current shear and volumetric stresses and the current nonlinear parameters cannot be determined directly because the nonlinear parameters are dependent on the current stress and vice versa. Hence, the iterative algorithm is added to solve for the current stress state, in which the nonlinear parameters are assumed at the beginning of each time increment  $g_\alpha^t = g_\alpha^{t-\Delta t}$  ;  $\alpha = 0,1,2$  and  $\Delta \psi^t = \Delta \psi^{t-\Delta t}$ . Then, the trial stresses can be determined as follows:

$$\Delta S_{ij}^{t,tr} = \frac{1}{\bar{J}^{t,tr}} \left\{ \Delta e_{ij}^t + \frac{1}{2} g_1^{t,tr} \sum_{n=1}^N J_n \left[ \exp(-\lambda_n \Delta \psi^t) - 1 \right] q_{ij,n}^{t-\Delta t} \right\} \quad (2-16)$$

$$\Delta \sigma_{kk}^{t,tr} = \frac{1}{\bar{B}^{t,tr}} \left\{ \Delta \varepsilon_{kk}^t + \frac{1}{3} g_1^{t,tr} \sum_{n=1}^N B_n \left[ \exp(-\lambda_n \Delta \psi^t) - 1 \right] q_{kk,n}^{t-\Delta t} \right\} \quad (2-17)$$

where  $\bar{J}^{t,tr}$  and  $\bar{B}^{t,tr}$  have the same forms as Eqs. (2-12) and (2-13), respectively, but the nonlinear parameters are assumed to be functions of the last converged stress state.

In this study, the iterative scheme is used to calculate the correct stress state from the current strain increment. As discussed earlier, this scheme allows using relatively large time increments, reduces accumulated residual error, and enhances convergence. In this iterative scheme, the residual strain should be defined and can be determined by calculating the current strain. The residual strain equation can be shown as:

$$R_{ij}^t = \Delta e_{ij}^t + \frac{1}{3} \Delta \varepsilon_{kk}^t \delta_{ij} - \Delta \varepsilon_{ij}^t \quad (2-18)$$

where  $\Delta \varepsilon_{ij}^t$  is provided from the structural level. The Newton-Raphson typed iterative algorithm is used to minimize the strain residual in Eq. (2-18). This requires defining the Jacobian matrix, which in this case is the consistent tangent compliance and is determined as:



$$\begin{aligned}
S_{ijkl} &= \frac{\partial R_{ij}^t}{\partial \Delta \sigma_{ij}^t} \\
&= \bar{J}^t \delta_{ik} \delta_{jl} + \frac{1}{3} (\bar{B}^t - \bar{J}^t) \delta_{ij} \delta_{kl} + \\
&\quad \left\{ \begin{aligned} &\frac{\partial \bar{J}^t}{\partial \Delta \sigma^t} \sigma_{ij}^t + \frac{1}{3} \left( \frac{\partial \bar{B}^t}{\partial \Delta \sigma^t} - \frac{\partial \bar{J}^t}{\partial \Delta \sigma^t} \right) \sigma_{kk}^t \delta_{ij} - \\ &\frac{1}{2} \frac{\partial g_1^t}{\partial \Delta \sigma^t} \sum_{n=1}^N J_n \left[ \exp(-\lambda_n \Delta \psi^t) q_{ij,n}^{t-\Delta t} - g_2^{t-\Delta t} \left( \frac{1 - \exp(-\lambda_n \Delta \psi^t)}{\lambda_n \Delta \psi^t} \right) S_{ij}^{t-\Delta t} \right] - \\ &\frac{\partial \sigma^t}{\partial \Delta \sigma_{kl}^t} \left\{ \frac{1}{2} \frac{\partial a_\sigma^t}{\partial \Delta \sigma^t} g_1^t \sum_{n=1}^N J_n \left[ \begin{aligned} &\exp(-\lambda_n \Delta \psi^t) \left( \frac{\lambda_n q_{ij,n}^{t-\Delta t} \Delta t}{a_\sigma^{t^2}} + g_2^{t-\Delta t} \frac{S_{ij}^{t-\Delta t}}{a_\sigma^t} \right) - \right. \\ &\left. g_2^{t-\Delta t} \left( \frac{1 - \exp(-\lambda_n \Delta \psi^t)}{\lambda_n \Delta t} \right) S_{ij}^{t-\Delta t} \right] - \\ &\frac{1}{9} \frac{\partial g_1^t}{\partial \Delta \sigma^t} \sum_{n=1}^N B_n \left[ \exp(-\lambda_n \Delta \psi^t) q_{kk,n}^{t-\Delta t} - g_2^{t-\Delta t} \left( \frac{1 - \exp(-\lambda_n \Delta \psi^t)}{\lambda_n \Delta \psi^t} \right) \sigma_{kk}^{t-\Delta t} \right] \delta_{ij} - \\ &\frac{1}{9} \frac{\partial a_\sigma^t}{\partial \Delta \sigma^t} g_1^t \sum_{n=1}^N B_n \left[ \begin{aligned} &\exp(-\lambda_n \Delta \psi^t) \left( \frac{\lambda_n q_{kk,n}^{t-\Delta t} \Delta t}{a_\sigma^{t^2}} + g_2^{t-\Delta t} \frac{\sigma_{kk}^{t-\Delta t}}{a_\sigma^t} \right) - \right. \\ &\left. g_2^{t-\Delta t} \left( \frac{1 - \exp(-\lambda_n \Delta \psi^t)}{\lambda_n \Delta t} \right) \sigma_{kk}^{t-\Delta t} \right] \delta_{ij} \end{aligned} \right\} \end{aligned} \right. \quad (2-19)
\end{aligned}$$

The flowchart of this algorithm is shown in Figure 2.1.

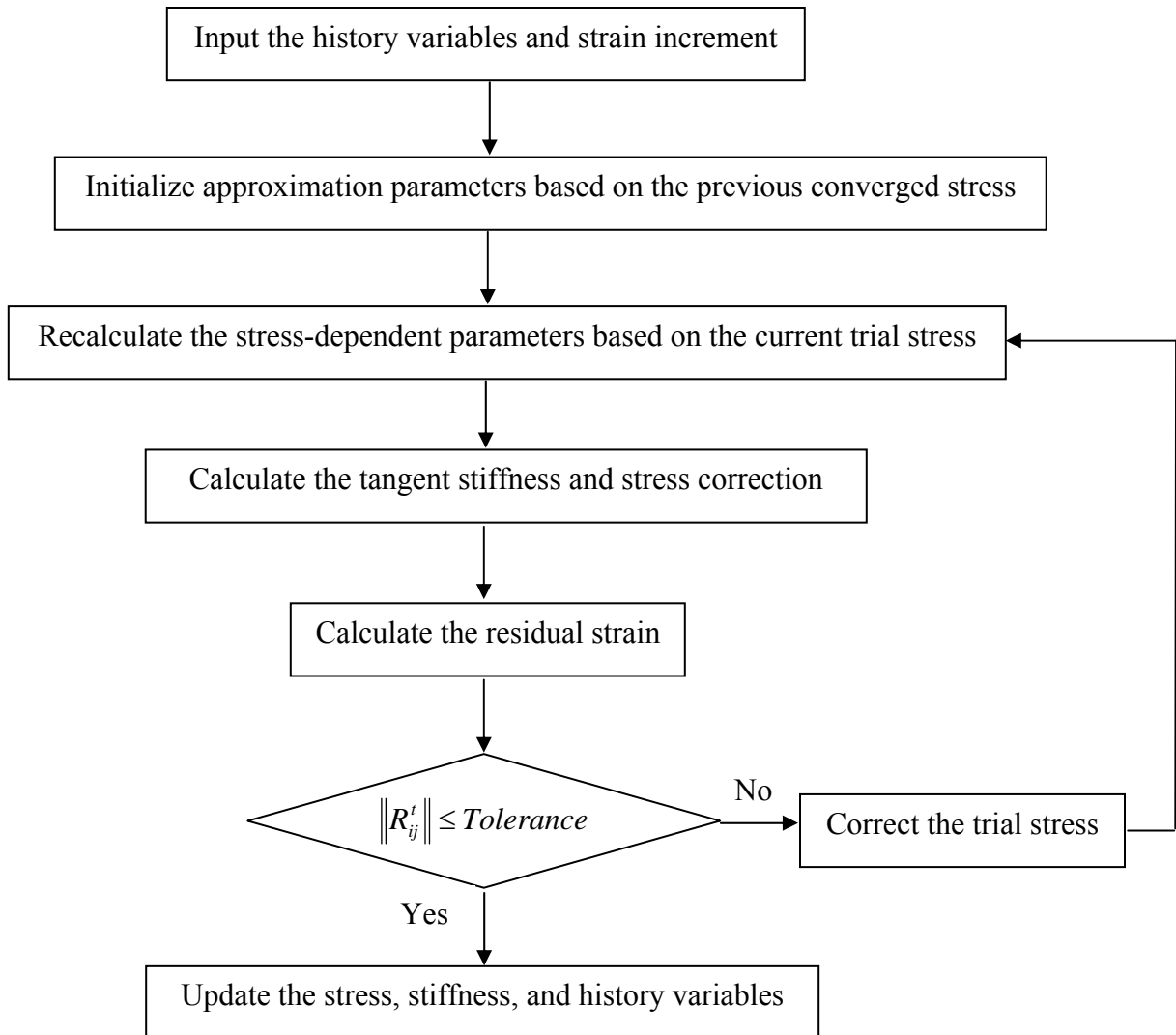


**Figure 2.1** The Flowchart of the Recursive-Iterative Algorithm.

In this study, the nonlinear viscoelastic constitutive model is implemented in the ABAQUS FE package. Iterative equation solutions are performed both at the structural and material levels simultaneously. Two convergence criteria are used in the ABAQUS iterative linear solver: force residual and displacement correction. The force residual vector is defined by a difference between the external force  $P$  and the internal force  $Ku$ ,

where  $K$  is the structure's stiffness matrix and  $u$  is the displacement solution. The displacement correction is defined by a ratio of the displacement correction and incremental displacement. Convergence at the structural level is achieved when the residual force is less than 0.05% of the applied force and the displacement correction is less than 0.01%. At the material level, the residual strain is defined in terms of strain (see Eq.(2-18)), and the given tolerances allow the maximum strain error to be 1 microstrain. Tolerances should be defined properly in every problem within numerical values of interest. Relaxing the tolerance at any level will accumulate errors as time increases, which leads to divergence. Further discussion regarding the effects of residual values on the overall viscoelastic material responses is presented by Haj-Ali and Muliana (2004).

## **EXPERIMENTAL MEASUREMENTS**

The Simple Shear Test (SST) was used to conduct the experimental measurements according to the American Association of State Highway and Transportation Officials (AASHTO) TP7 procedure (AASHTO 1995). The test specimen has a diameter of 150 mm and a height of 50 mm. A specimen was glued to SST platens using a device that ensured proper alignment and parallel faces. A thermocouple was inserted between the platens and the specimen to monitor the actual temperature of the specimen during testing. A linear variable differential transducer (LVDT) was used to measure the horizontal deformation, and the engineering shear

strain was calculated from the horizontal displacement and specimen height. A picture of an instrumented specimen inside the testing chamber is shown in Figure 2.2.



**Figure 2.2** A Photograph of the Testing Chamber.

The test was conducted at multiple frequencies and temperatures starting from the lowest temperature to the highest. At a given temperature, the test was conducted from the highest to the lowest frequency. One hundred cycles were applied for each frequency. The temperatures, frequencies, and strain levels were as follows:

- Temperature: 52, 46, 40, 27°C
- Frequency: 0.01, 0.02, 0.05, 0.1, 0.2, 0.5, 1.0, 2.0, 5.0, 10.0, 30.0 Hz
- Strain: 0.01, 0.04, 0.07, 0.1%

Two HMA mixes with different aggregate size distributions were tested in this study. The first one will be referred to as a fine mix, while the other one will be referred to as a coarse mix (Masad and Somadevan, 2002).

## DATA ANALYSIS

The dynamic compliance  $|J^*|$  (stress amplitude/strain amplitude) and phase angle  $\delta$  (the lag between the stress and strain functions) are determined as functions of frequency for each of the strain and temperature combinations. Then, the storage compliance  $J' = |J^*| \cos \delta$  and loss compliance  $J'' = |J^*| \sin \delta$  are calculated. The Prony series shown in Eq. (2-20) is used to fit each of these functions. The error function shown in Eq. (2-21) is minimized to fit the data.

$$J'_{Model} = J_0 + \sum_{n=1}^N \frac{J_n}{1 + \omega^2 \tau_n^2} \quad (2-20)$$

$$J''_{Model} = \sum_{n=1}^N \frac{J_n \omega \tau_n}{1 + \omega^2 \tau_n^2}$$

$$ERR = \left( \frac{J'_{Model}}{J'_{Exp}} - 1 \right)^2 + \left( \frac{J''_{Model}}{J''_{Exp}} - 1 \right)^2 \quad (2-21)$$

Once the Prony series coefficients are determined in the frequency domain, the series is formulated in terms of compliance as a function of time as in Eq. (2-22). All the analysis discussed hereafter applies to the compliance functions in the time domain.

$$J(t) = J_0 + \sum_{n=1}^N J_n \left( 1 - \exp\left(\frac{-t}{\tau_n}\right) \right) \quad (2-22)$$

The time-temperature shifting is used to obtain the master curve for each strain level with a reference temperature of 40°C. Nonlinear least squares regression was used in the time-temperature shifting. Figures 2.3 and 2.4 show the relationship between temperature and time-temperature factor  $a_T$  for the fine and coarse mixes, respectively. The graphs show that the temperature shift factors are almost independent of the strain level. Hence, the temperature shift factor will be taken to be the average at each strain level. These average temperature shift factors are shown in Table 2.1.

**Table 2.1** The Temperature Shift Factors.

Temp. °C	Time-Temperature Shift Factor $a_T$	
	Fine Mix	Coarse Mix
52	0.1369	0.1254
46	0.3620	0.3443
40	1.0000	1.0000
27	10.6630	12.9997

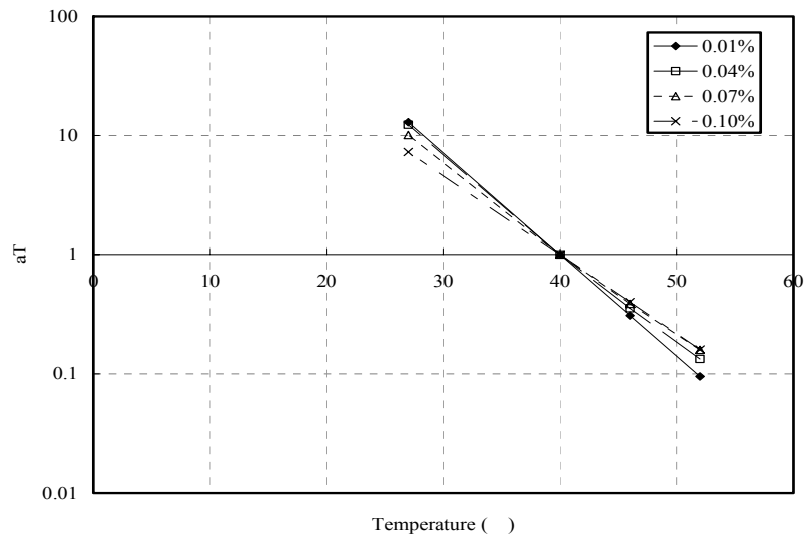


**Figure 2.3** The Relationship Between Time-Temperature Shift Factor and Temperature for the Fine HMA Mix.

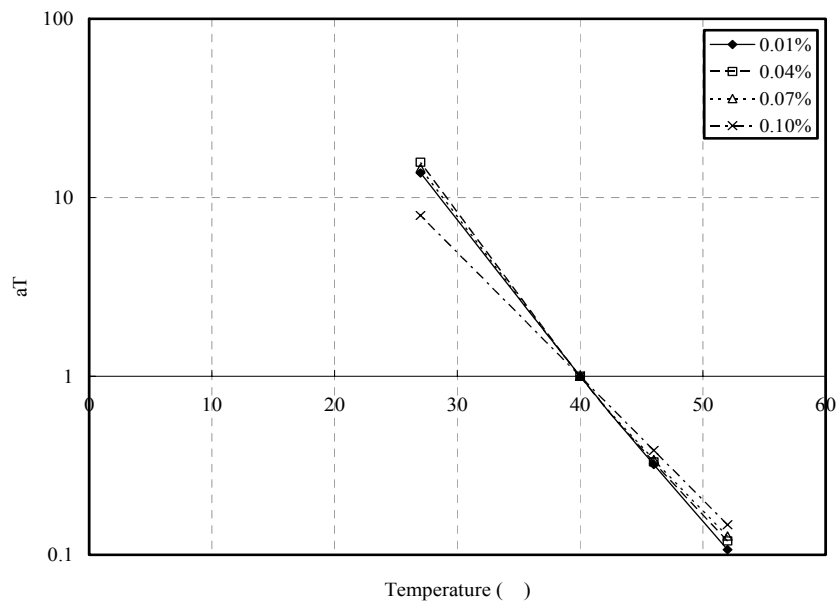


**Figure 2.4** The Relationship Between Time-Temperature Shift Factor and Temperature for the Coarse HMA Mix.

The result of the multiplication of the parameters  $g_1$  and  $g_2$ , which is denoted as  $g_1g_2$ , is obtained by vertical shifting of the master curves at all strain levels to a reference strain level, which in this case is 0.01%. The  $g_1g_2$  values are shown in Table 2.2. Figures 2.5 and 2.6 show the relationship between  $g_1g_2$  and strain levels for the fine and coarse mixes, respectively. As expected, the  $g_1g_2$  value increases with an increase in strain level. It is noted that unloading part of the creep compliance curve is needed in order to determine the  $g_1$  and  $g_2$  values separately (Lou and Schapery, 1971). However, only the loading part of the creep compliance can be determined from the frequency domain measurements, which can be used to calculate the multiplication of these two parameters ( $g_1g_2$ )

**Table 2.2** The Nonlinear Parameters  $g_1g_2$  at Different Strain Levels.

Strain Level	Nonlinear Parameter $g_1g_2$	
	Fine Mix	Coarse Mix
0.01%	1.0000	1.0000
0.04%	1.8486	1.7826
0.07%	2.3999	2.4328
0.1%	2.9628	2.9880



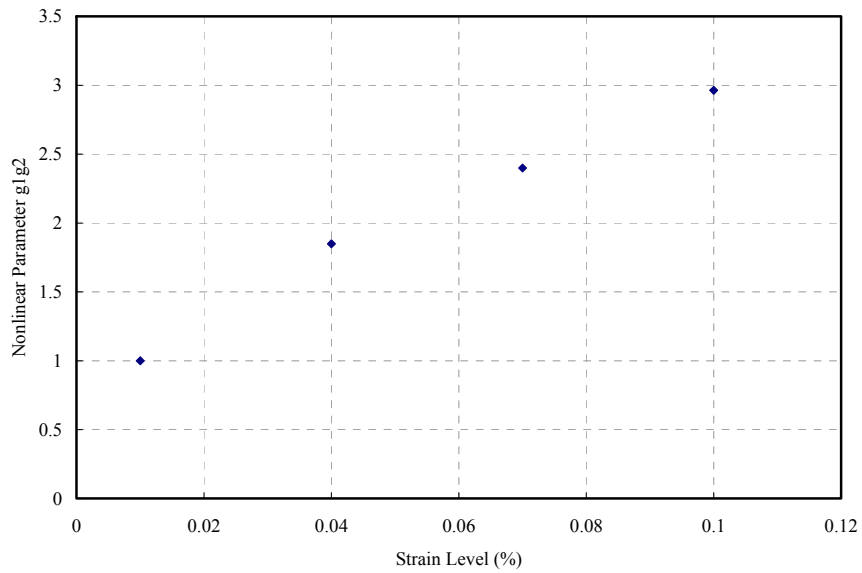


**Figure 2.5** The Relationship Between Nonlinear Parameter and Strain Level for the Fine HMA Mix.

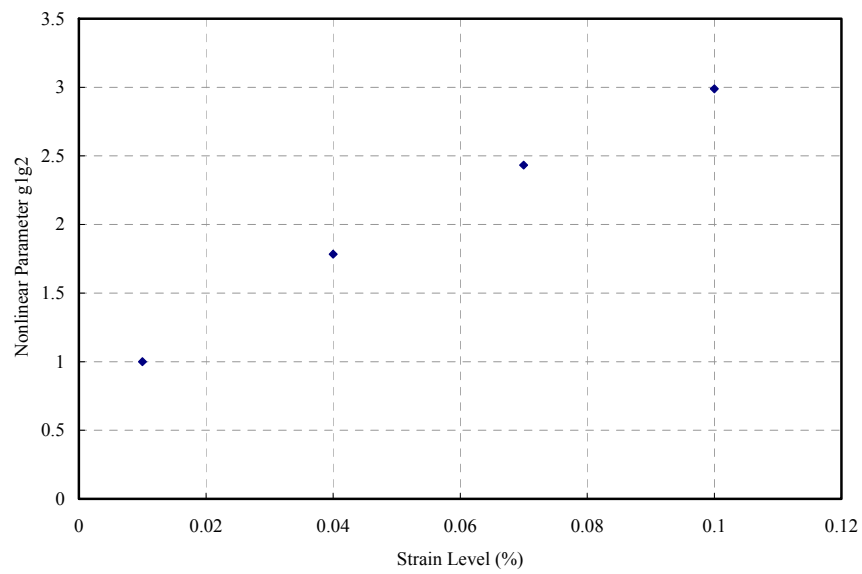


**Figure 2.6** The Relationship Between Nonlinear Parameter and Strain Level for the Coarse HMA Mix.

The master curves at the different strain levels are also shifted horizontally using nonlinear least squares analysis to the reference strain of 0.01% in order to determine the time-strain shift factors ( $a_s$ ) and obtain the long-term HMA behavior. The long-term linear viscoelastic Prony coefficients are obtained by fitting all the data shifted horizontally to the 0.01% strain. These coefficients are shown in Table 2.3. The time-strain shift factors for the fine and coarse mixes are shown as Table 2.4. Consequently, time-temperature shift factors (Table 2.1), nonlinear parameters (Table 2.2), and the long-term linear viscoelastic coefficients (Table 2.3) obtained from the experimental test will be used as input properties to the material subroutine.

**Table 2.3** Linear Viscoelastic Material Coefficients.

Linear Viscoelastic Material Coefficients				
n	Fine Mix		Coarse Mix	
	$J_n$	$\lambda$	$J_n$	$\lambda$
1	1.15E-06	1	2.00E-06	1
2	1.49E-06	0.1	2.72E-06	0.1
3	3.17E-06	0.01	6.45E-06	0.01
4	6.37E-06	0.001	1.20E-05	0.001
5	2.61E-06	0.0001	3.69E-05	0.0001
6	9.61E-05	0.00001		
$J_0$	6.75E-07		9.85E-07	

## MODEL VERIFICATION

Model verification is conducted in two stages. The first stage includes a comparison between the FE predictions and the closed form solution of the modified superposition principle (MSP). In the second stage, inverse analysis is conducted to determine the ability of the parameters obtained in establishing the master curve and used in FE analysis to match the experimental measurements at different combinations of temperatures and strain levels.

The two-step loading shown in Figure 2.7 is used in the first-step verification.

The strain response under this loading can be described as:

$$\varepsilon_r = \left[ g_0^a D_0 + g_1^a g_2^a \Delta D \left( \frac{t}{a_s^a} \right) \right] \sigma^a \quad \text{For } 0 < t < t_a \quad (2-23)$$

$$\varepsilon_r = g_0^b D_0 \sigma_b + g_1^b \left[ g_2^a \sigma_a \Delta D(\psi) + (g_2^b \sigma_b - g_2^a \sigma_a) \Delta D \left( \frac{t - t_a}{a_s^b} \right) \right] \quad \text{For } t_a < t < t_b \quad (2-24)$$

where

$$\psi = \frac{t_a}{a_s^a} + \frac{t - t_a}{a_s^b}$$

If  $\sigma_b$  is set to zero as in Figure 2.8, then  $g_1^b$  should be equal to 1, and Eq. (2-24)

becomes:

$$\varepsilon_r = g_2^a \sigma_a \Delta D(\psi) - g_2^a \sigma_a \Delta D \left( \frac{t - t_a}{a_s^b} \right) \quad (2-25)$$

The nonlinear viscoelastic subroutine implemented in ABAQUS will be used to calculate the response of the two-step loading and recovery behavior and then compare with the results calculated from Eqs. (2-23) ~ (2-25).

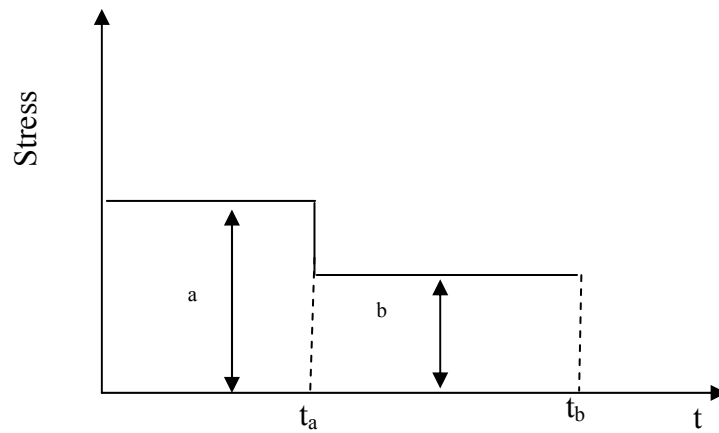


**Figure 2.7** Diagram of Two-Step Loading.

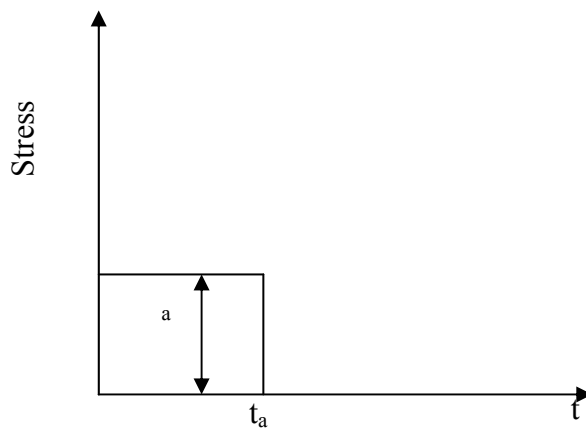


**Figure 2.8** Diagram of One-Step Loading.

The first case in Figure 2.7 will be represented by applying a uniaxial stress of 40 kPa for 1800 sec and then reducing the force to 20 kPa. The second case is for uniaxial stress by applying 40 kPa during 1800 sec and then releasing the force shown in Figure

2.8. The nonlinear parameter  $g_1$  and  $g_2$  are assumed as linear functions of the octahedral stress invariant as shown in Eq. (2-26):

$$\begin{aligned} g_1 &= 1 + 0.00001 * \tau_{oct} \\ g_2 &= 1 + 0.0001 * \tau_{oct} \end{aligned} \quad (2-26)$$

The results from the loading in Figures 2.7 and 2.8 are shown in Figures 2.9 and 2.10, respectively. The results clearly show that the finite element model (FEM) results with the nonlinear material subroutine agree with the results calculated by MSP.

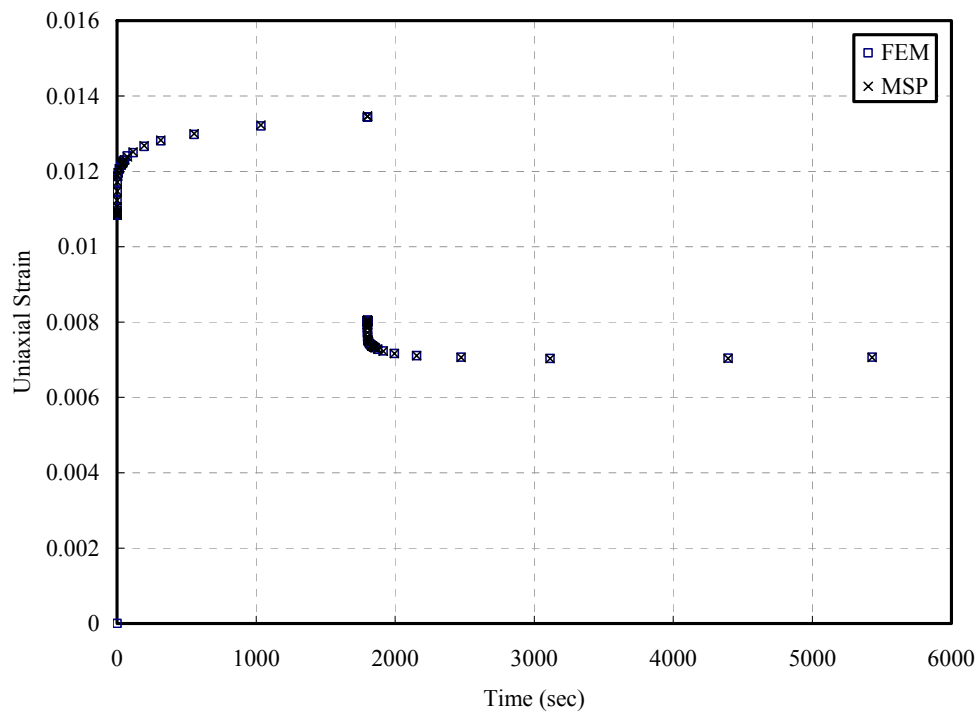


**Figure 2.9** Model Verification Using Two-Step Loading Shown in Figure 2.7.

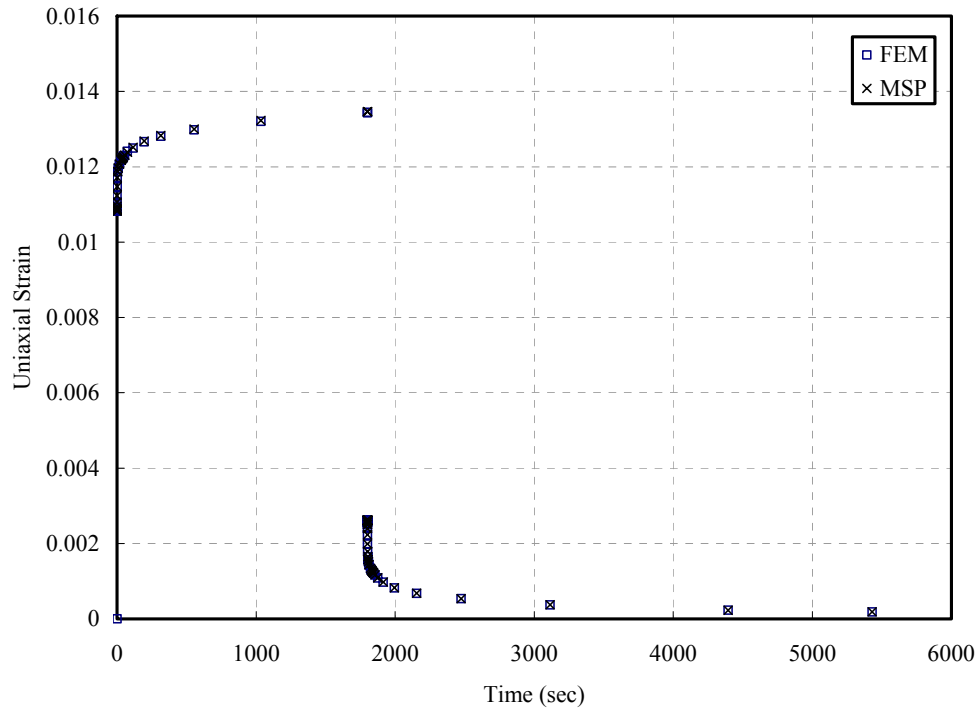


**Figure 2.10** Model Verification Using One-Step Loading Shown in Figure 2.8.

The FE model with the input parameters is used to conduct inverse analysis by comparing the numerical results with the experimental measurements at different temperature and strain-level combinations. The results for the fine mixture are shown in Figures 2.11 to 2.14, while the results for the coarse mixture are shown in Figures 2.15 to 2.18. In general, the numerical results have reasonable agreement with the experimental measurements. The errors in predicting the measured  $J(t)$  values are shown in Table 2.4. The error at the reference condition ( $T = 40^{\circ}\text{C}$  and strain level = 0.01%) is less than 10%, while it increases when the material condition is not at the reference condition. These errors are primarily due to assuming  $a_T$  to be a function of

temperature only irrespective of the strain level. However, as shown in Figures 2.3 and 2.4,  $a_T$  varies as a function of strain level which is not accounted for in the analysis.

**Table 2.4** Percent Difference Between Model Results and Experimental Measurements.

Strain Level	Error in Creep Compliance J(t) (%)							
	Fine Mix				Coarse Mix			
	52°C	46°C	40°C	27°C	52°C	46°C	40°C	27°C
0.01%	8.86	11.31	2.29	15.67	11.18	12.98	7.43	23.92
0.04%	18.71	17.72	12.26	17.98	21.64	11.72	11.86	20.63
0.07%	25.36	17.41	15.94	17.11	29.31	17.37	17.15	21.75
0.1%	26.70	21.20	20.25	20.04	33.72	22.14	20.50	18.62

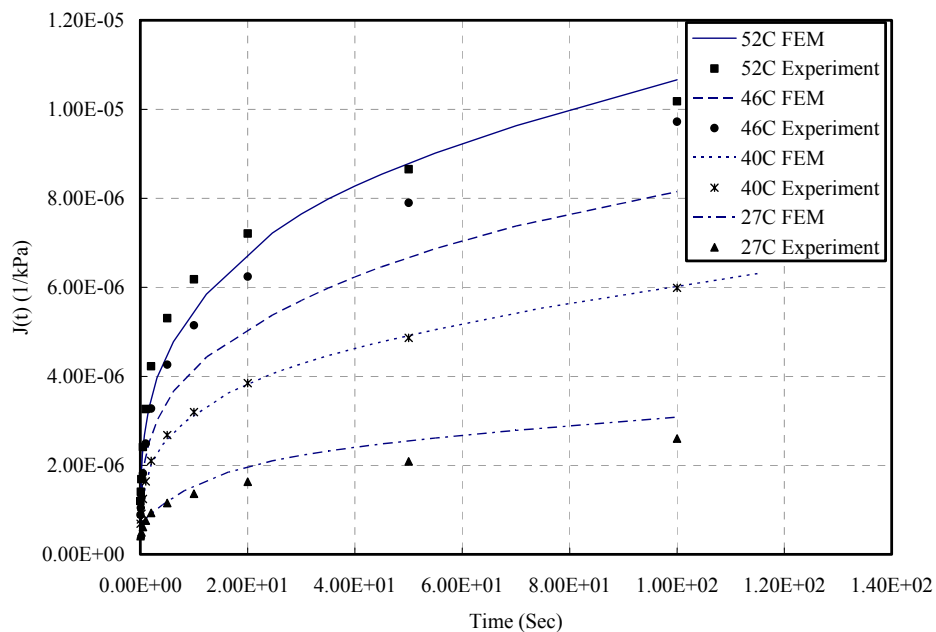


**Figure 2.11** The Verification of Strain Level 0.01% for Fine HMA Mixes.

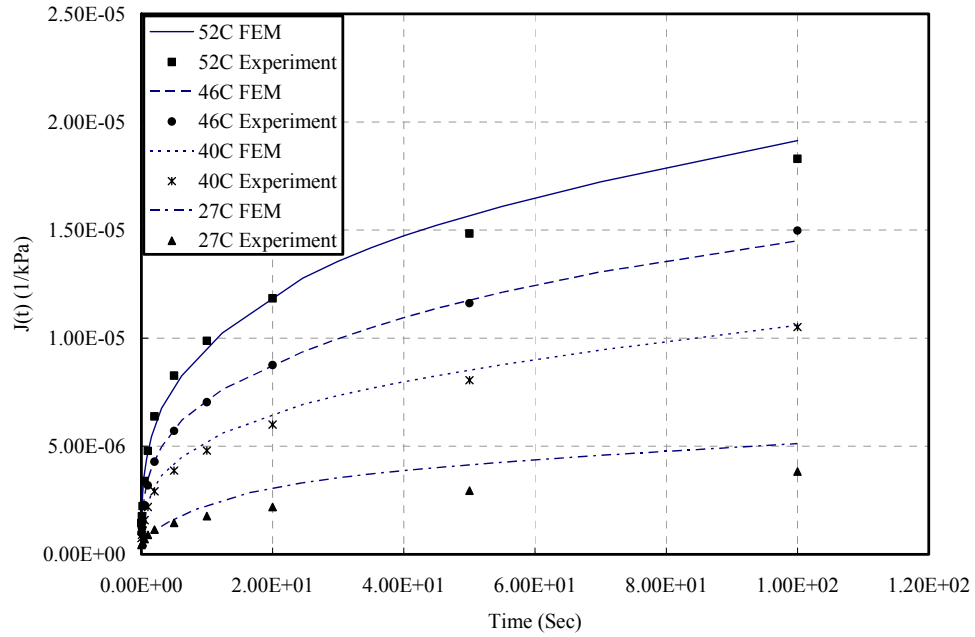


**Figure 2.12** The Verification of Strain Level 0.04% for Fine HMA Mixes.

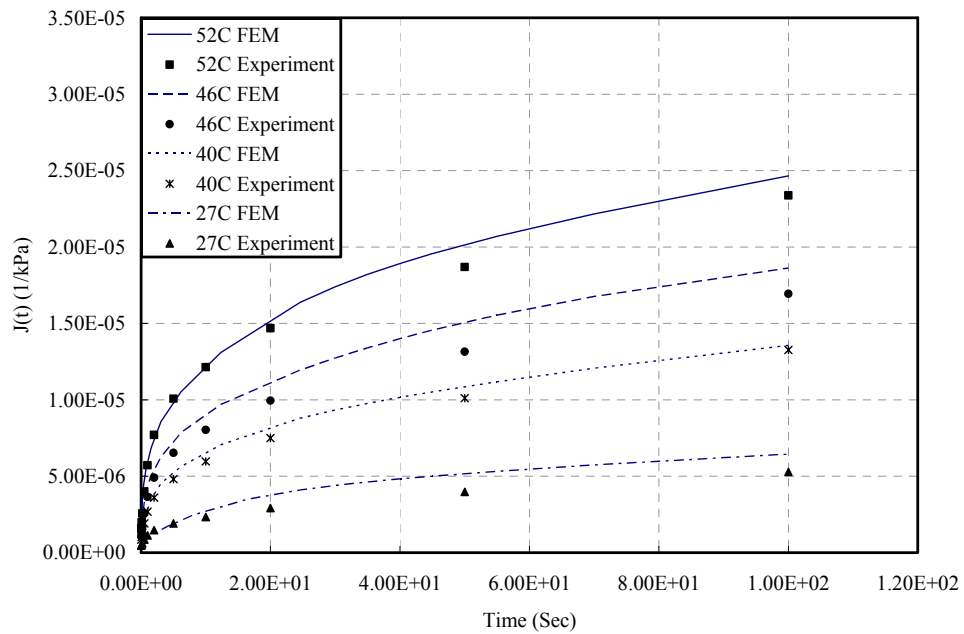


**Figure 2.13** The Verification of Strain Level 0.07% for Fine HMA Mixes.



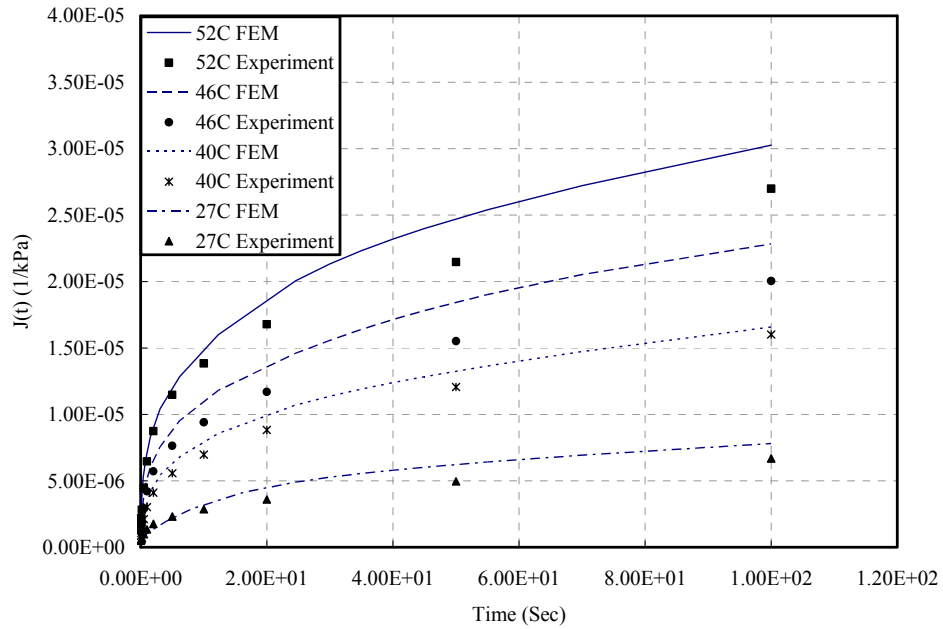


**Figure 2.14** The Verification of Strain Level 0.1% for Fine HMA Mixes.

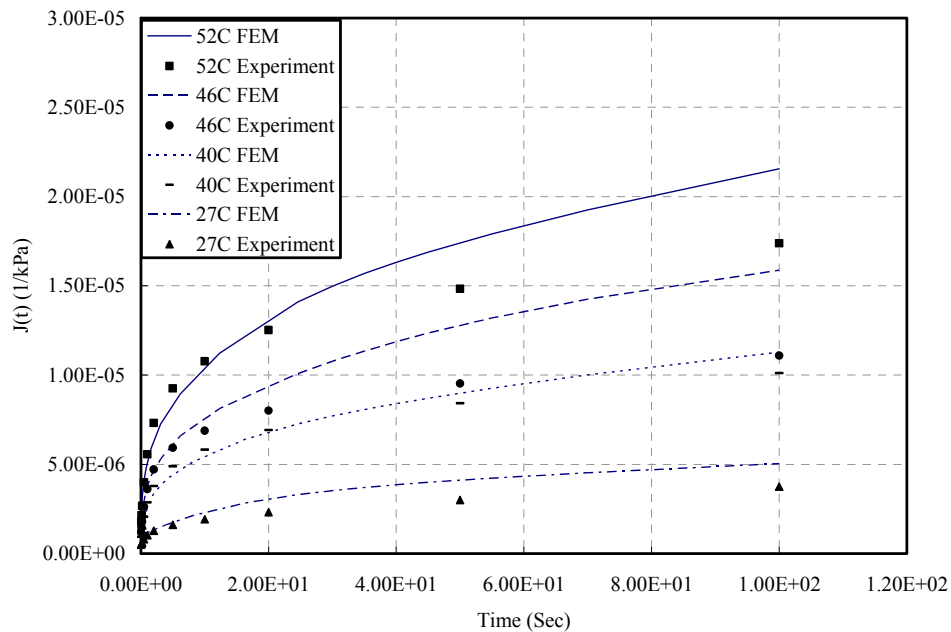


**Figure 2.15** The Verification of Strain Level 0.01% for Coarse HMA Mixes.

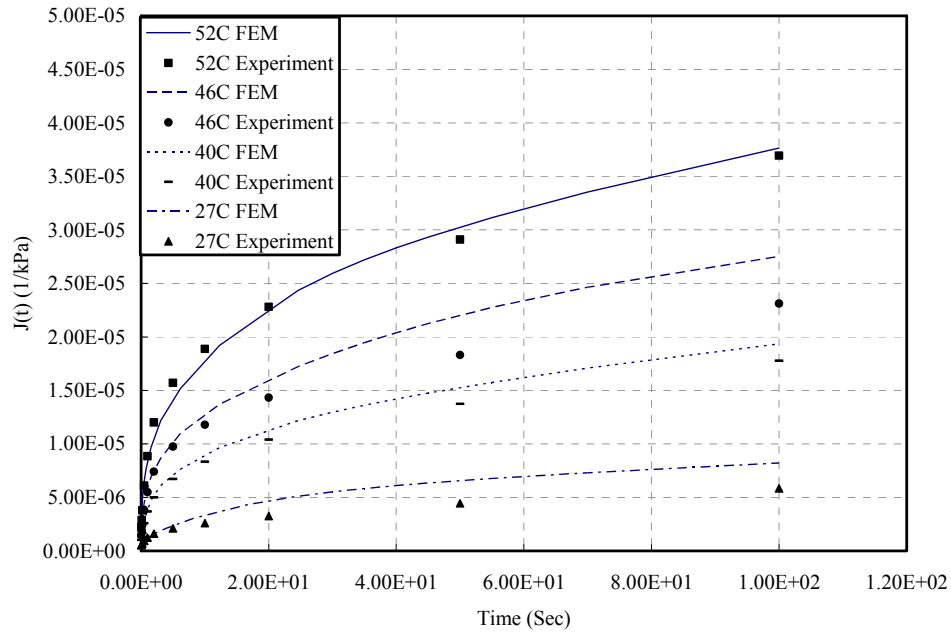


**Figure 2.16** The Verification of Strain Level 0.04% for Coarse HMA Mixes.

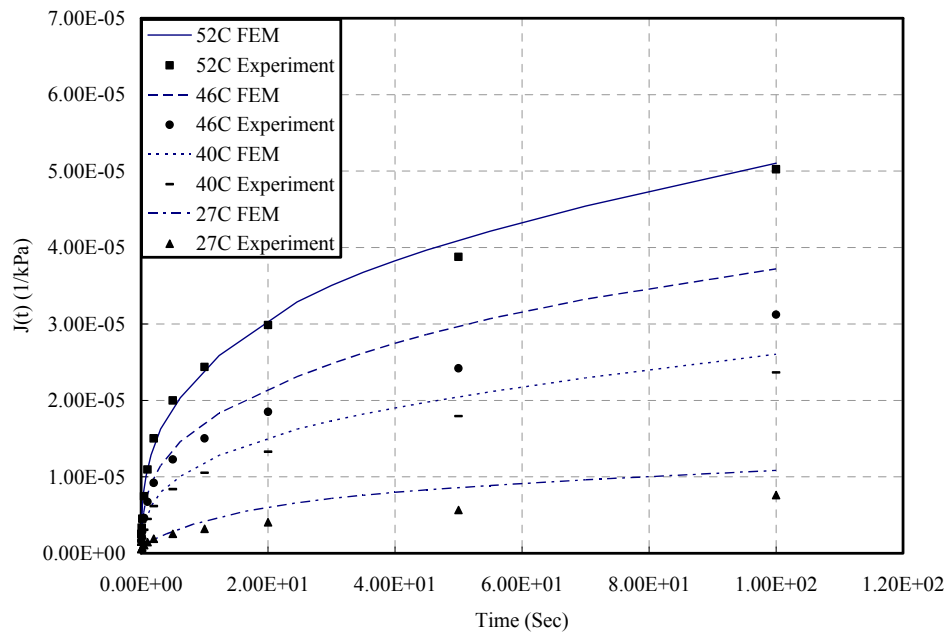


**Figure 2.17** The Verification of Strain Level 0.07% for Coarse HMA Mixes.

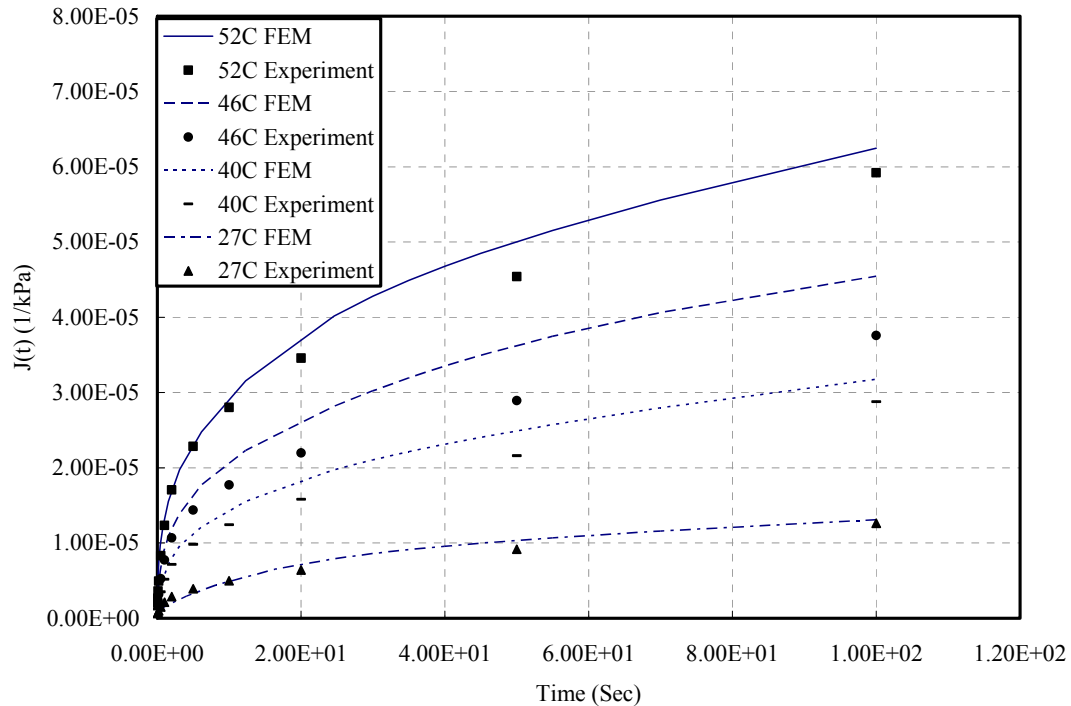


**Figure 2.18** The Verification of Strain Level 0.1% for Coarse HMA Mixes.

## SUMMARY OF FINDINGS

The Schapery nonlinear viscoelastic model parameters were obtained by analyzing the response of two asphalt mixes tested at different temperatures, frequencies, and strain levels. The time-strain shift factors were obtained by shifting the master curves at the different strain levels horizontally to the reference strain 0.01%. The nonlinear parameters were calculated by vertical shifting of the master curves at all strain levels to the same reference strain. The long-term linear viscoelastic coefficients were determined by fitting the Prony series to the data shifted horizontally at the reference strain. The time-temperature shift factors varied slightly as a function of strain

level. However, in order to simplify the analysis, the time-temperature shift factors were averaged for the different strain levels.

The material model was verified by comparing the FE predictions to the closed form solution for creep loading and recovery. Inverse analysis was also conducted, and the results showed that the FE model had reasonable agreement with the experimental measurements at different combinations of temperatures and strain levels. The strain horizontal shifting and nonlinear parameters can be used to predict HMA long-term nonlinear viscoelastic behavior by performing experiments at multiple strain levels and short time intervals.

In this study, the asphalt mix is assumed to exhibit isotropic behavior. The current research of the authors focuses on expanding the model to describe the anisotropic response under various loading and boundary conditions.

**CHAPTER III**  
**NONLINEAR VISCOELASTIC ANALYSIS OF UNAGED AND AGED**  
**ASPHALT BINDERS\***

**OVERVIEW**

This study presents analyses of the nonlinear viscoelastic behavior of unaged and aged asphalt binders tested using a Dynamic Shear Rheometer (DSR) at several temperatures and frequencies. It was not possible to conduct all DSR tests at the same range of stresses, which is necessary for establishing the master curve for nonlinear viscoelastic materials. Therefore, the stress levels for each test, at a given temperature and frequency, were normalized by the ultimate stress level of that test. Consequently, all test results were transformed to a common range of normalized stresses that were used in establishing the master curve.

A phenomenological model was used to obtain the creep response of the binders in the time domain from the normalized frequency domain measurements. Then, the Schapery single integral equation was used to model the binder nonlinear creep response. A master curve at a reference temperature of 30 °C was formed using the time-temperature superposition principle (TTSP) at selected normalized stress levels. The Schapery's nonlinear stress dependent parameters ( $g_1 g_2$ ) were determined by vertical shifting the master curves at the different normalized stress levels. An aging shift factor

---

\* Reprinted with permission from "Nonlinear Viscoelastic Analysis of Unaged and Aged Asphalt Binders" by Eyad Masad, Chien-Wei Huang, Gordon Airey and Anastasia Muliana, 2008. *Construction and Building Materials*, Vol. 22, pp. 2170-2179, Copyright [2008] by Elsevier.

was used to obtain the aged binder response from the properties of the unaged binder. The aging-time shift factor was found to be a function of temperature, but independent of stress level. The nonlinear viscoelastic model was implemented in the ABAQUS finite element (FE) software and used to back calculate the creep response of the unaged and aged binders. The FE results were in very good agreements with the experimental measurements.

## **INTRODUCTION**

Asphalt binders exhibit both linear and nonlinear viscoelastic behavior. The nonlinear viscoelastic properties depend on the stress or strain levels (Ferry, 1961). Cheung and Cebon (1997a, b) indicate that asphalt binders behave linearly at low stress levels and nonlinearly at higher stress levels. Airey et al. (2002 and 2004) conducted stress sweep tests using a DSR to obtain the linearity limits of various asphalt binders at different temperatures. The results showed that the strain dependent linear viscoelastic (LVE) limit is between 2% and 6% at low temperatures and the stress dependent LVE limit is between 1.5 and 7 kPa at high temperatures.

Kose et al. (2000) and Masad and Somadevan (2002) conducted finite element analysis of asphalt mix microstructure, which was modeled as a composite of two phases (asphalt binder and aggregates). The analysis aimed at calculating the strain distribution within the aggregate and binder phases at different macroscopic strain levels applied to the mixture. It was found that the orders of magnitude difference in stiffness between the aggregate and binder phases caused high strain levels to localize within the asphalt

binder. The average binder strain was to be about eight times larger than the macroscopic bulk strain of the mixture, and some parts of the binder phase experienced strain levels within the nonlinear viscoelastic range.

The Schapery's single integral model has been widely used to characterize the nonlinear viscoelastic behavior of engineering materials (Christensen, 1968; Schapery, 1969, and Schapery, 2000). Lou and Schapery (1971) extended the Schapery's integral model to characterize the nonlinear time-dependent behavior of glass fiber reinforced epoxy, while Shield et al. (1998) used Schapery's model to analyze the nonlinear behavior of asphalt mixtures.

Several numerical algorithms that are compatible with finite element analysis have been developed for solving the integral form in the Schapery's viscoelastic model (Touati and Cederbaum, 1997, 1998, and Haj-Ali and Muliana, 2004). Touati and Cederbaum (1997, 1998) presented a numerical scheme and used it to predict the nonlinear stress relaxation of the orthotropic laminated plate. Sadd et al. (2004) implemented Schapery's theory in a recursive finite element scheme to represent the micromechanical behavior of asphalt mixtures. Haj-Ali and Muliana (2004) developed a recursive-iterative integration algorithm to analyze the nonlinear viscoelastic behavior of polymeric materials.

## **OBJECTIVES AND SCOPE OF THE STUDY**

Previous work has shown that asphalt binders exhibit nonlinear viscoelastic behavior especially under high strain levels that binders may experience in the mix.

However, most current binder tests, specifications and mathematical models are developed assuming linear viscoelastic behavior. The objective of this study is to develop a framework for nonlinear viscoelastic analysis of asphalt binders that take into account the possible interactions between stress level, temperature, time of loading (or frequency) and aging. This framework will be useful for researchers and practitioners in describing and comparing the behavior of asphalt binders under various temperatures, aging and loading conditions. It can also be useful to mathematically quantify the influence of binder modification on the model's parameters and binder performance.

This study is organized as follows:

1. Brief presentation of the Schapery's nonlinear viscoelastic model.
2. Description of experimental measurements using DSR on unaged and aged asphalt binders at different stress levels, temperatures, and frequencies.
3. Determination of the parameters of the nonlinear viscoelastic model from the experimental measurements. These parameters include the coefficients of the Prony series that describes the LVE behavior of the binder, nonlinear stress-dependent parameters, and stress, temperature and aging shift factors.
4. Use of a finite element model to simulate the nonlinear viscoelastic behavior of the binders at different temperatures and stress levels.



## THE SCHAPERY'S NONLINEAR VISCOELASTIC MODEL

The strain response of the Schapery's integral form (1969) due to an applied stress  $\sigma^r$  is shown in Eq. (2-1). The reduced time  $\psi^t$  in Eq. (2-1) can be given by:

$$\psi^t = \int_0^t \frac{d\xi}{a_T a_s a_g} \quad (3-1)$$

where,  $a_T$  is the temperature shift factor,  $a_s$  is the strain or stress shift factor, and  $a_g$  is the aging shift factor. The Prony series is used to represent the transient compliance  $\Delta D$  shown in Eq. (2-3).

The three dimensional isotropic constitutive relations can be decoupled into deviatoric and volumetric parts and it can be presented in Eq. (2-4). The deviatoric and volumetric viscoelastic strain components can be expressed in Eq. (2-5) and (2-6), respectively.

Assuming the Poisson's ratio  $\nu$  to be time-independent and using the recursive method, the deviatoric and volumetric strain components can be written in terms of hereditary integral formulation shown in Eqs. (2-8) and (2-9), respectively. The incremental shear and bulk strains are also formulated and used in the finite element implementation, which are shown in Eqs. (2-10) and (2-11), respectively.

This study employs the iterative scheme at material level to correct stress state from the current strain increment. In the iterative scheme algorithm, the residual strain should be defined and the residual strain equation can be shown as Eq. (2-18). The Newton-Raphson typed iterative algorithm is used to minimize the strain residual in Eq. (2-18).

## EXPERIMENTAL MEASUREMENTS AND DATA ANALYSIS

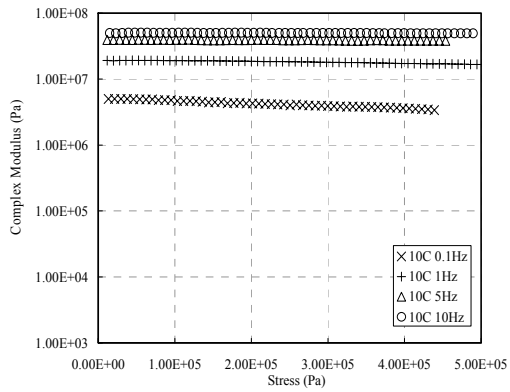
The DSR test was used to characterize the linear and nonlinear viscoelastic parameters of asphalt binders. The test applies a sinusoidal, oscillatory stress to a thin disc of asphalt between two parallel plates. The plate geometries used in this study were 8 mm in diameter with 2 mm testing gap at low temperatures (10, 20 and 30 °C) and 25 mm in diameter with 1 mm testing gap at a high temperature (40 °C). The binder was from a Venezuelan crude source and it was designated as 50 penetration grade according to the British standard BS3690 (penetration of 49 dmm and softening point of 52 °C). Short-term aging was conducted using the standard rolling thin film oven (RTFO) according to the ASTM D 2872 procedure. The unaged binder was tested at temperatures of 10, 20, 30 and 40 °C with frequencies of 0.1, 1, 5 and 10 Hz. The aged binder was tested using temperatures 20, 30, 40 °C and frequencies of 0.1, 1, 5 and 10 Hz. Stress sweeps at each temperature/frequency combination were performed from the minimum torque limit of the DSR to either the maximum torque value or a 30% reduction in complex modulus.

The magnitude of the dynamic complex compliance  $|J^*|$  and phase angle  $\delta$  were obtained from the test at each temperature and frequency. Then, the storage compliance  $J'$  and loss compliance  $J''$  were calculated ( $J' = |J^*| \cos \delta$  and  $J'' = |J^*| \sin \delta$ ). The coefficients of the Prony series of the shear compliance ( $J_n$  and  $\lambda_n$ ) were determined by minimizing the difference between the shear compliance in the constitutive model and the experimental measurements using the error function in Eq. (2-21).

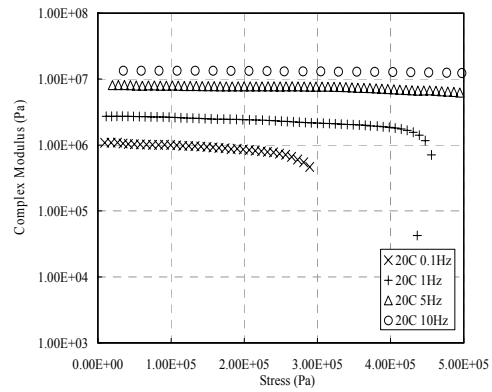
The stress sweep test data for the unaged and aged binders are shown in Figures 3.1 and 3.2, respectively. These two figures show that the range of stress that can be applied on the binder is a function of temperature and frequency. This is considered a limitation for the modeling efforts as the same range of stress levels is needed to establish the master curve of a nonlinear viscoelastic material. In order to overcome this limitation, the stress levels of each test at a given temperature and frequency were normalized by the ultimate stress level of that test. This ultimate stress was determined following the method proposed in a number of studies to determine the maximum stress that an asphalt mix can sustain (Reese 1997, Rowe and Bouldin 2000, Kim 2003). This method relies on plotting the function  $N|G^*|/|G_{mi}^*|$  versus stress level, where  $N$  is the data point number,  $|G^*|$  is the magnitude of the dynamic complex modulus, and  $|G_{mi}^*|$  is the magnitude of the initial dynamic complex modulus for each combination of temperature and frequency. Examples of the data are shown in Figure 3.3. The ultimate stress is selected at the end data point for the cross-annotation data type in Figure 3.3; while the ultimate stress is selected at the peak of the data for the square-annotation data type in Figure 3.3. This normalization causes points at the same distance from the maximum stress for the different test temperatures and frequencies to be represented by the same normalized stress level. The normalized data of the unaged and aged binders are shown as Figures 3.4 and 3.5, respectively.

The analysis was conducted at four different normalized stress levels (0.01, 0.6, 0.8 and 1.0) for both the unaged and aged asphalt binders. In this study, the linear viscoelastic behavior is selected at the lowest normalized stress level of 0.01. The

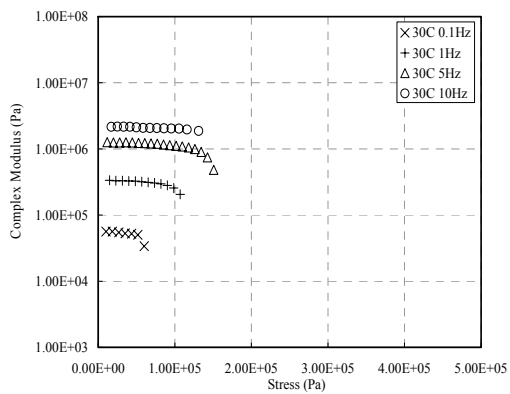
analysis was determined for the unaged binder, and then the behavior of the aged binder was represented using an aging shift factor.



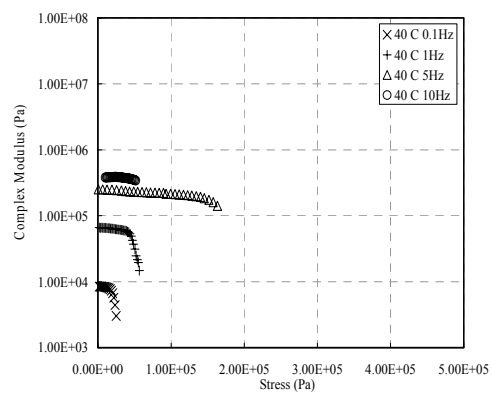
(a) 10 °C



(b) 20 °C

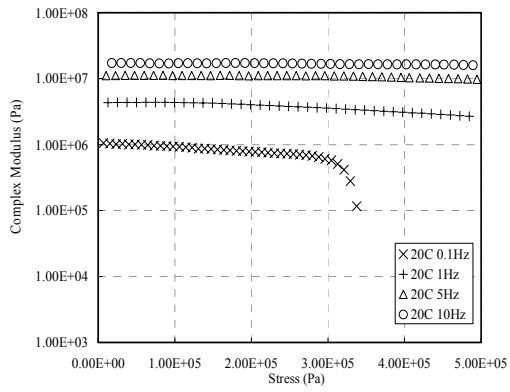


(c) 30 °C

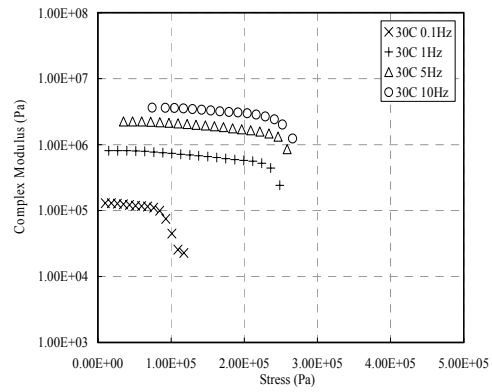


(d) 40 °C

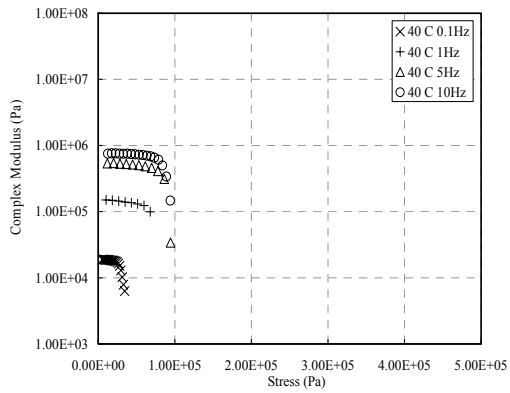
**Figure 3.1** The Stress Sweep Test Data of Unaged Asphalt Binder.



(a) 20 °C



(b) 30 °C



(c) 40 °C

**Figure 3.2** The Stress Sweep Test Data of Aged Asphalt Binder.

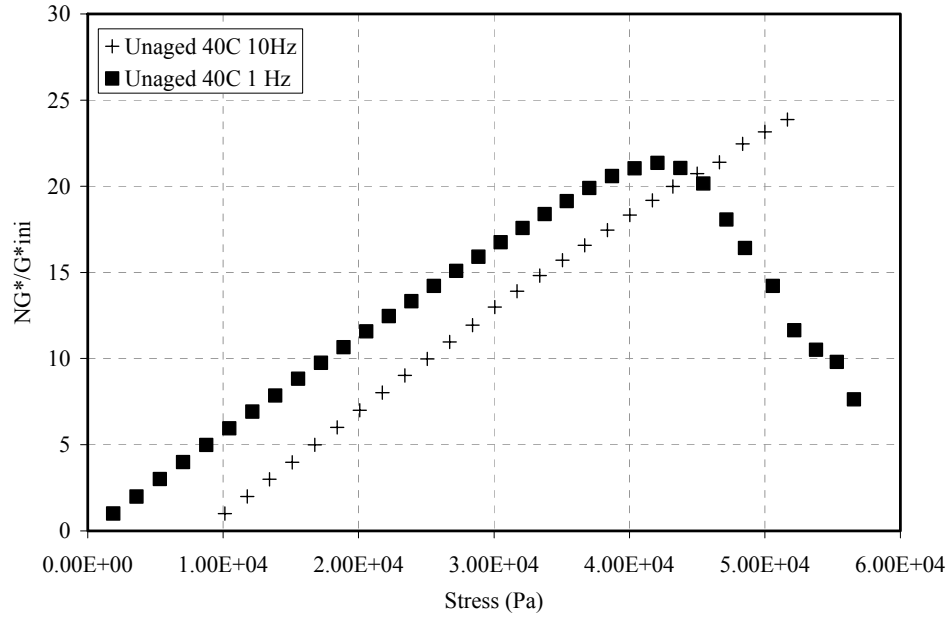
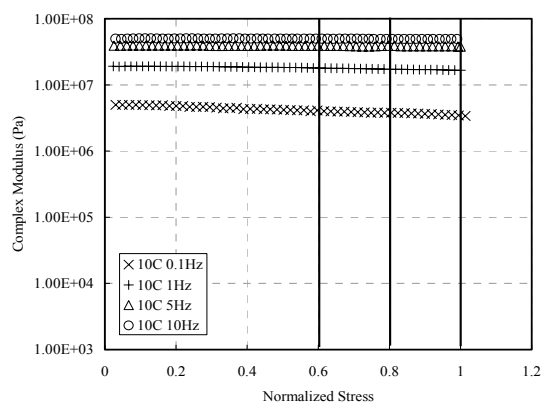
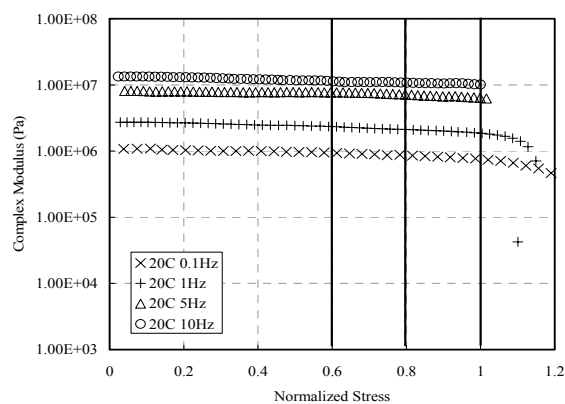


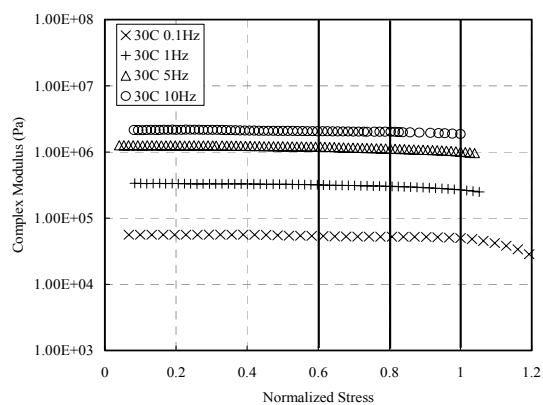
**Figure 3.3** The Relationship Between  $N|G^*|/|G_{ini}^*|$  and Stress.



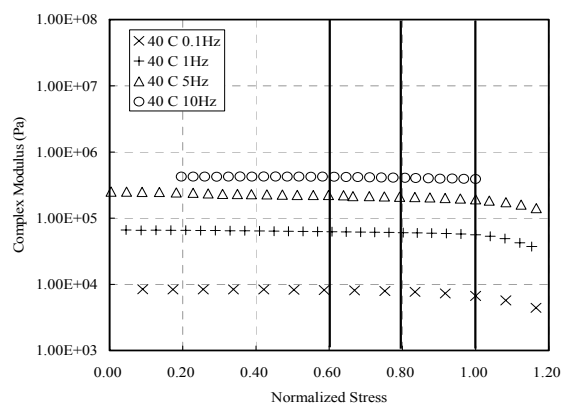
(a) 10°C



(b) 20°C



(c) 30°C



(d) 40°C

**Figure 3.4** The Stress Sweep Test Data of Unaged Asphalt Binder After Normalizing by the Ultimate Stress.

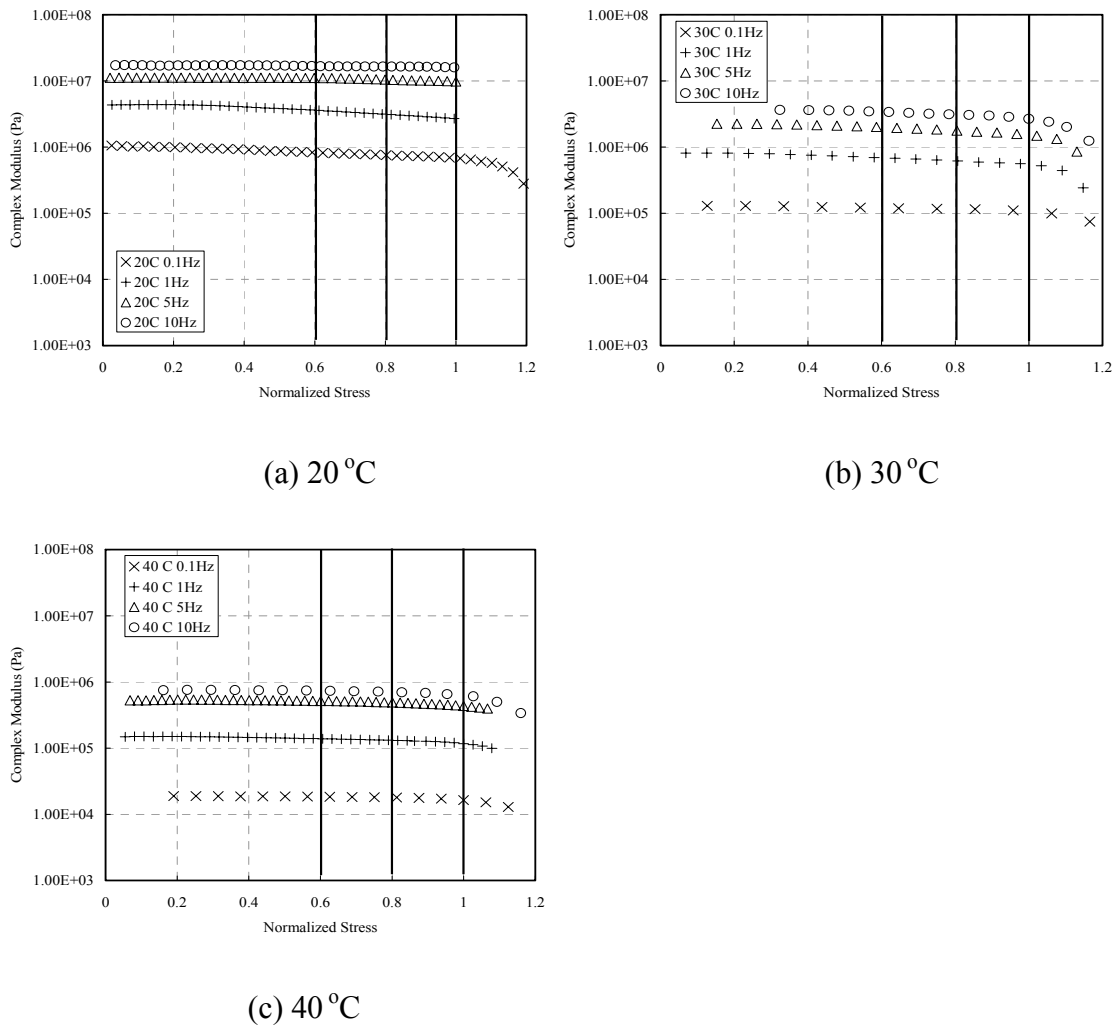


**Figure 3.5** The Stress Sweep Test Data of Aged Asphalt Binder After Normalizing by the Ultimate Stress.

### Time-Temperature Shift

A temperature 30 °C was used as the reference temperature for the unaged binder. The TTSP was used to conduct time-temperature shifting at each normalized stress level. Nonlinear regression using least squares analysis was used in the time-temperature shifting. The relationship between the shift factor  $a_T$  and temperature for different



stress levels is shown in Figure 3.6. These results show that  $a_T$  is independent of stress level; consequently, the  $a_T$  values were averaged for the different stress levels at each temperature as presented in Table 3.1.

**Table 3.1** The Temperature Shift Factor for Each Temperature.

Temp.	$a_T$
10	225.00
20	26.50
30	1.00
40	0.10

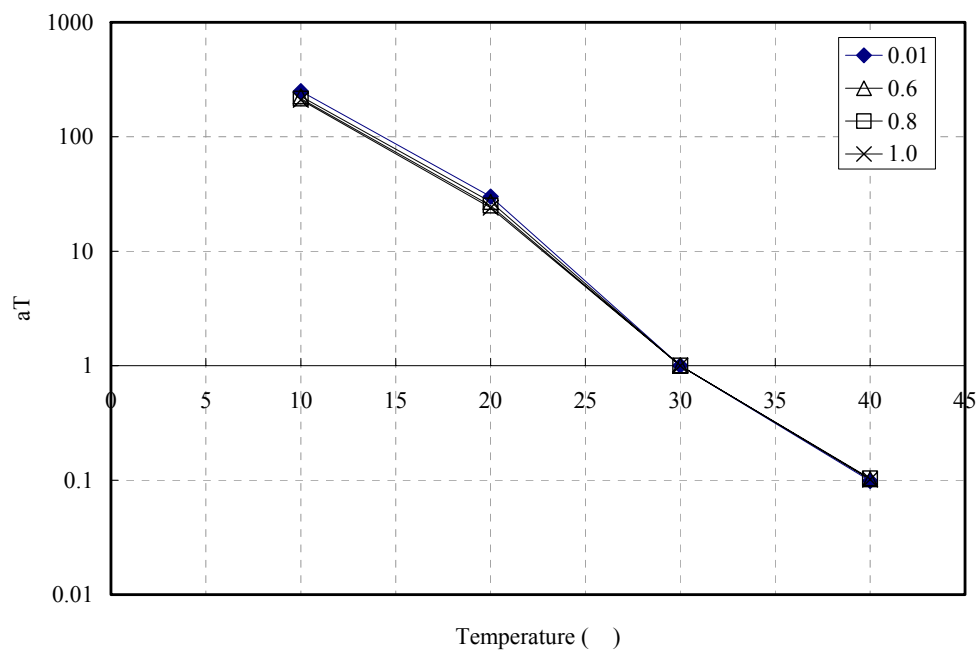


**Figure 3.6** The Relationship Between Temperature Shift Factor ( $a_T$ ) and Temperature.

### Nonlinearity Stress Shift

The nonlinear parameters  $g_1g_2$  were determined by vertically shifting the higher stress master curves to the linear stress level. The results in Figure 3.7 show increasing nonlinear parameters with an increase in stress level; the nonlinear parameters are given in Table 3.2. The experimental data after vertical shifting are shown in Figure 3.8.

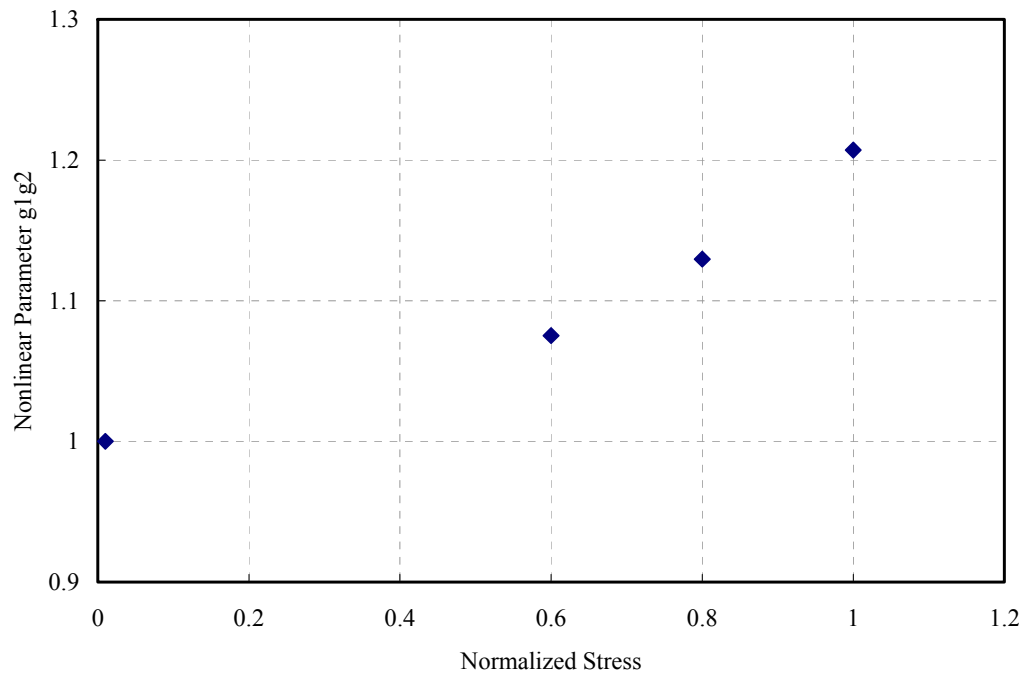
The master curves at different stress levels were shifted horizontally, shown as Figure 3.9, in order to predict the long term behavior of the asphalt binder, and the Prony series was calibrated to fit the long term response of the binder. The stress horizontal shift factors are shown as Table 3.2, and the Prony coefficients are shown in Table 3.3. The Prony series (similar to that in Eq. (3-3)) fitted to the long term response was used in representing the linear viscoelastic response of the binder. The stress horizontal shifting is advantageous as it allows prediction of the linear binder response at longer time periods by performing experiments at stress levels higher than the linear range but at shorter time intervals. The  $g_1g_2$  can be further used to predict the nonlinear response of the asphalt binders at the long term intervals.

**Table 3.2** The Nonlinear Parameters and Stress Shift Factors at Different Stress Levels.

Normalized Stress	$g_1g_2$	$a_s$
0.01	1.00	1.00
0.6	1.08	0.96
0.8	1.13	0.93
1.0	1.21	0.84

**Table 3.3** Linear Viscoelastic Coefficients of the Prony Series.

n	$J_n$	$\lambda_n$
0	3.57E-09	-
1	1.03E-07	18.23
2	2.13E-06	0.25
3	2.71E-08	146.01
4	4.56E-05	0.01
5	8.21E-07	0.88
6	3.16E-07	3.54
7	6.61E-06	0.07
8	4.90E-01	1.71E-06

**Figure 3.7** The Relationship Between Nonlinear Parameter and Normalized Stress Level.

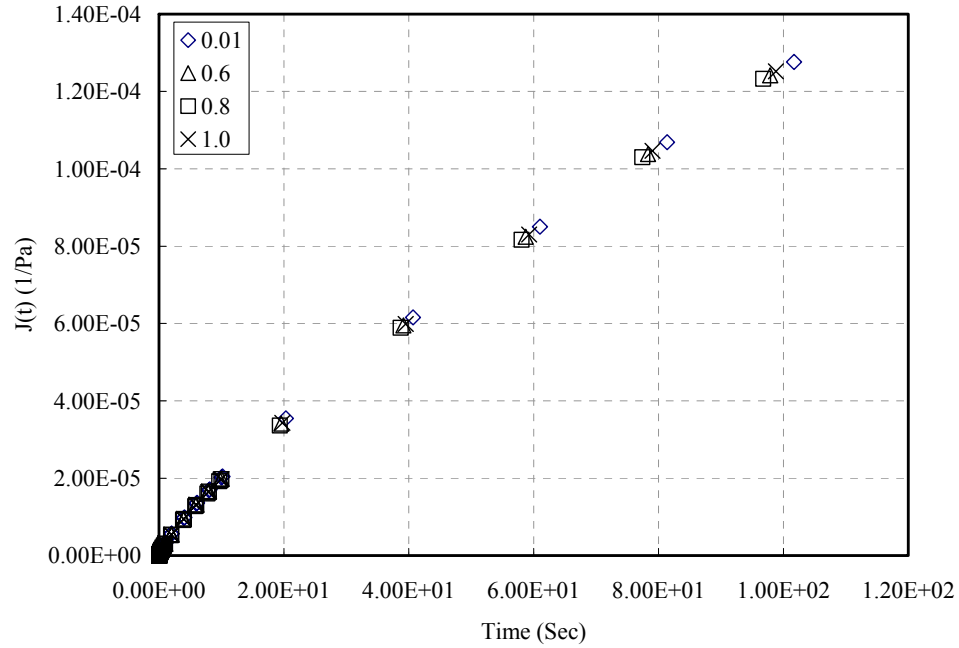


**Figure 3.8** The Master Curve After Stress Vertical Shifting.

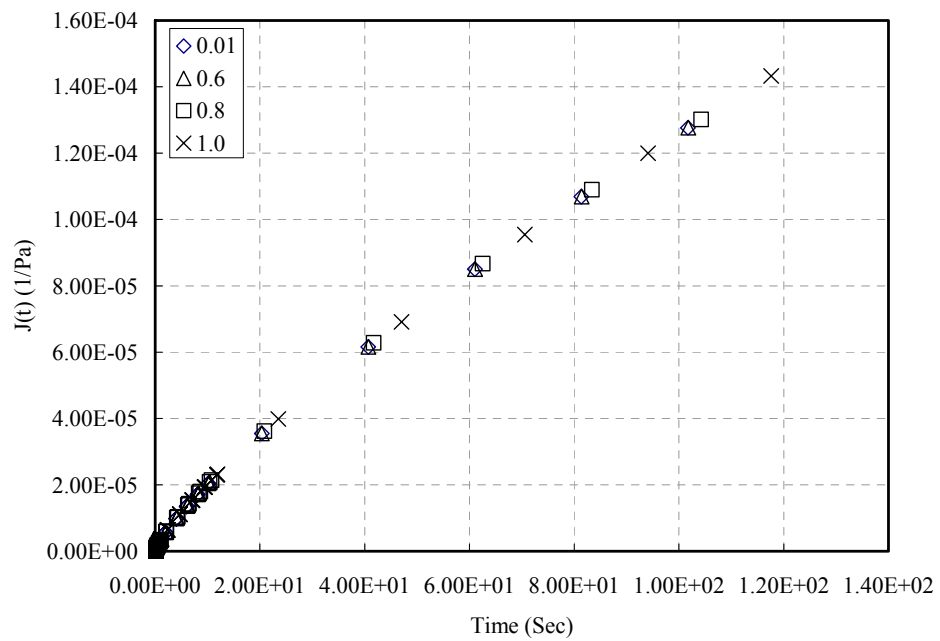


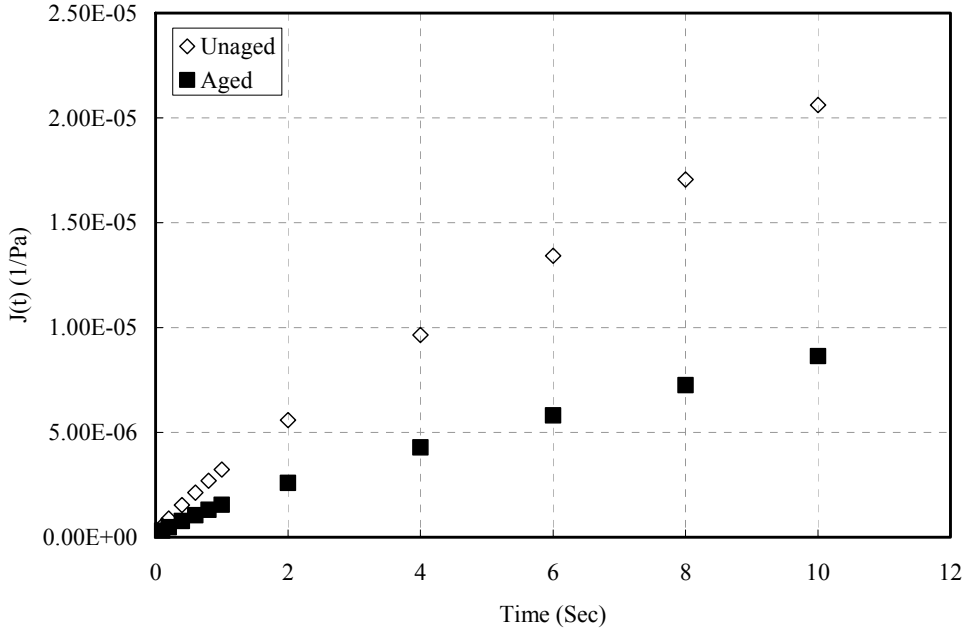
**Figure 3.9** The Master Curve After Stress Horizontal Shifting.

### **Aging Shift**

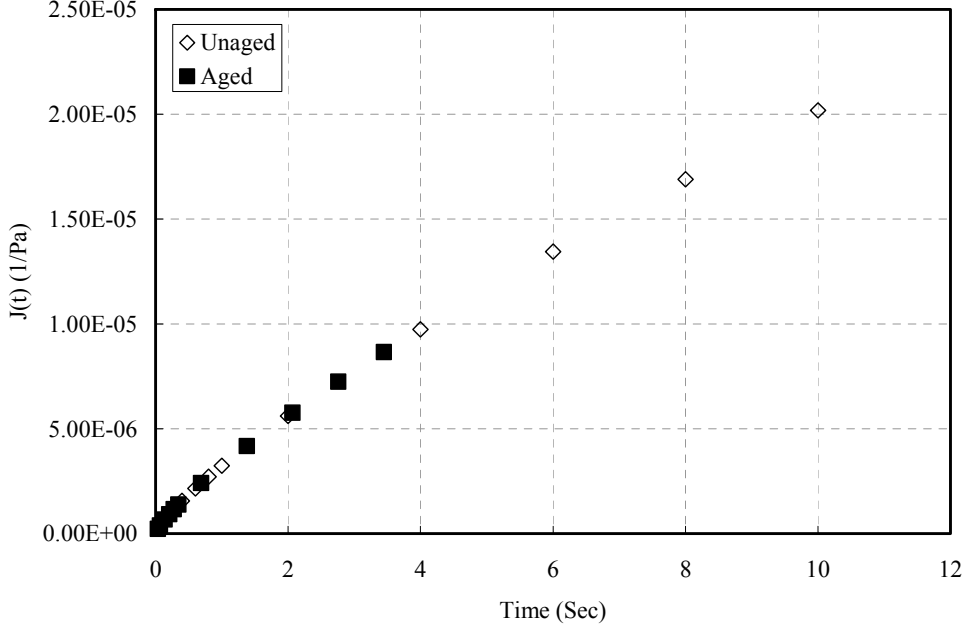
This study obtained the aging shift factor by horizontal shifting the aged asphalt binder data to the unaged asphalt binder data. The aging shift factor was calculated for each temperature and normalized stress levels. Examples of the experimental data before and after aging shifting are shown as Figure 3.10. By evaluating the average and variance in Table 3.4 of the aging shift factor for the different temperatures and stress levels, it can be concluded that the aging shift factor is mostly a function of temperature, while it is almost independent of normalized stress levels. Hence, the average aging shift factor for all stress levels at each given temperature was calculated and used to represent the response of the aged binder. This finding indicates that the behavior of the aged asphalt binder can be obtained by using unaged binder parameters (temperature shift factor, nonlinear parameters, Prony series coefficients) and the aging shift factor for each temperature.

**Table 3.4** The Aging Shift Factor for Each Combination of Temperature and Normalized Stress Levels.

Temp. °C	Aging Shift Factors					
	Normalized Stress				Averaged at Each Temperature	Variance Between Stress Levels
	0.01	0.6	0.8	1.0		
20	1.3	1.15	1.05	1.05	1.14	0.0140
30	2.9	2.6	2.5	2.4	2.60	0.0467
40	2.7	2.7	2.65	2.6	2.66	0.0023
Averaged at Each Stress Level	2.3	2.15	2.07	2.02		
Variance Between Temperatures	0.7600	0.7525	0.7808	0.7108		



(a) Before applying the aging shift factor.



(a) After applying the aging shift factor.

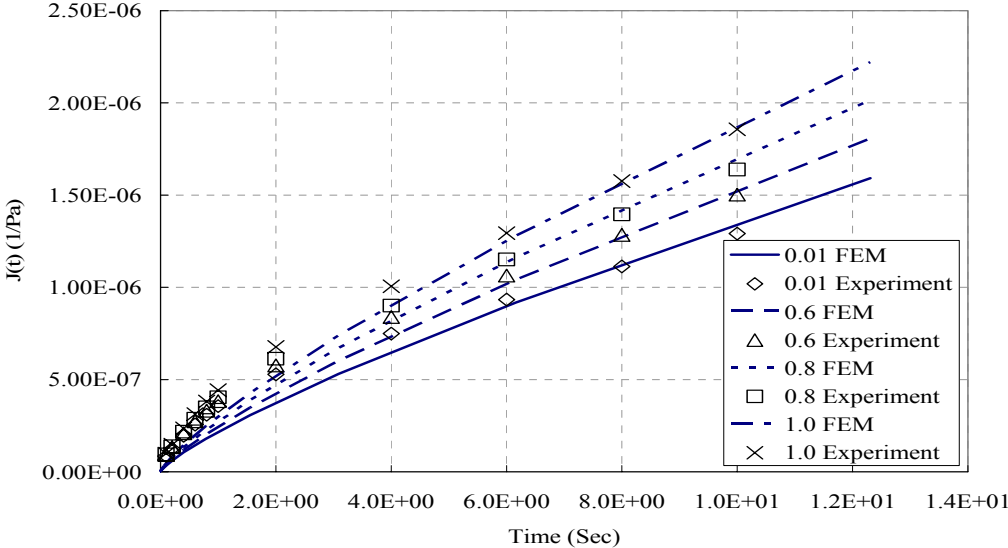
**Figure 3.10** Data Before and After Applying the Aging Shift Factor.

## FINITE ELEMENT ANALYSIS OF BINDER RESPONSE

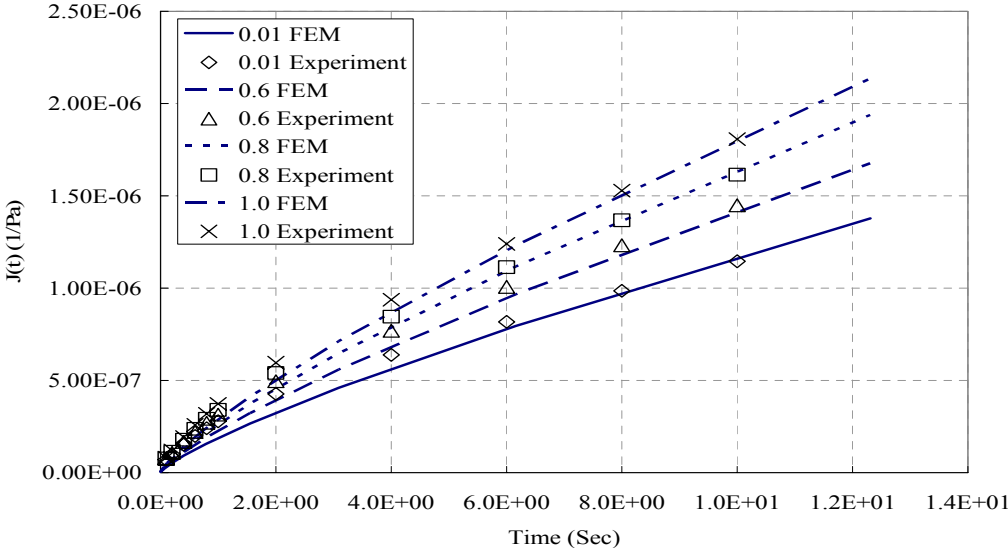
The material parameters of the unaged binder ( $a_T$ ,  $a_s$ ,  $g_1g_2$ , Prony series coefficients of long term response), and the aging shift factors, were used as the input to the finite element subroutine. The finite element analysis was used to calculate the creep response at each of the temperature and normalized stress levels. The model consisted of a three-dimensional element (C3D8R) representing the asphalt specimen subjected to shear creep loading. The deformation and rotation of the nodes in the bottom of the element were fixed, while the different stress levels were applied at the upper face of the element. For brevity, only the results of unaged and aged binders at a temperature of 20°C are shown in Figure 3.11. The results show that the model gives a very good prediction of the experimental measurements. The results in Figure 3.11b indicate that the response of the aged binder can be obtained by simply shifting the data of the unaged binder by the aging factor  $a_g$ .

The Prony series was fitted to the numerical results, and the coefficients of this series were used to determine the binder response in the frequency domain. Consequently, the numerical results in the frequency domain were compared with the DSR experimental data. Examples of the unaged and aged comparisons of  $J'$  and  $J''$  for linear and nonlinear responses are shown in Figures 3.12 and 3.13. In general, the results show that the numerical results are in very good agreement with the experimental measurements for the linear and nonlinear stresses.



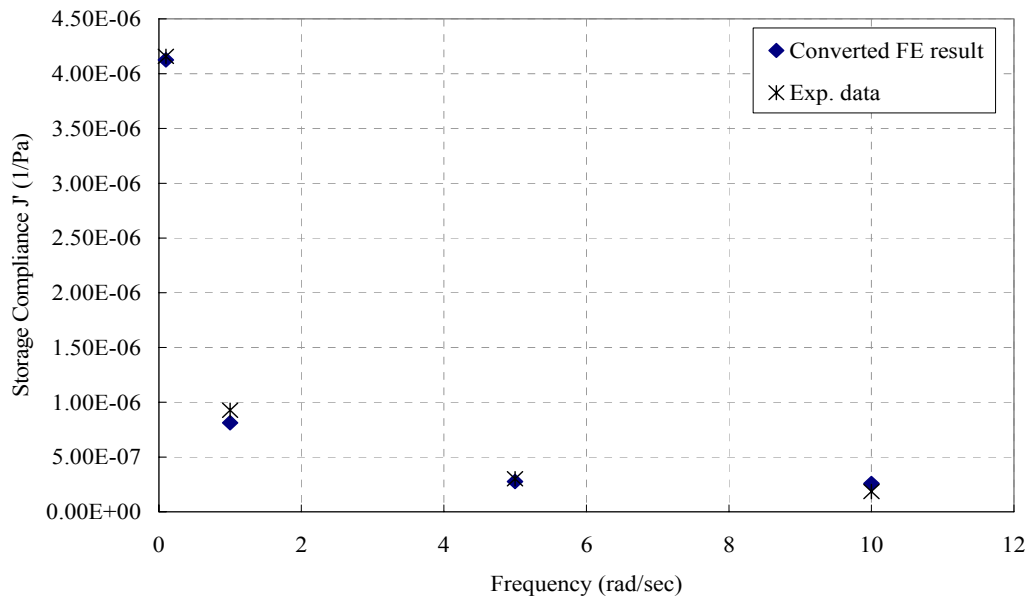
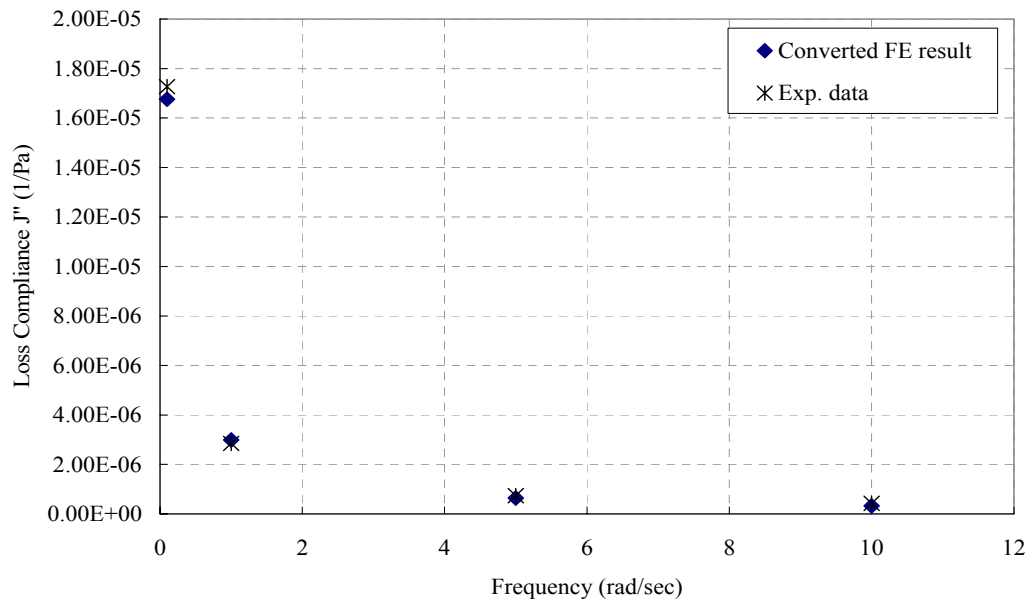


(a) Unaged binder

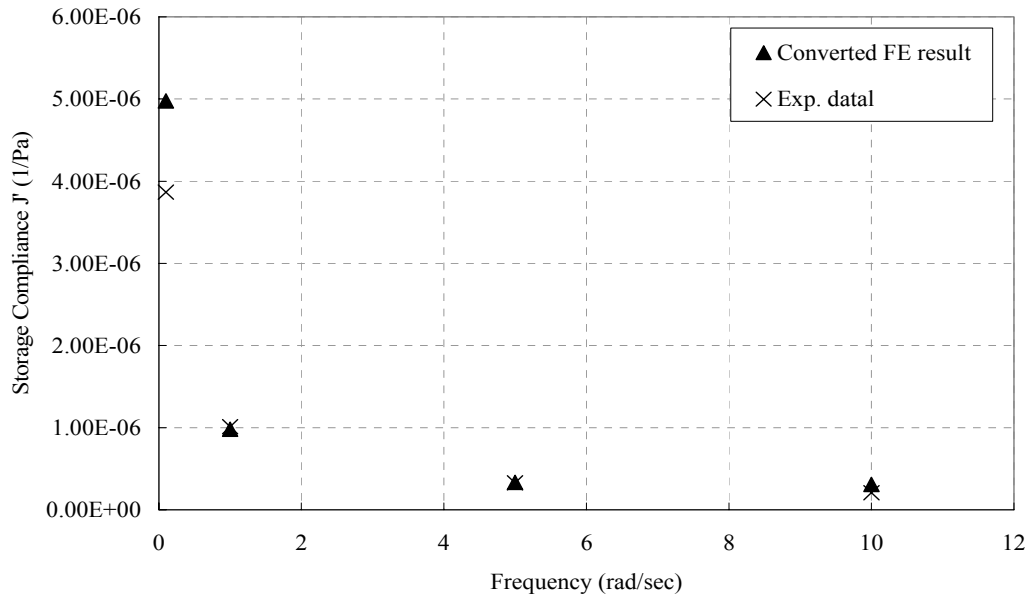
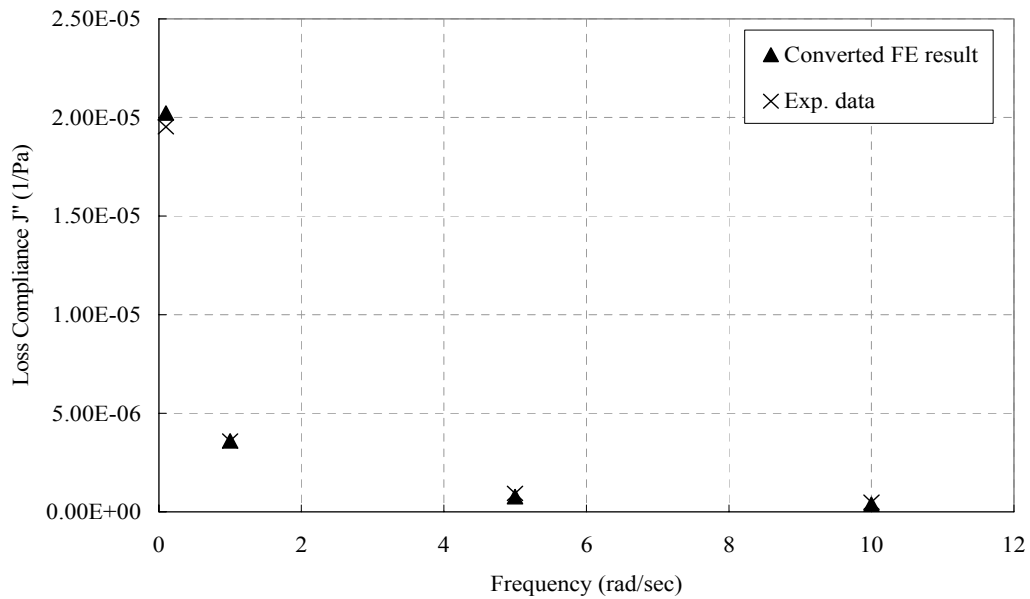


(b) Aged binder

Figure 3.11 Verification of the Finite Element Analysis at a Temperature of 20 °C.

(a) Storage compliance ( $J'$ )(b) Loss compliance ( $J''$ )

**Figure 3.12** Viscoelastic Properties ( $J'$  and  $J''$ ) for Unaged Binder at 30°C and Linear Stress Level (Normalized Stress of 0.01).

(a) Storage compliance ( $J'$ )(b) Loss compliance ( $J''$ )

**Figure 3.13** Viscoelastic Properties ( $J'$  and  $J''$ ) for Unaged Binder at 30 °C and Nonlinear Stress Level (Normalized Stress of 1).

## CONCLUSIONS

This study presents a framework for the analysis of the nonlinear viscoelastic behavior of unaged and aged asphalt binders at different temperatures and stresses. Due to the influence of test temperatures on the stress levels that the binder can sustain prior to failure, the experimental measurements do not have a common range of stress levels that can be used in developing the master curve of nonlinear viscoelastic materials. This limitation was overcome by introducing the normalized stress concept in which the stress values of each test at a given temperature and frequency were normalized by the ultimate stress of that test. The response at the actual stress is obtained by dividing the actual stress by the ultimate stress and using the normalized stress in the model.

The data at the different stress levels were shifted horizontally to obtain the long term response of the binder. This means that the long term response of the binder can be obtained by conducting short term tests at multiple stress levels. The nonlinear response of the binder is determined by vertical shifting between the nonlinear stresses and the linear stress. The advantages of the analysis approach can be realized in providing a mathematical framework for describing the nonlinear response of asphalt binders, and in the possibility of describing the behavior of aged binders by using the unaged binder parameters ( $a_T, a_s, g_1, g_2$ , Prony series coefficients of long term response) and aging shift factors.

The analysis conducted on this study was limited to only one asphalt binder source. It is necessary to evaluate the applicability of the analysis method for more asphalt binders that exhibit different properties from different sources. Specifically,

chemically modified binders need to be examined in order to determine the applicability of the aging shifting factors to these binders.

**CHAPTER IV**

**CHARACTERIZATION OF ASPHALT BINDER RESISTANCE TO  
PERMANENT DEFORMATION BASED ON NONLINEAR VISCOELASTIC  
ANALYSIS OF MULTIPLE STRESS CREEP RECOVERY (MSCR) TEST**

**OVERVIEW**

A significant emphasis has been placed in the asphalt community on development of a method to characterize the resistance of asphalt binders to permanent deformation. The multiple stress creep recovery (MSCR) test has been proposed as a means of accomplishing this objective. In this test, an asphalt binder is subjected to creep loading at different stress levels with recovery (unloading) periods between stresses. The current analysis method of the MSCR test uses the strain accumulated at the end of the test to derive an index describing the resistance of asphalt binders to permanent deformation. However, the accumulated strain is not due only to permanent strain; some of this accumulated strain is viscoelastic strain that might not fully recover depending on the duration of the unloading period. In order to ensure that asphalt binders are characterized based on the actual permanent strain at the end of the test, a method to separate the actual permanent strain (irrecoverable) from the viscoelastic strain (recoverable with time) is needed.

The challenge in separating the recoverable and irrecoverable components is that these two components occur simultaneously during loading, and the recoverable component can exhibit nonlinear behavior. This study presents an analytical method to

analyze the MSCR test results and determine the actual irrecoverable and nonlinear recoverable response. Subsequently, the irrecoverable strain is used to develop an index by which to evaluate the resistance of asphalt binders to permanent deformation. The analytical approach is corroborated by analyzing asphalt binders that have been used as part of the Accelerated Loading Facility (ALF) experiment of the Federal Highway Administration (FHWA). The new permanent deformation index shows excellent correlation with the performance of the asphalt binders in the ALF experiment.

## **INTRODUCTION**

In this study, the response of an asphalt binder is characterized by three components. The first is the instantaneous elastic component, the second is the viscoelastic component (or delayed elastic) that is fully recovered provided that sufficient unloading time is allowed, and the third is the permanent or viscous component. These three components can exhibit linear or nonlinear behavior.

The Superpave method for characterizing the resistance of asphalt binders to permanent deformation is based on linear viscoelasticity theory. In this method, a permanent deformation index is derived to quantify the energy dissipation due to combined viscoelastic (delayed elastic) and viscous deformation. Asphalt linear viscoelastic properties are measured during small oscillatory stress or strain testing modes. However, experimental results have clearly shown that these properties are not sufficient to describe the performance of modified asphalt binders (Bahia et al. 2001, D'Angelo et al., 2007). These studies have emphasized the need to characterize asphalt

binders based on tests and analysis methods that are capable of capturing permanent deformation after cycles of creep and recovery.

Bahia et al. (2001) recommended the repeated creep recovery test (RCRT) using the Dynamic Shear Rheometer (DSR) to test asphalt binders. This test applies one creep stress level for 1.0 second and then removes the stress for 9.0 seconds. A linear viscoelastic model is fit to the data in order to derive a parameter to characterize the accumulated strain after applying a certain number of cycles. This parameter is the viscosity of a linear dashpot representation of Newton viscous deformation.

Recently, D'Angelo et al. (2007) recommended the use of the multiple stress creep recovery (MSCR) test to measure the stress dependency of asphalt binder response. This test applies several stress levels with 10 loading-recovery cycles for each stress level. The stress is applied for 1.0 second followed by a 9.0 second recovery within each cycle. The analysis method of the MSCR test is based on calculating what is referred to as the non-recoverable compliance  $J_{nr}$ , which is equal to the maximum accumulated strain at the end of the test divided by the maximum stress level applied to the binder. This method does not restrict the analysis to a linear viscoelastic response; however, it considers all the accumulated strain at the end of the test to be irrecoverable. In reality, some of this accumulated strain could be recovered depending on the loading and unloading time durations.

The MSCR test provides valuable data regarding the stress dependency of the binder. However, there is a need to analyze the MSCR results using an approach that can separate the viscoelastic (recoverable) and permanent (irrecoverable) strain



components without imposing the assumption of linear material behavior. This study offers a new method by which to separate of the permanent and nonlinear viscoelastic components. This method uses Schapery's single integral model to describe the nonlinear viscoelastic behavior of asphalt binders (Christensen, 1968; Schapery, 1969, and Schapery, 2000).

### **OBJECTIVES AND TASKS**

The primary objective of this study was to develop a method to analyze the MSCR binder test results and propose an index to characterize the resistance of asphalt binders to permanent deformation. This objective is achieved through the following six tasks:

1. Conduct the MSCR test on binders with similar high temperature performance grades (PG) and binders that have been tested as part of mixtures in the Accelerated Loading Facility (ALF) experiment of the Federal Highway Administration (FHWA).
2. Develop a method to analyze and model the viscoelastic (recoverable) and permanent (irrecoverable) strain components.
3. Compare the permanent strain of binders that have similar high temperature PG grades.
4. Examine the ability of the viscosity parameter of a linear dashpot viscous to describe the permanent deformation of asphalt binders.

5. Examine the nonlinear response of binders and its implications in understanding their behavior.
6. Propose a new index based on the actual permanent strain and compare the new index to the recorded permanent deformation of ALF mixtures.

## **EXPERIMENTAL MEASUREMENTS**

The MSCR test involves applying 11 shear stress levels (25, 50, 100, 200, 400, 800, 1600, 3200, 6400, 12800, and 25600 Pa) using DSR. Ten loading-unloading cycles are applied at each stress level. The test applies step shear loading where one load cycle is comprised of 1.0 second of loading followed by 9.0 seconds of unloading. No additional rest periods are applied between different stress levels.

In the first part of this study, four modified binders (PG 70-22, PG 70-28, PG 76-22, and PG 76-28) were each tested at four temperatures (58 °C, 64 °C, 70 °C, and 76 °C). The data were analyzed using the new method described in the following section in order to compare the results with the current PG grades determined using the current Superpave method.

The second part of the study involved analyzing the results of testing five ALF binders (Air Blown PG 71-28, SBS PG 71-38, ELVALOY PG 76-30, Control PG 73-23, and SBSLG PG 74-28) at a temperature of 64 °C. These ALF binder results were compared with permanent deformation data of ALF asphalt mixtures.

The ALF test is a full-scalar pavement test. In the ALF test, a super-single tire applies a load of 45 kN at a travel speed 19 km/hr over a 10 m tested section. Testing

was conducted at a temperature of 64 °C (D' Angelo et al., 2007, and Stuart, K. et al., 1999).

### **NONLINEAR PLASTO-VISCOELASTIC ANALYSIS PROCEDURE**

The response of asphalt binders subjected to an applied stress includes recoverable and irrecoverable strain components, which can be described as shown in Eq.

(4-1):

$$\varepsilon^{total} = \varepsilon^{rec} + \varepsilon^{irrec} \quad (4-1)$$

where  $\varepsilon^{rec}$  is the recoverable strain and  $\varepsilon^{irrec}$  is the irrecoverable strain. The recoverable strain component can be instantaneous (elastic) or time-dependent (viscoelastic).

A number of studies have shown that asphalt binders could exhibit nonlinear viscoelastic behavior (Airey et al., 2002, 2004; Touati and Cederbaum, 1997, 1998). This nonlinear response is caused by the high strains developed in asphalt binders within the asphalt mix (Masad and Somadevan, 2002). Schapery's nonlinear viscoelastic model is employed in this study to represent the nonlinear recoverable strain component (Schapery, 1969). The recoverable strain under a constant applied stress  $\sigma$  can be expressed as in Eq. (2-1).

The effects of Schapery nonlinear parameters are shown in Figures 4.1 to 4.3. Figure 4.1 shows the effect of  $g_0$ , which shifts the creep strain vertically with an increase in  $g_0$ , but it does not affect the transient behavior nor does it affect the material response during unloading. The nonlinear parameters  $g_1$  and  $g_2$  dominate the nonlinearity of the transient portion. Figures 4.2 and 4.3 represent that the material

response during loading is controlled by both  $g_1$  and  $g_2$ , while only  $g_2$  determines the material behavior during unloading. The loading and unloading strain increases with an increase in the nonlinear parameters  $g_1$  and  $g_2$ .

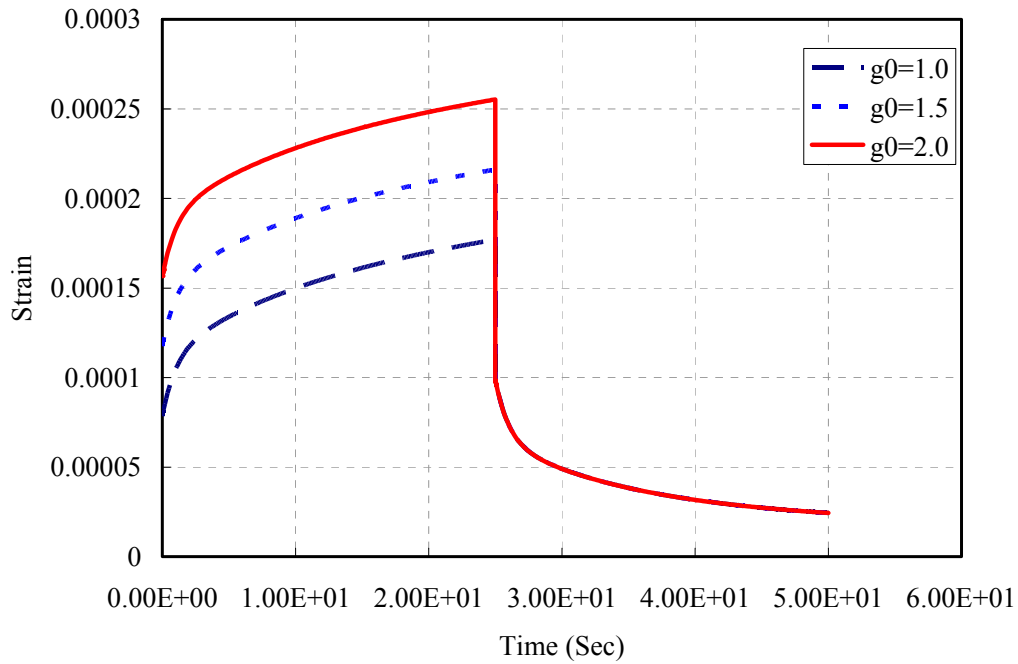


**Figure 4.1** The Effect of Nonlinear Parameter  $g_0$ .

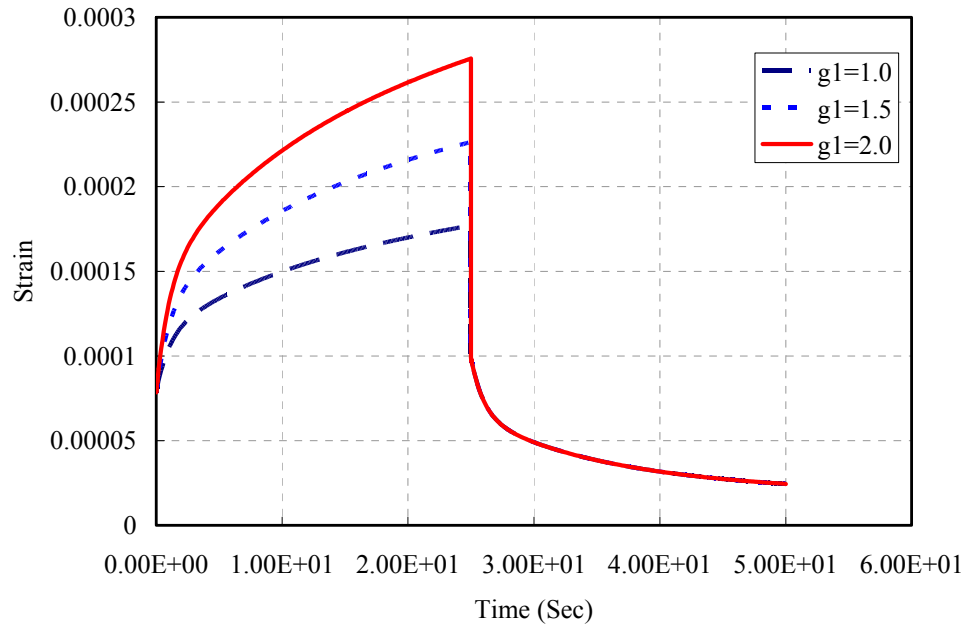


**Figure 4.2** The Effect of Nonlinear Parameter  $g_1$ .

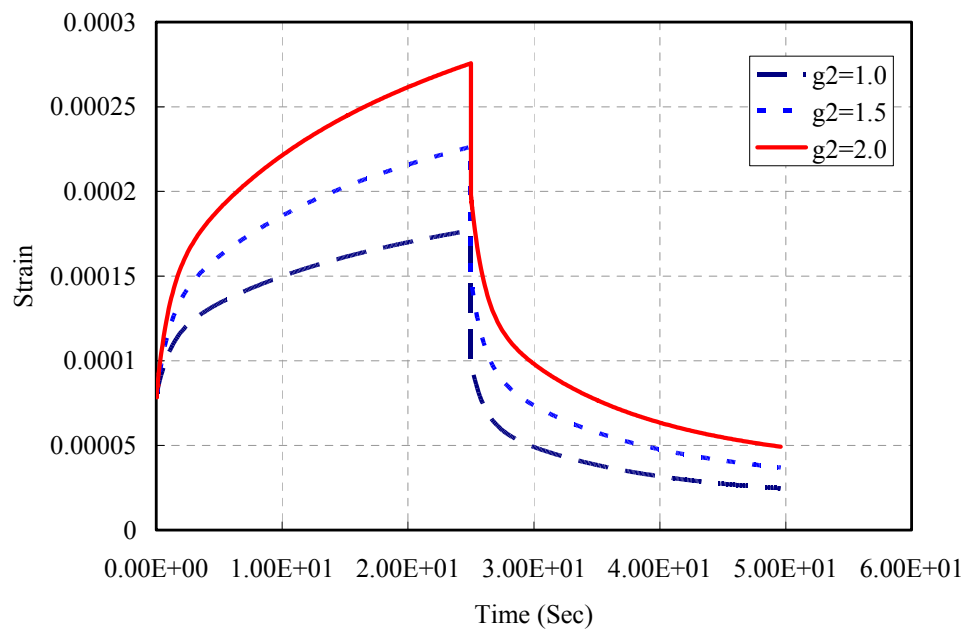


**Figure 4.3** The Effect of Nonlinear Parameter  $g_2$ .

In this study, the entire recoverable strain component is assumed to be time-dependent ( $D_0 = 0$ ). This was motivated by the experimental observation that it is very difficult to select the time at which the response could be considered to be instantaneous at the high temperatures used in this study. In addition, the analysis has revealed that the transient part of the compliance (the second part on the right of Eq. [2-1]) is sufficient to describe the entire recoverable response of asphalt binders.

In Eq. (2-1), the transient linear compliance  $\Delta D$  can be represented by a Prony series as shown in Eq. (2-2).

A schematic of binder creep loading and recovery is shown in Figure 4.4. The recoverable strain components during loading and recovery (unloading) in the first cycle are given in Eqs. (4-2) and (4-3), respectively:

$$\varepsilon_1^c(t) = g_1^1 g_2^1 \sigma_1 \Delta D(t) + \varepsilon^{irrec}(t) \quad (4-2)$$

$$\varepsilon_1^r(t) = \left[ g_2^1 \sigma_1 \Delta D(t) - g_2^1 \sigma_1 \Delta D(t - t_a) \right] + \varepsilon^{irrec}(t_a) \quad (4-3)$$

where the superscript of nonlinear parameters is the loading cycle number, and the subscript of stress and strain components presents the loading cycle number. The expressions  $\varepsilon^c$  and  $\varepsilon^r$  are the total strain during loading and unloading, respectively. The term  $t_a$  is the loading time as shown in Figure 4.4.

The first step of this analysis procedure is to obtain the coefficients of the Prony series that describe the linear transient compliance (Eq. [2-2]). These coefficients were obtained by analyzing the binder response during the first loading cycle of the lowest stress level ( $g_1^1 = g_2^1 = 1$ ), which in this study is at a stress level of 25 Pa. The

irrecoverable strain is constant once the load is removed at  $t = t_a$  as is illustrated in Figure 4.4. Therefore, the recoverable strain  $\Delta\varepsilon_1^{r1}$  between  $t_a$  and  $t_b$ , shown in Figure 4.4, is used to obtain the coefficients of the linear transient compliance. The expression for  $\Delta\varepsilon_1^{r1}$  is shown in Eq. (4-4), which can be derived from Eqs. (4-2) and (4-3) and by substituting Eq. (2-1) in these two equations. The Prony series coefficients ( $D_n$  and  $\lambda_n$ ) are obtained by minimizing the error between the measurements of  $\Delta\varepsilon_1^{r1}$  and Eq. (4-4).

$$\begin{aligned} \Delta\varepsilon_1^{r1}(t) &= \varepsilon_1^c(t_a) - \varepsilon_1^r(t) \\ &= \sigma_1 \left\{ \begin{aligned} &\sum_{n=1}^N D_n [1 - \exp(-\lambda_n t_a)] - \\ &\sum_{n=1}^N D_n [1 - \exp(-\lambda_n t)] + \sum_{n=1}^N D_n [1 - \exp(-\lambda_n (t - t_a))] \end{aligned} \right\} \end{aligned} \quad (4-4)$$

By applying the modified superposition principle (MSP) of the nonlinear response for the second loading cycle, the recoverable strain components during loading and unloading are obtained as shown in Eqs. (4-5) and (4-6), respectively:

$$\varepsilon_2^c(t) = g_1^2 \left[ g_2^1 \sigma_1 \Delta D(t) - g_2^1 \sigma_1 \Delta D(t - t_a) + (g_2^2 \sigma_2) \Delta D(t - t_b) \right] + \varepsilon^{irrec}(t) \quad (4-5)$$

$$\varepsilon_2^r(t) = \left[ \begin{aligned} &g_2^1 \sigma_1 \Delta D(t) - g_2^1 \sigma_1 \Delta D(t - t_a) + \\ &(g_2^2 \sigma_2) \Delta D(t - t_b) - g_2^2 \sigma_2 \Delta D(t - t_c) \end{aligned} \right] + \varepsilon^{irrec}(t_c) \quad (4-6)$$

As discussed earlier, the Prony series  $\Delta D$  is a function of  $D_n$  and  $\lambda_n$ , which are obtained from the first loading cycle. Thus, the only unknown viscoelastic parameter in Eq. (4-6) is  $g_2^2$ . However, the irrecoverable strain component  $\varepsilon^{irrec}(t_c)$  must be subtracted from Eq. (4-6) in order to determine  $g_2^2$ . Since the irrecoverable strain ceases once the load is removed at  $t_c$ , the term  $\Delta\varepsilon_2^{r2}$  is the recovered strain from  $t = t_2$  to  $t = t_d$ .

In other words, the irrecoverable strain beyond  $t_c$  and before the next cycle is applied equal to  $\varepsilon^{irrec}(t_c)$ . The expression for  $\Delta\varepsilon_2^{r2}$  is represented by Eq. (4-7). Consequently, the nonlinear parameter  $g_2^2$  can be obtained by minimizing the error between the measurements of  $\Delta\varepsilon_2^{r2}$  and Eq. (4-7). In this study,  $t_2$  is selected as the 10<sup>th</sup> measurement during unloading.

$$\begin{aligned} \Delta\varepsilon_2^{r2}(t) &= \varepsilon_2^r(t_2) - \varepsilon_2^r(t) \\ &= \sigma_1 \left\{ \begin{aligned} &\sum_{n=1}^N D_n [1 - \exp(-\lambda_n t_2)] - \sum_{n=1}^N D_n [1 - \exp(-\lambda_n (t_2 - t_a))] - \\ &\sum_{n=1}^N D_n [1 - \exp(-\lambda_n t)] + \sum_{n=1}^N D_n [1 - \exp(-\lambda_n (t - t_a))] \end{aligned} \right\} + \quad (4-7) \\ &\quad g_2^2 \sigma_2 \left\{ \begin{aligned} &\sum_{n=1}^N D_n [1 - \exp(-\lambda_n (t_2 - t_b))] - \sum_{n=1}^N D_n [1 - \exp(-\lambda_n (t_2 - t_c))] - \\ &\sum_{n=1}^N D_n [1 - \exp(-\lambda_n (t - t_b))] + \sum_{n=1}^N D_n [1 - \exp(-\lambda_n (t - t_c))] \end{aligned} \right\} \end{aligned}$$

Once the nonlinear parameter  $g_2^2$  is obtained, the measurements of  $\Delta\varepsilon_2^{r3}$ , shown in Figure 4.4, are used to obtain the nonlinear parameter  $g_1^2$ . The term  $\Delta\varepsilon_2^{r3}$  is the difference between the creep strain at  $t = t_c$  and the unloading strain at  $t = t_2$ . The expression for  $\Delta\varepsilon_2^{r3}$  is shown in Eq. (4-8). Consequently, the term  $g_1^2$  can be obtained by minimizing the error between the measurements of  $\Delta\varepsilon_2^{r3}$  and Eq. (4-8).



$$\begin{aligned}
\Delta \varepsilon_2^{r3} &= \varepsilon_2^c(t_c) - \varepsilon_2^r(t_2) \\
&= g_1^2 \left\{ \begin{aligned} &\left[ \sigma_1 \sum_{n=1}^N D_n [1 - \exp(-\lambda_n t_c)] - \sigma_1 \sum_{n=1}^N D_n [1 - \exp(-\lambda_n (t_c - t_a))] \right] + \\ &\left[ (g_2^2 \sigma_2) \sum_{n=1}^N D_n [1 - \exp(-\lambda_n (t_c - t_b))] \right] \end{aligned} \right\} \\
&\quad - \left\{ \begin{aligned} &\left[ \sigma_1 \sum_{n=1}^N D_n [1 - \exp(-\lambda_n t_2)] - \sigma_1 \sum_{n=1}^N D_n [1 - \exp(-\lambda_n (t_2 - t_a))] \right] + \\ &\left[ (g_2^2 \sigma_2) \sum_{n=1}^N D_n [1 - \exp(-\lambda_n (t_2 - t_b))] - \right. \\ &\left. \left[ g_2^2 \sigma_2 \sum_{n=1}^N D_n [1 - \exp(-\lambda_n (t_2 - t_c))] \right] \right] \end{aligned} \right\} \quad (4-8)
\end{aligned}$$

Because the response of asphalt binder is hereditary or time-dependent, the material response at the current loading cycle is a function of the previous loading cycles. Therefore, it is necessary to apply the MSP to each loading cycle. Similarly to Eqs. (4-5) and (4-6), the strain response functions were derived for all loading cycles. These equations were coded in a program using Mathematica<sup>TM</sup> software to obtain all the required model parameters (Prony series coefficients,  $g_1$  and  $g_2$ ).

Once the Prony series coefficients and nonlinear parameters are obtained, the recoverable strain can be calculated as a function of time for all cycles. Consequently, the irrecoverable strain as a function of time is obtained by subtracting the recoverable strain from the total strain. The analysis procedure is illustrated in Figure 4.5.

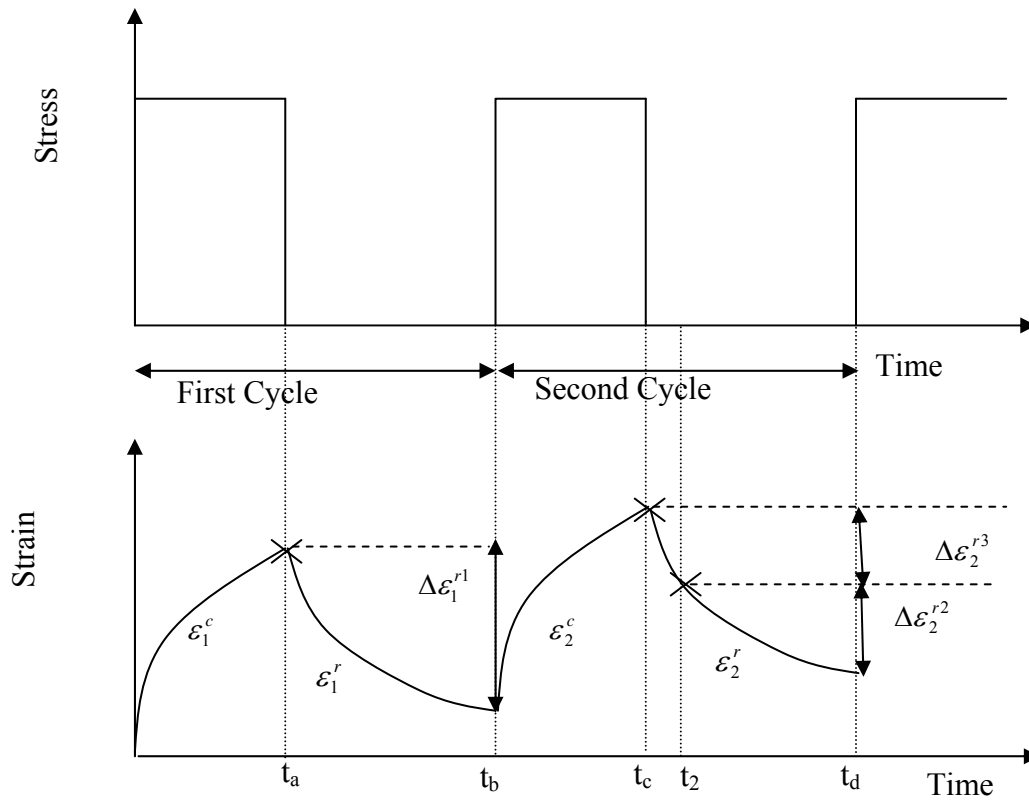


**Figure 4.4** A Schematic Diagram of Creep and Recovery Loading and Strain Response.

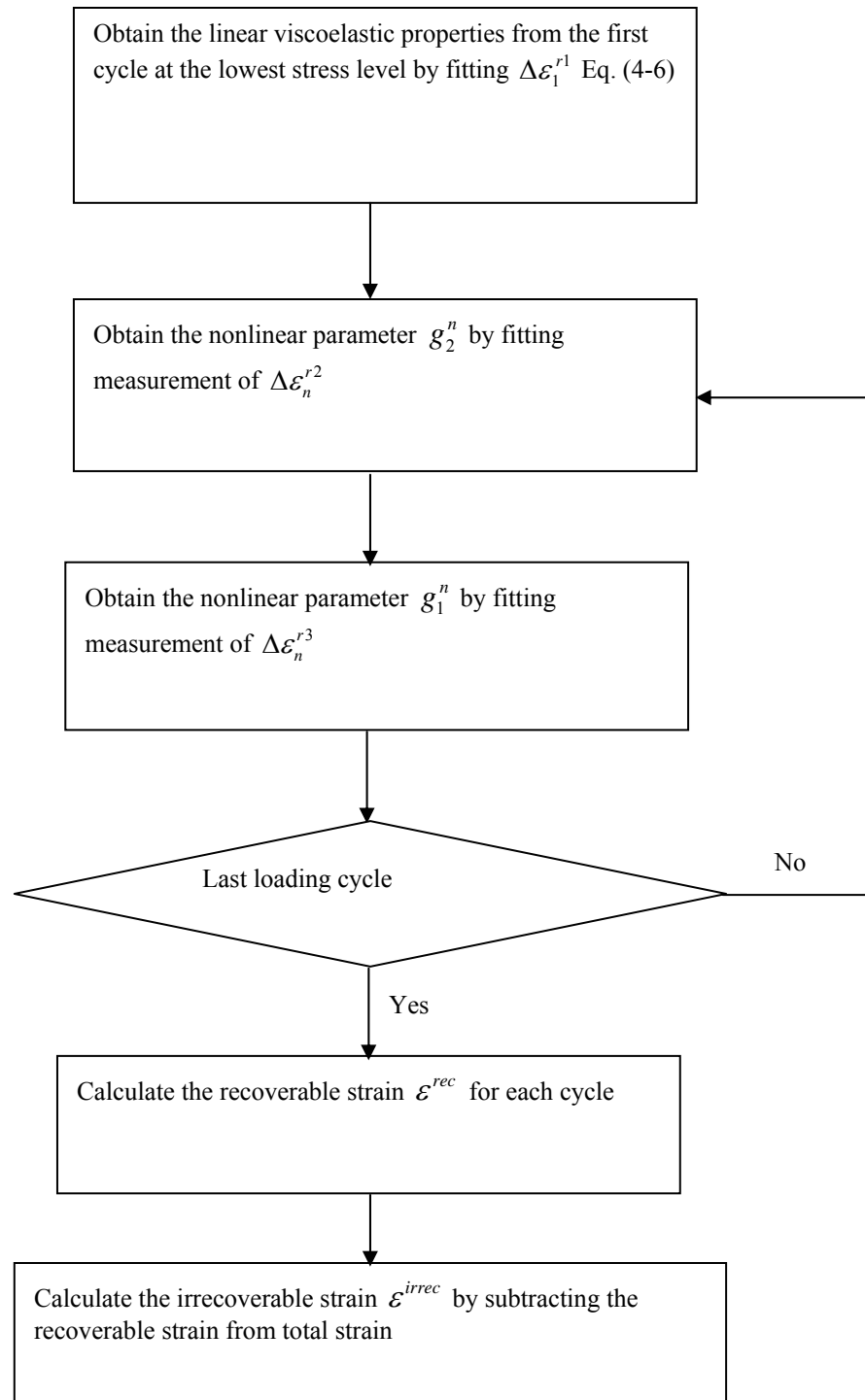


**Figure 4.5** A Flowchart of the Procedure for the Analysis of Strain Components.

## ANALYSIS OF RESULTS

### Nonlinear Viscoelastic Parameters

Examples of the results of decoupling strain components for the PG 70-22 binder at 58 °C are shown in Figure 4.6. This figure shows the first two stress levels (25 and 50 Pa) only in order to simplify the representation of results. As expected, the results show that the irrecoverable strain component accumulates as the number of load cycles increased and as the stress level increases. In addition, the irrecoverable strain was constant when the load was removed; it was a function of time during loading.

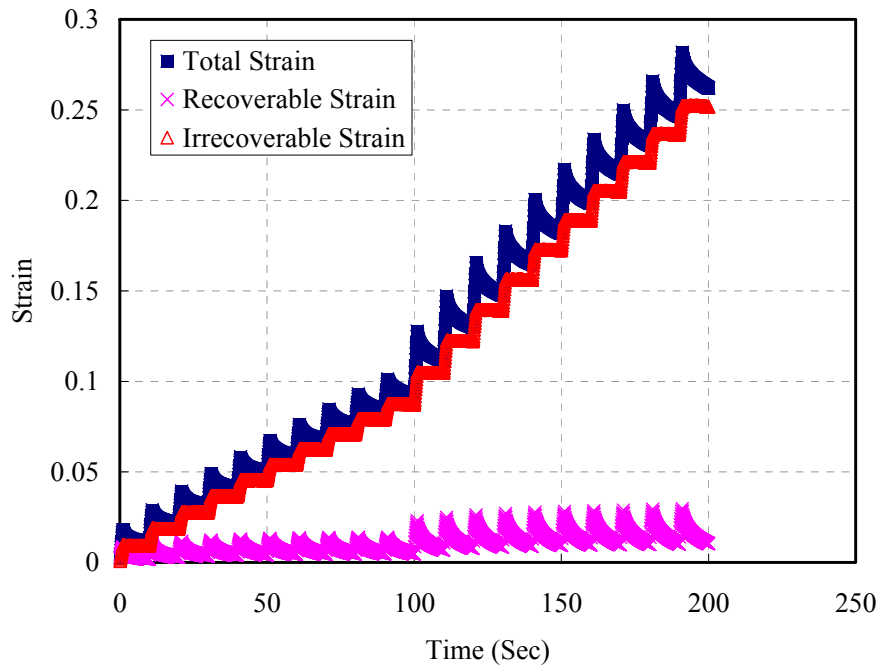
Figure 4.7 compares the maximum irrecoverable strain at each loading cycle for the different binders. The results show that the irrecoverable strain increases with an increase in temperature. Moreover, the PG 76 binder had a smaller irrecoverable strain than the PG 70 binder. However, binders with the same high temperature PG grade (PG 76 or PG 70) exhibited different accumulated permanent strain levels, indicating that the current high temperature grading system does not sufficiently predict the resistance to the accumulation of permanent strain.

Figure 4.8 is an example of the results of the nonlinear viscoelastic parameters for all stress levels used in the MSCR test. These results show that nonlinear parameter  $g_1$  was almost constant with a value of 1, while  $g_2$  and  $g_1 * g_2$  increased with increasing number of cycles at the same stress level (every 10 cycles) during most of the loading cycles. This increase means that the material experienced softening, leading to an increase in the resulting recoverable strain. However, the rate of increase in  $g_2$  and  $g_1 * g_2$  decreased after 40 cycles (fourth stress level), indicating a reduction in the

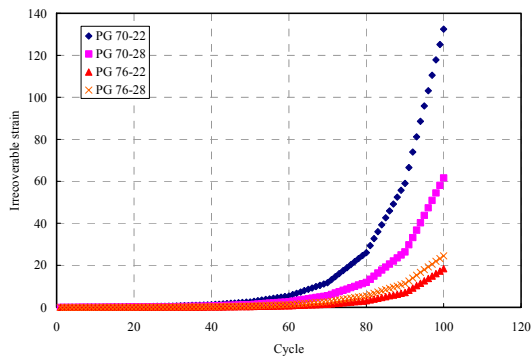
recoverable strain. This behavior could be caused by binder hardening due to considerable accumulation of permanent strain after 40 cycles.

An interesting phenomenon in Figure 4.8 is the drop of  $g_1 * g_2$  and  $g_2$  when the stress increases from one stress level to the other. The exact causes of this phenomenon are not clear. However, a possible explanation is that the increase in stress level causes a sudden increase in permanent strain (permanent change in binder structure) and binder hardening, leading to a reduction in binder recoverable strain. The reduction of  $g_1 * g_2$  and  $g_2$  to values less than one indicates that the accumulation of permanent strain causes binder hardening such that the viscoelastic strain decreases to a level below that determined from the linear viscoelastic response. Another example of binder response is shown in Figure 4.9. These results show that this binder did not exhibit a significant nonlinear response throughout the test.

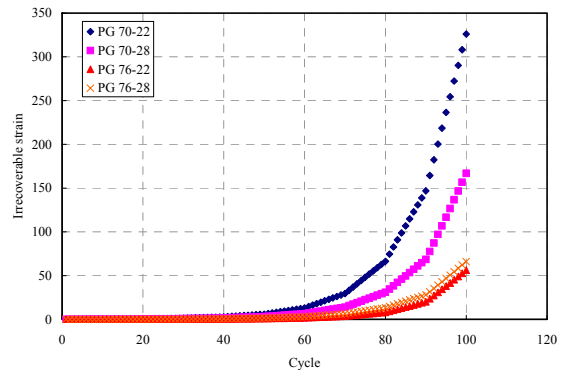
In general, the use of the nonlinear viscoelastic model is important as some of the nonlinear response could be mistakenly considered permanent strain if the linear viscoelasticity theory is used.



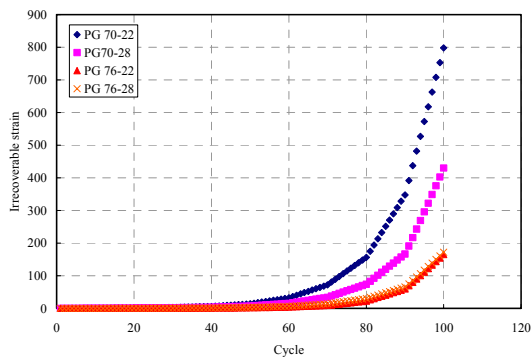
**Figure 4.6** The Strain Components of PG 70-22 at 58 °C.



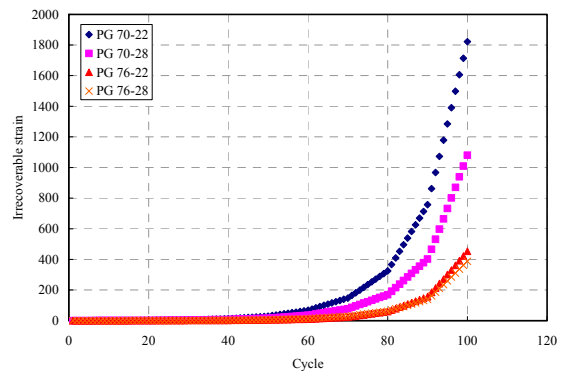
(a) 58 °C



(b) 64 °C



(c) 70 °C



(d) 76 °C

**Figure 4.7** Comparisons of Irrecoverable Strain for Different Binders at Different Temperatures.

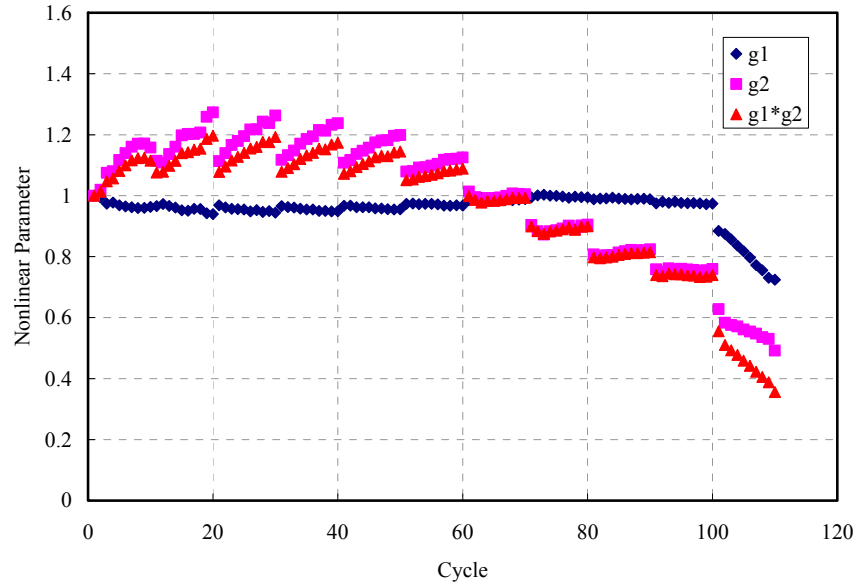


**Figure 4.8** The Nonlinear Parameters of Binder PG 70-22 at 58 °C.

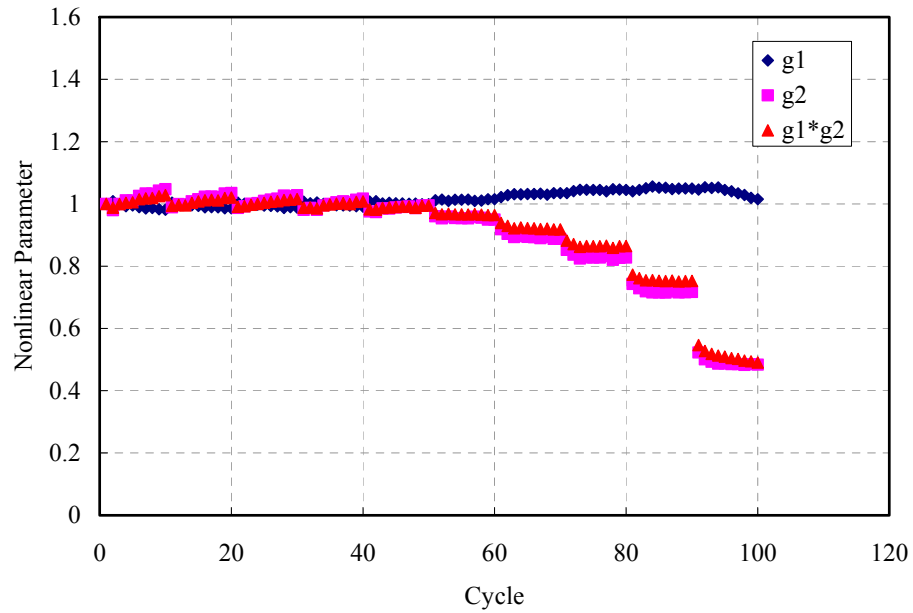


**Figure 4.9** The Nonlinear Parameters of PG 70-28 Binder at 64 °C.



### Validity of Using a Linear Model for Describing Permanent Strain

As discussed previously, some studies use a linear viscous model to represent the accumulation of permanent strain in asphalt binders. The validity of this approach is evaluated here by using Eq. (4-9), which represents a linear viscoelastic model with a linear viscous representation (referred to as linear dashpot), to analyze the data:

$$\Delta D(\psi^t) = \sum_{n=1}^N D_n (1 - \exp(-\lambda_n \psi^t)) + \phi_f t \quad (4-9)$$

where  $\phi_f$  is the viscosity coefficient of the dashpot. The Prony series and dashpot coefficients in Eq. (4-9) can be obtained by fitting the measurements at the first loading-recovery cycle using Eqs. (4-2) and (4-3) without  $\varepsilon^{irrec}$ . Then the coefficients obtained are used with  $\phi_f t$  replacing  $\varepsilon^{irrec}$  in Eqs. (4-2) and (4-3) along with the superposition principle to describe the response during the remaining cycles. Figures 4.10 and 4.11 are the result of using the linear dashpot to analyze the binder PG 70-22 at 58 °C for stress levels 1 to 6 (25 to 800 Pa) and stress levels 7 to 9 (1600 to 6400 Pa), respectively. These figures show that the linear dashpot approach overestimates the permanent strain during one to six stress levels, but underestimates the permanent strain after the eighth stress level (time greater than 800 sec).

Figure 4.12 is a comparison of the irrecoverable strain obtained using a linear dashpot approach and the new method developed in this study. This figure shows that the relationship between the irrecoverable strain increment and stress is a high order polynomial and not a straight line as would be predicted by the dashpot approach.

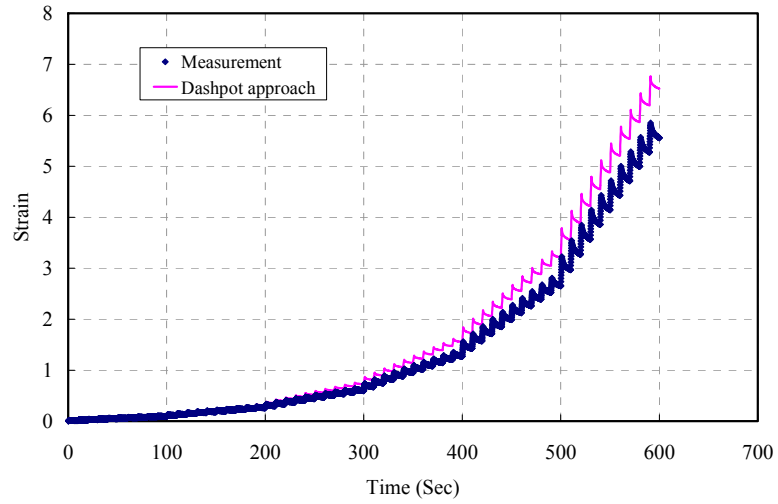


**Figure 4.10** The Comparison of Experimental Measurements of Permanent Strain and Linear Dashpot Analysis Results for Stress Levels 1 to 6.

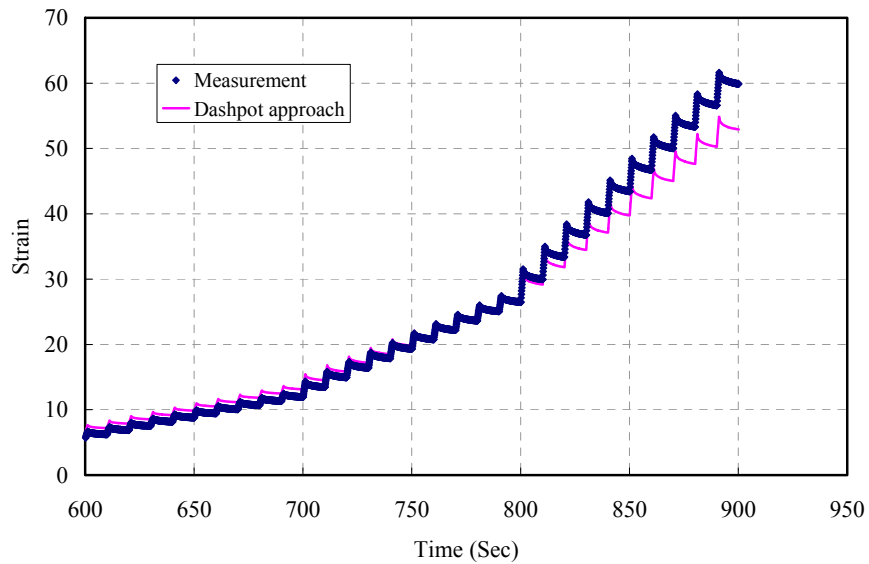


**Figure 4.11** The Comparison of Experimental Measurements of Permanent Strain and Linear Dashpot Analysis Results for Stress Levels 7 to 9.

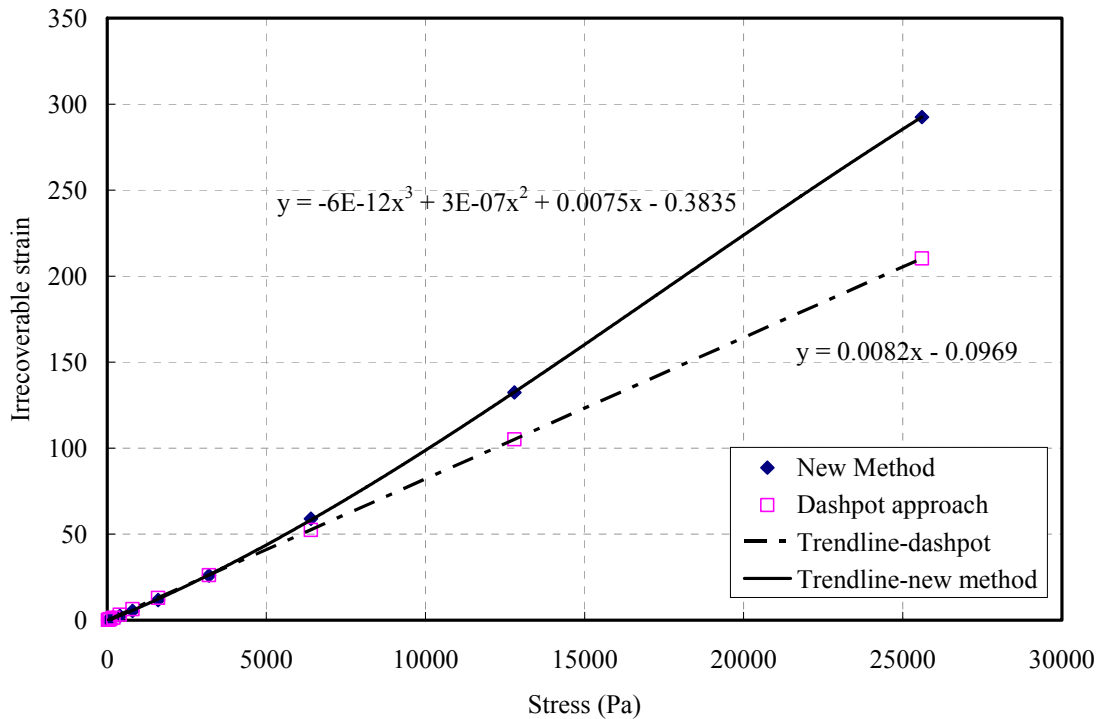


**Figure 4.12** The Comparison of Irrecoverable Strain Using the New Method and the Dashpot Approach.

### Nonlinearity in ALF Binders

The nonlinear parameter responses for ALF binders—air blown, SBS, ELVALOY, control, and SBSLG—are shown in Figures 4.13 to 4.17, respectively. The results show that air blown and SBSLG binders exhibited nonlinear viscoelastic behavior. The  $g_1 * g_2$  is around 1 for air blown binder, indicating that during loading the response remained almost linear, but nonlinearity was evident during unloading ( $g_2 > 1$ ). The SBSLG binder experienced nonlinear response during loading ( $g_1 * g_2 > 1$ ) and unloading ( $g_2 > 1$ ). The SBS and ELVALOY binders remained linear during loading

and unloading throughout most of the test. The control binder also experienced linear behavior during most of the test. However, it deviated from linearity and exhibited hardening behavior ( $g_2 < 1$  and  $g_1 * g_2 < 1$ ) earlier than either SBS or ELVALOY. These results indicate that asphalt binders vary in their nonlinear response; hence, it was necessary to apply the nonlinear viscoelastic model to characterize the asphalt binder in order to accurately determine permanent strain.

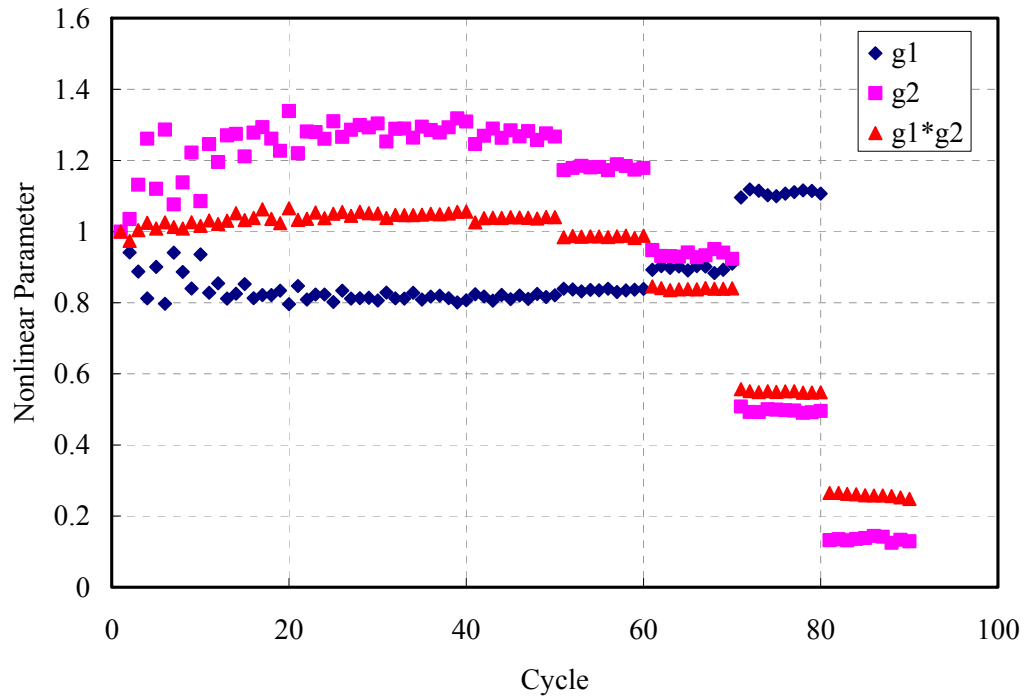


**Figure 4.13** The Results of Nonlinear Parameters for the Air Blown Binder.

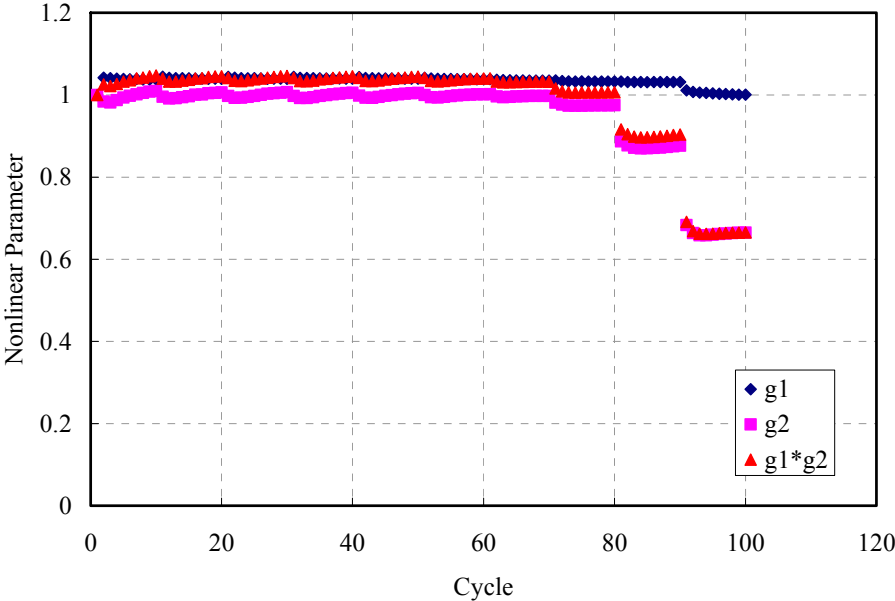


Figure 4.14 The Results of Nonlinear Parameters for the SBS-Modified Binder.

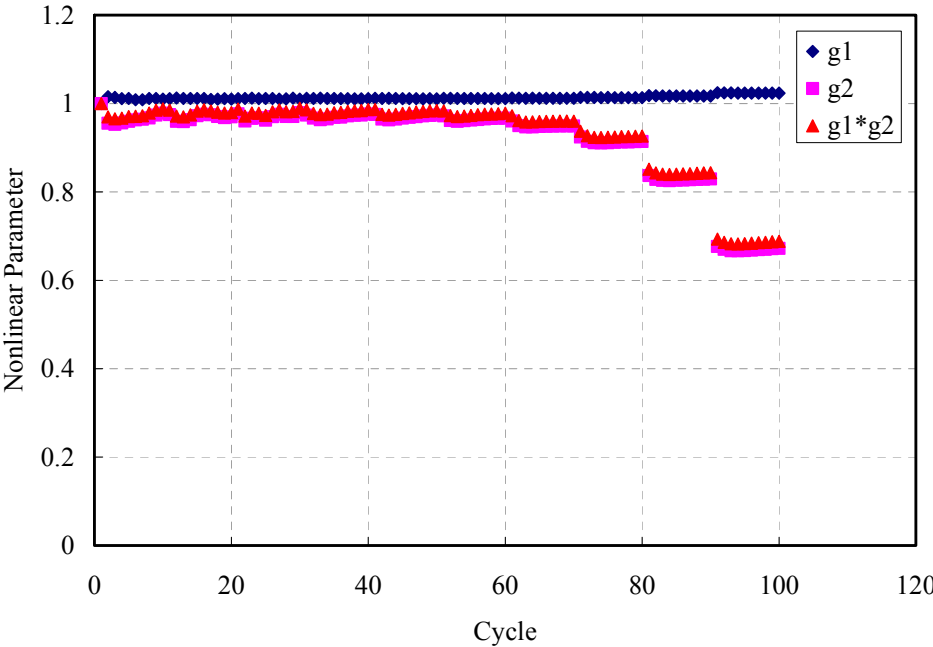
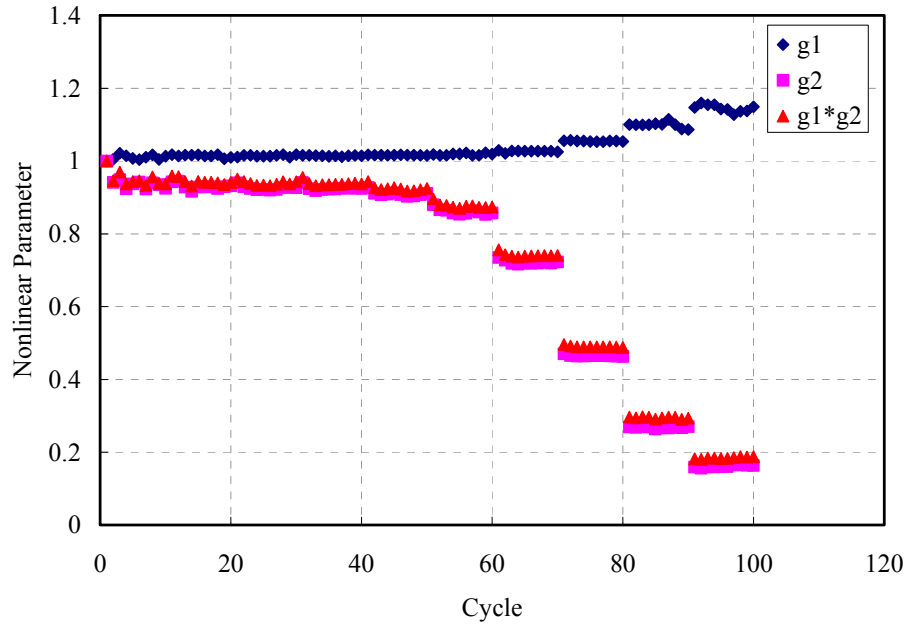
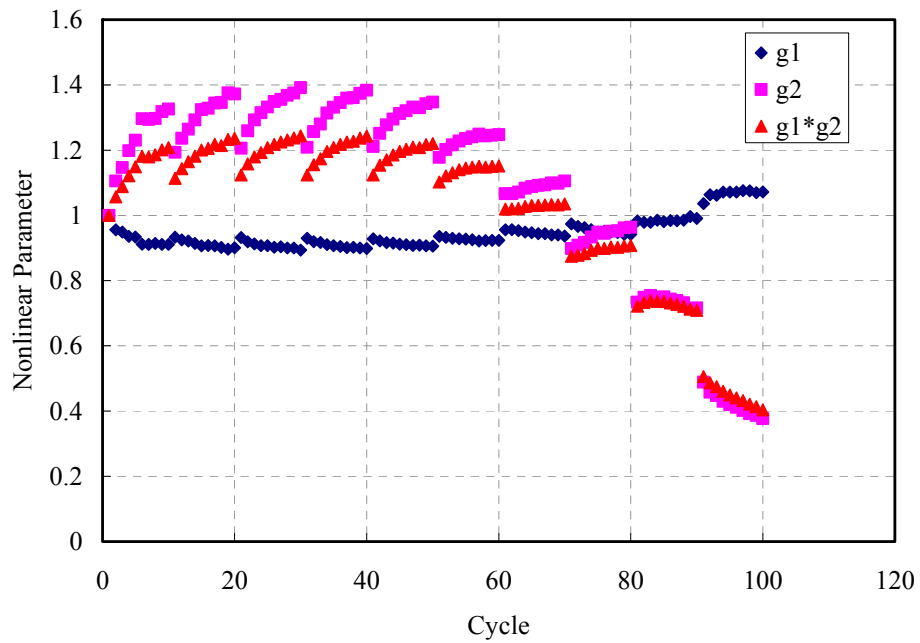


Figure 4.15 The Results of Nonlinear Parameters for the ELVALOY-Modified Binder.



**Figure 4.16** The Results of Nonlinear Parameters for the Control Binder.



**Figure 4.17** The Results of Nonlinear Parameters for the SBSLG-Modified Binder.

### Analysis of ALF Binder Permanent Deformation

The primary objective of this study was to develop a method for analyzing the resistance of asphalt binders to permanent deformation. The current approach of analyzing binder resistance to permanent deformation uses the accumulated strain  $\gamma_{ir}$  at the last loading-unloading cycle of maximum stress level (25600 Pa). This accumulated strain is then divided by the maximum stress  $\tau$  (25600 Pa) to calculate  $J_{nr}$ , as shown in Eq. (4-10) (D' Angelo et al., 2007):

$$J_{nr} = \frac{\gamma_{ir}}{\tau} \quad (4-10)$$

A different approach is proposed in this study to quantify the resistance to permanent deformation. First, the irrecoverable strain was determined at every loading cycle following the approach presented in this study and outlined in Figure 4.5. Then, the irrecoverable strain was averaged by the number of cycles within each stress level. The average irrecoverable strain at every stress level was then divided by the ultimate stress that the material was able to sustain. This maximum stress was defined as the stress that precedes the stress level at which the calculated  $g_2$  dropped by 20 percent. The drop of  $g_2$  indicates that the material has lost its ability to recover strain during unloading, which could be indicative of damage, rendering any further analysis of permanent strain after this point inaccurate.

The ultimate stresses for all binders are shown in Table 4.1. The relationship between applied stress level and  $J_{nr}$  at that stress level is shown in Figure 4.18. This figure shows that the rate of increase in  $J_{nr}$  becomes higher with an increase in stress

level. This result supports the point that the irrecoverable strain response increases with an increase in stress level.

The comparison of the current method used by D'Angelo et al. (2007) for the analysis of the MSCR test and the one developed in this study for the analysis of the MSCR test is shown in Table 4.2. This comparison shows that both methods conform to the ranking of the ALF rutting reasonably well. Figures 4.19 and 4.20 present a comparison of both methods of analysis with ALF rutting. Figures 4.19 and 4.20 show that the results prove that  $J_{nr}$  calculated using the method developed in this study provides a better correlation with ALF rutting than does the current MSCR analysis approach.

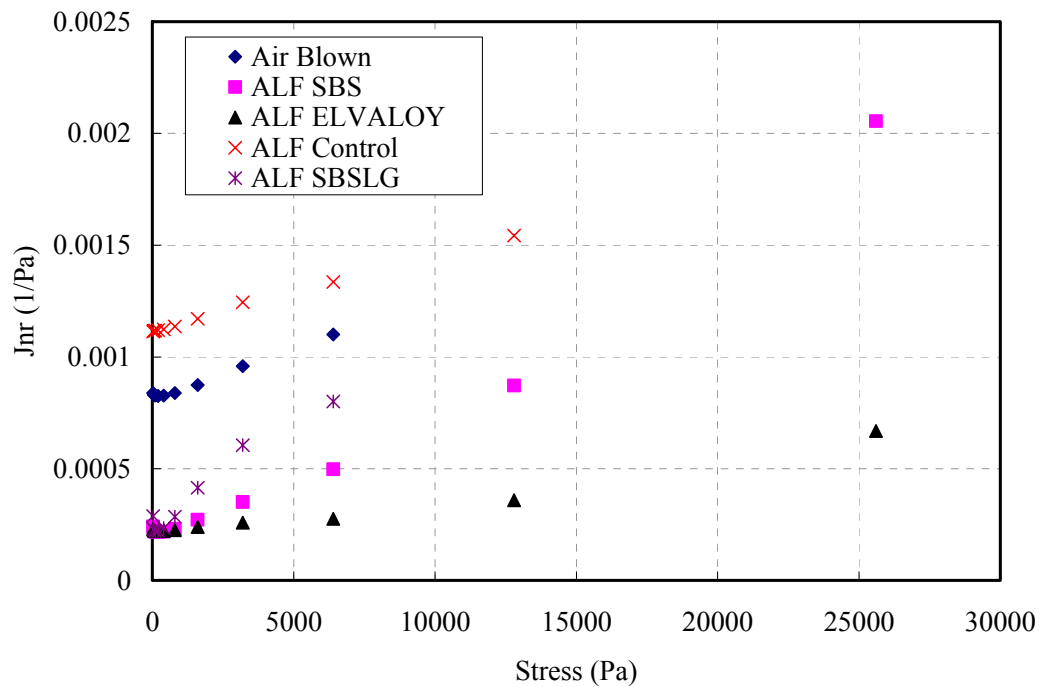
**Table 4.1** The Ultimate Stress for Each Binder.

Binder	Ultimate Stress (Pa)
Air Blown	6400
ALF SBS	25600
ALF ELVALOY	25600
ALF Control	12800
ALF SBSLG	6400



**Table 4.2** The Results of  $J_{nr}$  and the Ranking.

Binder	New Method		Without Separation		ALF Measurements	
	$J_{nr}$ (1/Pa)	$J_{nr}$ Ranking	$J_{nr}$ (1/Pa)	$J_{nr}$ Ranking	Rutting (mm)	Ranking
Air Blown	1.10E-3	3	0.17	3	1.27	3
SBS	2.05E-3	5	0.19	4	1.73	5
ELVALOY	6.69E-4	1	0.08	1	1.12	2
Control	1.54E-3	4	0.2	5	1.42	4
SBSLG	8.E-4	2	0.09	2	1.09	1

**Figure 4.18** The Relationship between Stress and  $J_{nr}$ .

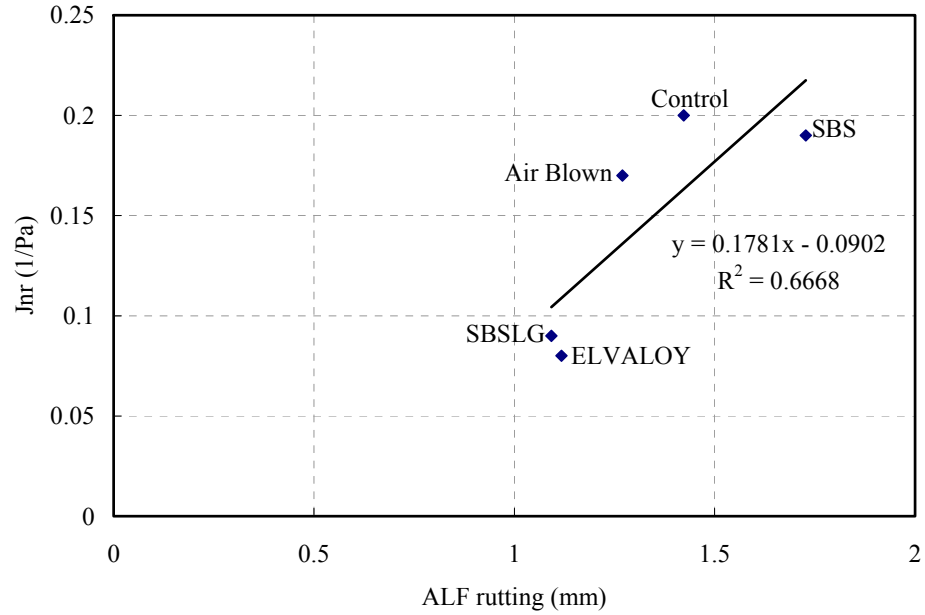


**Figure 4.19** The Comparison of  $J_{nr}$  without Separation and ALF Rutting.

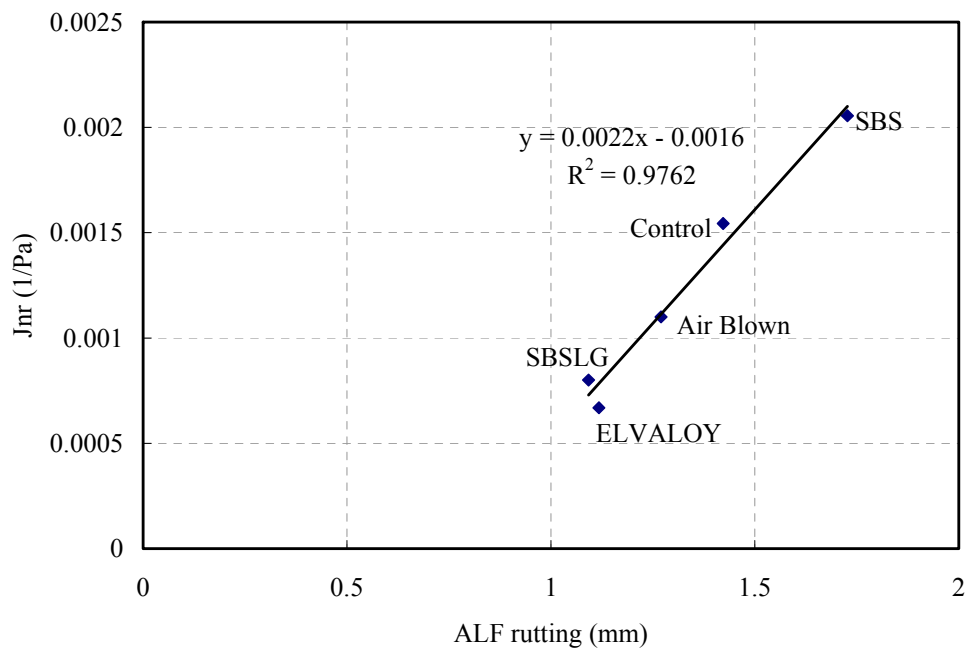


**Figure 4.20** The Comparison of  $J_{nr}$  with Separation and ALF Rutting.

## CONCLUSIONS

A new method was developed in this study to separate recoverable (nonlinear viscoelastic) strain from irrecoverable (permanent) strain developed in asphalt binders. Schapery's nonlinear viscoelastic model was used to analyze the recoverable strain. This method was utilized to analyze MSCR tests of asphalt binders to determine their resistance to permanent deformation. The primary findings of this study are as follows:

- Modified binders that had the same high temperature PG grade developed different degree of irrecoverable strain. This result supports previous findings indicating that the current Superpave system does not accurately rank modified asphalt binders based on their resistance to permanent deformation.
- A linear viscous model (linear dashpot) was not able to accurately describe the accumulation of permanent strain in asphalt binders.
- Asphalt binders varied in their nonlinear viscoelastic response during loading and unloading. The viscoelastic response of some asphalt binders remained linear throughout the MSCR test. Other binders, however, exhibited nonlinear response during loading and/or unloading. The recoverable strain decreased after a certain level of accumulation of permanent strain. This decrease was marked by a reduction in the nonlinear viscoelastic parameter ( $g_2$ ).
- The use of a linear viscoelastic model to analyze the recoverable strain response leads to errors in separating the nonlinear viscoelastic strain from

the irrecoverable strain for the binders evaluated. As a result, the calculation of the irrecoverable strain is not be accurate and leads to errors in ranking these binders based on their resistance to permanent deformation.

- The results of the new method for characterizing resistance of asphalt binders to permanent deformation conformed well to asphalt mixture permanent deformation measured in the ALF experiment. The new method offers an improvement over the current method used in the analysis of the MSCR test results.

**CHAPTER V**  
**NUMERICAL IMPLEMENTATION OF NONLINEAR**  
**VISCOELASTIC-VISCOPLASTIC MODEL**

**OVERVIEW**

This chapter includes the development of a general constitutive relationship for describing the behavior of asphalt mixtures. This constitutive relationship includes a nonlinear viscoelastic component to model the recoverable response and a viscoplastic component to model the irrecoverable response. The nonlinear viscoelastic component is modeled using Schapery model. The irrecoverable component is represented using Perzyna's viscoplasticity theory with a Drucker-Prager yield surface that is modified to capture the influence of stress state on response.

This study uses the user-defined material subroutine (UMAT) supported within ABAQUS to implement the nonlinear viscoelastic-viscoplastic model. This chapter includes parametric analysis using the finite element (FE) model in order to illustrate the effect of each of the model's parameters on model response. In addition, this chapter includes FE simulations of the response of a pavement structure using different parameters of the constitutive relationship. The purposes of these simulations are to demonstrate the capabilities of the FE model in describing the performance of asphalt pavements in terms of resistance to permanent deformation and fatigue damage.

## INTRODUCTION

Experimental measurements have shown that the response of asphalt mixtures contains recoverable and irrecoverable components (Perl et al., 1983, Sides et al., 1985, and Collop et al., 2003). Some of these studies modeled the recoverable response as elastic (time-independent) or viscoelastic (time-dependent). Similarly, the irrecoverable response has been modeled as plastic (time-independent) or viscoplastic (time-dependent). Moreover, Cheung and Cebon (1997a, b) and Airey et al. (2002 and 2004) indicated that the recoverable component can be nonlinear depending on the combination of temperature, loading rate and stress/strain level. Therefore, this study employs nonlinear viscoelasticity theory to describe the recoverable component; while Perzyna's viscoplasticity theory is used to model the irrecoverable component.

The Schapery single integral model is one of the most popular models to characterize the nonlinear viscoelastic constitutive behavior of engineering materials (Christensen, 1968; Schapery, 1969; Schapery, 2000). Touati and Cederbaum (1997, 1998) developed a numerical scheme of the Schapery theory to predict the nonlinear stress relaxation using the Runge-Kutta method and to analyze the orthotropic laminated plane. Sadd et al. (2004) employed the Schapery theory to represent the nonlinear viscoelastic behavior of asphalt mixes and implemented it in the ABAQUS finite element package using a recursive scheme. This model has been used recently by Haj-Ali and Muliana (2004) to analyze the three-dimensional nonlinear viscoelastic behavior of polymeric materials.

In terms of viscoplastic model, Sousa and Weissman (1994) improved the nonlinear viscoelastic model developed by Sousa et al. (1993) by incorporating the elastoplastic component with Von Mises yield surface, and isotropic and kinematic hardening. However, this model used nonlinear elastic and viscoelastic relationships to represent the recoverable component, and the viscoplastic component was not included within the model. Seibi et al. developed an elasto-viscoplastic constitutive model for hot mixes asphalt (HMA). This model used the Perzyna's theory of viscoplasticity with the Drucker-Prager yield surface to model the irrecoverable component; nevertheless this model only used the elastic model to represent the recoverable component. Lu and Wright (1998) and Oeser and Moller (2004) developed elasto-viscoplastic models to represent the asphalt mixtures behavior. Lu and Wright (1998) employed Perzyna's theory of viscoplasticity to model the irrecoverable component; while Oeser and Moller (2004) used a Hook-Kelvin-Newton element to present the elastic, viscoelastic, and viscoplastic components, respectively. However, these models do not include the nonassociated flow rule. Tashman (2003) developed a microstructural viscoplastic model with nonassociated flow rule for HMA. This model considered material anisotropy, damage effect and work hardening. Dessouky (2005) developed an elasto-viscoplastic model with Drucker-Prager yield surface and implemented it in a finite element program. However, those constitutive models do not consider the nonlinear viscoelastic behavior of recoverable component. Hence, this chapter employs the Schapery nonlinear viscoelastic model to represent the recoverable component, while the viscoplastic component is modeled by Perzyna's theory. Moreover, the Drucker-Prager

yield surface modified to account for the influence of stress state on mixture response is used as part of Perzyna's viscoplasticity theory (Dessouky 2005).

## **OBJECTIVES AND TASKS**

The objective of the research reported in this chapter is to implement a nonlinear viscoelastic-viscoplastic model in finite element (FE) and demonstrate the capabilities of this model in describing the performance of asphalt mixtures in terms of resistance to permanent deformation and fatigue damage. The research tasks are as follows:

1. Implement the nonlinear viscoelastic-viscoplastic model in FE.
2. Conduct the parametric analysis in order to demonstrate the influence of the model's parameters on mixture response.
3. Develop a FE model of asphalt pavement structure and study the response of this structure using different model's parameters.

## **DEVELOPMENT OF NONLINEAR VISCOELASTIC-VISCOPLASTIC MODEL**

The total response of asphalt material subjected to an applied stress can be decomposed into recoverable components (elastic, viscoelastic) and irrecoverable components (plastic, and viscoplastic). This study assumes that the asphalt material response contains nonlinear viscoelasticity and viscoplasticity to present the recoverable and irrecoverable components, respectively. The elastic response is included within the viscoelastic relationship, while the irrecoverable response is assumed to be all time-dependent. The total strain subjected an applied stress can be expressed as:



$$\varepsilon_{ij} = \varepsilon_{ij}^{nve} + \varepsilon_{ij}^{vp} \quad (5-1)$$

where,  $\varepsilon_{ij}$  is total strain,  $\varepsilon_{ij}^{nve}$  is the nonlinear viscoelastic strain representing the recoverable component, and  $\varepsilon_{ij}^{vp}$  is the viscoplastic strain representing the irrecoverable component.

### **Nonlinear Viscoelastic Model**

This study employs the Schapery nonlinear viscoelasticity theory to model the recoverable component. This model is presented in Chapter II, and a summary is presented here for completeness. The recoverable strain response under an applied stress  $\sigma^r$  is expressed as in Eq. (2-1). The reduced time in Eq. (2-1) can be a function of stress/strain shift factor, temperature shift factor, and other environment shift factors as shown in Eq. (2-2). This study uses the Prony series to represent the transient compliance  $\Delta D$  shown in Eq. (2-3).

The strain response for isotropic materials can be decoupled into deviatoric and volumetric parts as presented in Eq. (2-4). Applying the Schapery integral constitutive model, the deviatoric and volumetric strain can be expressed as Eq. (2-5) and (2-6), respectively. Assuming Poisson's ratio  $\nu$  to be time-independent, the shear and bulk compliances can be expressed as Eq. (2-7).

### Viscoplastic Model

This study uses an Extended Drucker-Prager model with nonassociated flow rule to model the viscoplasticity. From Eq. (5-1), the total strain rate can be represented as in Eq. (5-2).

$$\dot{\epsilon}_{ij} = \dot{\epsilon}_{ij}^{nve} + \dot{\epsilon}_{ij}^{vp} \quad (5-2)$$

where  $\dot{\epsilon}_{ij}^{nve}$  is the viscoelastic strain rate, and  $\dot{\epsilon}_{ij}^{vp}$  is the viscoplastic strain rate. This study uses the Perzyna's model to present the viscoplastic strain rate component as:

$$\dot{\epsilon}_{ij}^{vp} = \Gamma \langle \phi(f) \rangle \frac{\partial g}{\partial \sigma_{ij}} \quad (5-3)$$

where,  $\Gamma$  is a viscosity parameter which can be a constant or a function of time,  $g$  is the viscoplastic potential energy function which is a surface of the actual stress state in stress space, and  $\phi$  is the overstress function assumed as a function of yield surface  $f$  with  $N$  power. In Eq. (5-3),  $\Gamma \langle \phi(f) \rangle$  is a positive scalar which determines the magnitude of viscoplastic strain rate  $\dot{\epsilon}_{ij}^{vp}$ , and  $\frac{\partial g}{\partial \sigma_{ij}}$  is a vector which dominates the direction of  $\dot{\epsilon}_{ij}^{vp}$ . Once the potential energy function coincides with the yield surface function ( $g = f$ ), it is called associated flow rule. On the other hand, the nonassociated flow rule is defined as the potential energy function that does not coincide with the yield surface function ( $g \neq f$ ). Several studies have shown that hot mixes asphalt (HMA) exhibits nonassociated behavior. Hence, this study uses nonassociated flow rule to

model the viscoplasticity. In addition,  $\langle \bullet \rangle$  in Eq. (5-3) are McCauley brackets which imply that

$$\langle \phi(f) \rangle = \begin{cases} 0 & \phi(f) \leq 0 \\ \left( \frac{f}{\sigma_y^0} \right)^N & \phi(f) > 0 \end{cases} \quad (5-4)$$

where,  $\sigma_y^0$  and  $N$  are material constants. Eqs. (5-3) and (5-4) indicate that the viscoplasticity takes place only when the overstress function exceeds zero.

### ***Yield Surface Function***

The yield surface function determines the possible combinations of stresses that separate the recoverable from the irrecoverable response. In order to consider the effect of confinement, shear stress and dilative behavior of HMA, this study employs Extended Drucker-Prager yield surface, which is presented in  $I_1 - \tau$  plane shown in Figure 5.1, and the equation is shown as:

$$f = F(\sigma_{ij}) - \kappa(\varepsilon_e^{vp}) = \tau - \alpha I_1 - \kappa(\varepsilon_e^{vp}) \quad (5-5)$$

where,  $\alpha$  is material parameter,  $\kappa(\varepsilon_e^{vp})$  is a hardening function which is a function of effective viscoplastic strain  $\varepsilon_e^{vp}$ .  $\tau$  and  $I_1$  are the deviatoric shear stress modified to account for the stress state and first invariant stress, respectively, expressed as:

$$I_1 = \frac{1}{3} \sigma_{ii}$$

$$\tau = \frac{\sqrt{J_2}}{2} \left[ 1 + \frac{1}{d} + \left( 1 - \frac{1}{d} \right) \frac{J_3}{\sqrt{J_2^3}} \right] \quad (5-6)$$

where,  $J_2$  and  $J_3$  are second and third deviatoric stress invariants, respectively, which are defined as:

$$\begin{aligned} J_2 &= \frac{3}{2} S_{ij} S_{ij} \\ J_3 &= \frac{9}{2} S_{ij} S_{jk} S_{ki} \end{aligned} \quad (5-7)$$

where,  $S_{ij}$  is deviatoric stress. In Eq. (5-6),  $d$  is a material parameter which takes care of the sensitivity of yield surface to the first invariant stress  $I_1$ . The range of  $d$  is from 0.778 to 1. Applying uniaxial compression stress  $\sigma_{11}$ , the deviatoric shear stress  $\tau$

yields  $\tau = \sqrt{J_2} = \sigma_{11}$ ; while  $\tau = \frac{\sqrt{J_2}}{d} = \frac{\sigma_{11}}{d}$  for uniaxial tension case. This indicates that

at same stress level, the material in tension reaches the yield surface earlier than the material in compression. Hence, the material strength in compression is higher than the material strength in tension. The influence of  $d$  is illustrated in Figure 5.2. Consider the point A under the confinement pressure  $\sigma_3$ . Once increasing the axial stress  $\sigma_1$

(compression), both of  $I_1$  and  $\sqrt{J_2}$  will increase and follow line AB until reaching yield stress point B. On the other hand, if the axial stress is decreasing (extension), both

of  $I_1$  and  $\sqrt{J_2}$  will decrease and follow the line AC until researching yield stress point

C. The yield surface under extension in  $I_1 - \sqrt{J_2}$  plane is modified by reducing the slope ( $\alpha'$ ) and intercept ( $\kappa'$ ) multiplying by  $d$ .

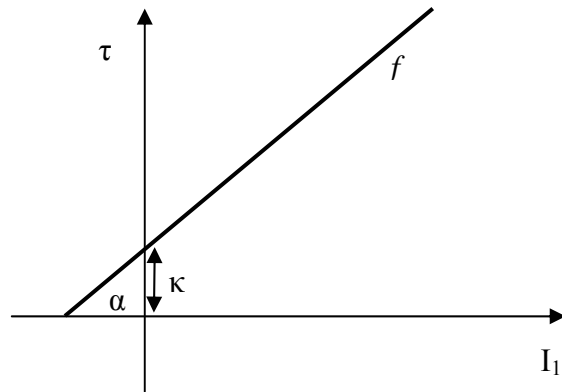


**Figure 5.1** The Extended Drucker-Prager Yield Surface.

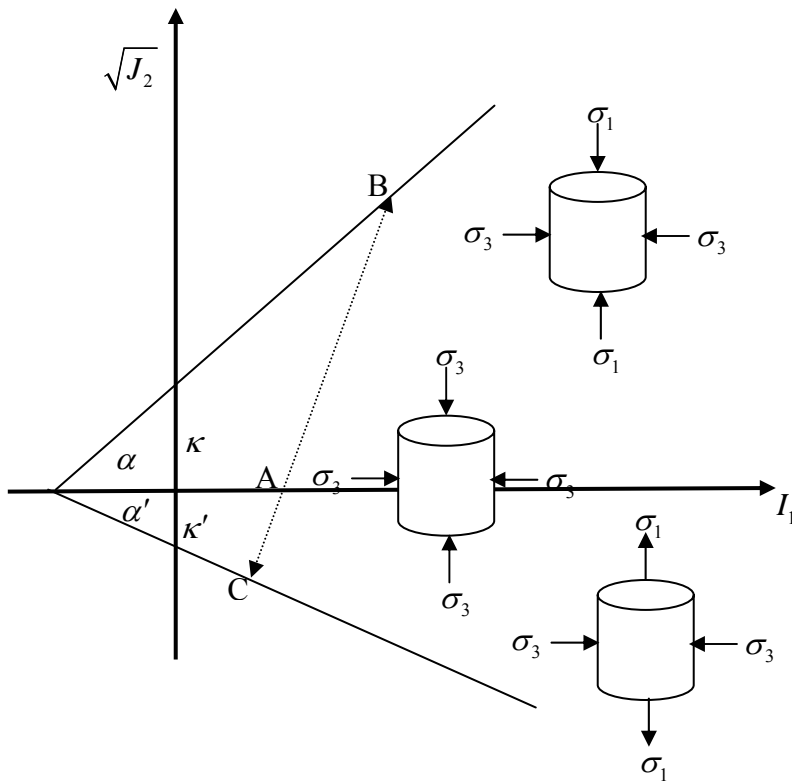


**Figure 5.2** The Influence of Stress Path on the  $I_1 - \sqrt{J_2}$  Plane.

### ***Viscoplastic Potential Energy Function***

Many researches indicated that HMA has nonassociated behavior which means that the direction of viscoplastic strain increment is not normal to yield surface. In addition, the experimental measurements show that using associated flow rule ( $g = f$ ) overestimates the dilation compared with experimental measurements (Masad et al., 2007). Hence, this study defines a potential energy function to be the same formula as the yield surface function and replaces  $\alpha$  with a smaller parameter  $\beta$  as shown in Eq. (5-8).

$$g = \tau - \beta I_1 \quad (5-8)$$

where,  $\beta$  is a material parameter.

In Eq. (5-3), the differential of potential energy function  $\frac{\partial g}{\partial \sigma_{ij}}$  has to be derived.

From Eq. (5-8),  $\frac{\partial g}{\partial \sigma_{ij}}$  can be shown as:

$$\frac{\partial g}{\partial \sigma_{ij}} = \frac{\partial \tau}{\partial \sigma_{ij}} - \beta \frac{\partial I_1}{\partial \sigma_{ij}} \quad (5-9)$$

The differential of  $I_1$  and  $\tau$  can be shown as:

$$\begin{aligned}
\frac{\partial I_1}{\partial \sigma_{ij}} &= \frac{1}{3} \delta_{ij} \\
\frac{\partial \tau}{\partial \sigma_{ij}} &= \frac{\frac{\partial J_2}{\partial \sigma_{ij}}}{4\sqrt{J_2}} \left[ 1 + \frac{1}{d} + \left(1 - \frac{1}{d}\right) \frac{J_3}{\sqrt{J_2^3}} \right] + \frac{\sqrt{J_2}}{2} \left(1 - \frac{1}{d}\right) \left( \frac{\frac{\partial J_3}{\partial \sigma_{ij}}}{\sqrt{J_2^3}} - \frac{3J_3}{2\sqrt{J_2^5}} \frac{\partial J_2}{\partial \sigma_{ij}} \right) \\
&= \frac{1}{2} \left[ \frac{\frac{\partial J_2}{\partial \sigma_{ij}}}{2\sqrt{J_2}} \left(1 + \frac{1}{d}\right) + \left( \frac{\frac{\partial J_3}{\partial \sigma_{ij}} J_2 - \frac{\partial J_2}{\partial \sigma_{ij}} J_3}{J_2^2} \right) \left(1 - \frac{1}{d}\right) \right]
\end{aligned} \tag{5-10}$$

where, the differential of  $J_2$  and  $J_3$  can be shown as:

$$\begin{aligned}
\frac{\partial J_2}{\partial \sigma_{ij}} &= 3S_{ij} \\
\frac{\partial J_3}{\partial \sigma_{ij}} &= \frac{27}{2} S_{ik} S_{kj} - 3J_2 \delta_{ij}
\end{aligned} \tag{5-11}$$

Substituting Eqs. (5-10) and (5-11) into (5-9), the differential of viscoplastic potential energy yields:

$$\frac{\partial g}{\partial \sigma_{ij}} = \frac{1}{2} \left[ \left( \frac{3S_{ij}}{2\sqrt{J_2}} \left(1 + \frac{1}{d}\right) + \left( \frac{\left( \frac{27}{2} S_{ik} S_{kj} - 3J_2 \delta_{ij} \right) J_2 - 3S_{ij} J_3}{J_2^2} \right) \left(1 - \frac{1}{d}\right) - \frac{2\beta}{3} \delta_{ij} \right) \right] \tag{5-12}$$

### ***Hardening Function***

The evolution of yield surface is defined by a hardening rule. Many hardening rules, such as isotropic hardening, kinematic hardening and combination hardening, are

presented to describe the evolution of yield surface. This study uses the isotropic hardening rule to evaluate the hardening behavior. In this study, the hardening function is an exponential function of effective viscoplastic strain based on the work of Dafalias (1990). The hardening function is shown as:

$$\kappa = \kappa_0 + \kappa_1 \left\{ 1 - \exp\left(-\kappa_2 (\varepsilon_e^{vp})\right) \right\} \quad (5-13)$$

where,  $\kappa_0$ ,  $\kappa_1$  and  $\kappa_2$  are material parameters, which defines the initial yield stress, the ultimate yield stress, and the shape of yield stress evolution, respectively.  $\varepsilon_e^{vp}$  is the effective viscoplastic strain.

For practical use, the hardening function must be related to an effective stress or an effective viscoplastic strain, which is a function of stress combination, and viscoplastic strain combination, respectively. Then, the hardening function can be correlated with any different loading test by plotting the effective stress against the effective viscoplastic strain. In other words, the relation between the effective stress and the effective viscoplastic strain should be reduced to a stress-strain curve for uniaxial stress test. Applying an uniaxial compression stress  $\sigma_{11}$ , the loading function  $F(\sigma_{ij})$  shown in Eq. (5-5) becomes a constant  $C$  times effective stress  $\sigma_e$  with power  $n$  (Chen and Han, 1988), shown as:

$$F(\sigma_{ij}) = \tau - \alpha I_1 = C \sigma_e^n \quad (5-14)$$

where,  $I_1 = \frac{1}{3} \sigma_{11}$  and  $\tau = \sigma_{11}$  for uniaxial compression case. Then, Eq. (5-14) becomes:



$$\left(1 - \frac{\alpha}{3}\right) \sigma_{11} = C \sigma_e^n \quad (5-15)$$

Observing Eq. (5-15), the constants  $C$  and  $n$  can be determined as:

$$C = \left(1 - \frac{\alpha}{3}\right) \quad (5-16)$$

$$n = 1$$

Substituting Eq. (5-16) into (5-14), the effective stress can be derived as:

$$\sigma_e = \frac{1}{C} (\tau - \alpha I_1) = \frac{3(\tau - \alpha I_1)}{3 - \alpha} \quad (5-17)$$

After obtaining the effective stress, this study employs the viscoplastic work rate per unit volume to derive the effective viscoplastic strain. The viscoplastic work rate can be presented as:

$$\dot{W}_{vp} = \sigma_{ij} \dot{\epsilon}_{ij}^{vp} = \sigma_{ij} \Gamma \langle \phi(f) \rangle \frac{\partial g}{\partial \sigma_{ij}} = \sigma_e \dot{\epsilon}_e^{vp} \quad (5-18)$$

where,  $\dot{\epsilon}_e^{vp}$  is the effective viscoplastic strain rate. From Eq. (5-3),  $\Gamma \langle \phi(f) \rangle$  can be obtained as:

$$\Gamma \langle \phi(f) \rangle = \frac{\sqrt{\dot{\epsilon}_{ij}^{vp} \dot{\epsilon}_{ij}^{vp}}}{\sqrt{\frac{\partial g}{\partial \sigma_{ij}} \frac{\partial g}{\partial \sigma_{ij}}}} \quad (5-19)$$

In Eq. (5-19), the term  $\frac{\partial g}{\partial \sigma_{ij}} \frac{\partial g}{\partial \sigma_{ij}}$  subjected to a compression uniaxial stress can be

derived as:

$$\frac{\partial g}{\partial \sigma_{ij}} \frac{\partial g}{\partial \sigma_{ij}} = \left(1 - \frac{\beta}{3}\right)^2 + 2\left(\frac{1}{2} + \frac{\beta}{3}\right)^2$$

and

$$\sigma_{ij} \frac{\partial g}{\partial \sigma_{ij}} = \sigma_{11} \left(1 - \frac{\beta}{3}\right) \tag{5-20}$$

Substituting Eqs. (5-20) and (5-19) into (5-18), the viscoplastic work rate can be shown

as:

$$\dot{W}_{vp} = \frac{\sigma_{11} \left(1 - \frac{\beta}{3}\right)}{\sqrt{\left(1 - \frac{\beta}{3}\right)^2 + 2\left(\frac{1}{2} + \frac{\beta}{3}\right)^2}} \sqrt{\dot{\epsilon}_{ij}^{vp} \dot{\epsilon}_{ij}^{vp}} = \sigma_e \dot{\epsilon}_e^{vp} = \sigma_{11} \dot{\epsilon}_e^{vp} \tag{5-21}$$

Then, the effective viscoplastic rate can be derived as:

$$\dot{\epsilon}_e^{vp} = \frac{\left(1 - \frac{\beta}{3}\right)}{\sqrt{\left(1 - \frac{\beta}{3}\right)^2 + 2\left(\frac{1}{2} + \frac{\beta}{3}\right)^2}} \sqrt{\dot{\epsilon}_{ij}^{vp} \dot{\epsilon}_{ij}^{vp}} = \frac{1}{\sqrt{1 + 2\left(\frac{\frac{1}{2} + \frac{\beta}{3}}{1 - \frac{\beta}{3}}\right)^2}} \sqrt{\dot{\epsilon}_{ij}^{vp} \dot{\epsilon}_{ij}^{vp}} \tag{5-22}$$

## THE NUMERICAL ALGORITHM OF NONLINEAR VISCOELASTIC-VISCOPLASTIC MODEL

In the finite element method, the strain rate is presented as time increment formulation. For small strain theory, the total strain and incremental strain can be decomposed into viscoelastic and viscoplastic components as shown in Eq. (5-23a). Moreover, the effective viscoplastic strain can be presented as incremental formulation

shown as Eq. (5-23b). The current stress is equal to previous stress plus current stress increment Eq. (5-23c).

$$\boldsymbol{\varepsilon}_{ij}^t = \boldsymbol{\varepsilon}_{ij}^{nve,t} + \boldsymbol{\varepsilon}_{ij}^{vp,t} = \boldsymbol{\varepsilon}_{ij}^{t-\Delta t} + \Delta \boldsymbol{\varepsilon}_{ij}^t = \boldsymbol{\varepsilon}_{ij}^{nve,t-\Delta t} + \boldsymbol{\varepsilon}_{ij}^{vp,t-\Delta t} + \Delta \boldsymbol{\varepsilon}_{ij}^{nve,t} + \Delta \boldsymbol{\varepsilon}_{ij}^{vp,t} \quad (5-23a)$$

$$\boldsymbol{\varepsilon}_e^{vp,t} = \boldsymbol{\varepsilon}_e^{vp,t-\Delta t} + \Delta \boldsymbol{\varepsilon}_e^{vp,t} \quad (5-23b)$$

$$\boldsymbol{\sigma}_{ij}^t = \boldsymbol{\sigma}_{ij}^{t-\Delta t} + \Delta \boldsymbol{\sigma}_{ij}^t \quad (5-23c)$$

In terms of nonlinear viscoelastic increment, the viscoelastic bulk and deviatoric strain increments can be shown in Eqs. (2-10) and (2-11), respectively. The variables  $q_{ij,n}^{t-\Delta t}$  and  $q_{kk,n}^{t-\Delta t}$  in Eqs. (2-10) and (2-11) are the shear and volumetric hereditary integrals, respectively, for every Prony series term  $n$  at previous time  $t - \Delta t$ . The hereditary integrals are updated at the end of every converged time increment, which will be used for the next time increment. The formulation of shear and volumetric hereditary integrals are shown in Eqs. (2-14) and (2-15), respectively.

For viscoplastic strain increment, this study employs Perzyna's model to describe the viscoplastic increment. The viscoplastic strain incremental formulation of Perzyna's model is shown as:

$$\Delta \boldsymbol{\varepsilon}_{ij}^{vp,t} = \Gamma \langle \phi(f) \rangle \frac{\partial g}{\partial \Delta \boldsymbol{\sigma}_{ij}} \Delta t = \Delta \gamma^{vp,t} \frac{\partial g}{\partial \Delta \boldsymbol{\sigma}_{ij}} \quad (5-24)$$

In Eq. (5-24), the viscoplastic multiplier can be shown as:

$$\Delta \gamma^{vp,t} = \Delta t \Gamma \langle \phi(f) \rangle = \Delta t \Gamma \left( \frac{f(\boldsymbol{\sigma}_{ij}^t, \boldsymbol{\varepsilon}_e^{vp,t})}{\sigma_y^0} \right)^N \quad (5-25)$$

Substituting Eqs. (5-22) and (5-24) into (5-23b), the effective viscoplastic strain increment can be shown as:

$$\varepsilon_e^{vp,t} = \varepsilon_e^{vp,t-\Delta t} + \Delta \varepsilon_e^{vp,t} = \varepsilon_e^{vp,t-\Delta t} + \frac{\Delta \gamma^{vp,t}}{\sqrt{1+2\left(\frac{\frac{1+\beta}{2} + \frac{\beta}{3}}{1-\frac{\beta}{3}}\right)^2}} \sqrt{\frac{\partial g}{\partial \Delta \sigma_{ij}} \frac{\partial g}{\partial \Delta \sigma_{ij}}} \quad (5-26)$$

The nonlinear viscoelastic-viscoplastic algorithm starts at a trial stress. In this study, the initial trial stress is assumed as nonlinear viscoelastic only and the trial stress is shown in Eqs. (2-16) and (2-17). Once the trial stress exceeds the yield surface, the calculation of viscoplastic strain increment is needed. On the other hand, the material only has viscoelastic strain increment and the viscoplastic strain increment is equal to 0, if the trial stress is not beyond the yield surface.

Alfano et al. (2001) developed an equivalent to the consistency condition for the plastic problem. From Eq. (5-25), the trial yield surface based on the trial stress can be shown as:

$$f^{tr} = \sigma_y^0 \left( \frac{\Delta \gamma^{vp,t}}{\Delta t \Gamma} \right)^{1/N} \quad (5-27)$$

A dynamic yield surface function  $\chi$  can be defined as:

$$\chi = \tau^{tr} - \alpha I_1^{tr} - \kappa \left( \left( \varepsilon_e^{vp,t} \right) \right) - \sigma_y^0 \left( \frac{\Delta \gamma^{vp,t}}{\Delta t \Gamma} \right)^{1/N} \quad (5-28)$$

This study uses a numerical scheme Newton-Raphson to calculate  $\Delta \gamma^{vp,t}$ . Once obtaining  $\Delta \gamma^{vp,t}$ , the viscoplastic strain increment can be determined by Eq. (5-24). In

Newton-Raphson scheme, the differential of  $\chi$  with  $\Delta\gamma^{vp}$  should be derived and it is shown as:

$$\begin{aligned}\frac{\partial\chi}{\partial\Delta\gamma^{vp}} &= -\frac{\partial\kappa}{\partial\Delta\varepsilon_e^{vp}} \frac{\partial\Delta\varepsilon_e^{vp}}{\partial\Delta\gamma^{vp}} - \frac{\sigma_y^0}{\Delta t \Gamma N} \left( \frac{\Delta\gamma^{vp}}{\Delta t \Gamma} \right)^{\frac{1}{N}-1} \\ &= -\frac{\partial\kappa}{\partial\Delta\varepsilon_e^{vp}} \frac{\partial\Delta\varepsilon_e^{vp}}{\partial\Delta\gamma^{vp}} - \frac{\sigma_y^0}{\Delta\gamma^{vp} N} \left( \frac{\Delta\gamma^{vp}}{\Delta t \Gamma} \right)^{\frac{1}{N}}\end{aligned}\quad (5-29)$$

The differential of hardening function  $\kappa$  with  $\Delta\varepsilon_e^{vp,t}$  can be shown as:

$$\begin{aligned}\frac{\partial\kappa}{\partial\Delta\varepsilon_e^{vp,t}} &= \frac{\partial \left[ \kappa_1 \left\{ 1 - \exp \left( -\kappa_2 \left( \varepsilon_e^{vp,t-\Delta t} + \Delta\varepsilon_e^{vp,t} \right) \right) \right\} \right]}{\partial\Delta\varepsilon_e^{vp,t}} \\ &= \kappa_1 \kappa_2 \exp \left( -\kappa_2 \left( \varepsilon_e^{vp,t-\Delta t} + \Delta\varepsilon_e^{vp,t} \right) \right)\end{aligned}\quad (5-30)$$

The  $\frac{\partial\Delta\varepsilon_e^{vp}}{\partial\Delta\gamma^{vp}}$  in Eq. (5-29) can be shown as:

$$\frac{\partial\Delta\varepsilon_e^{vp,t}}{\partial\Delta\gamma^{vp,t}} = \frac{1}{\sqrt{1+2 \left( \frac{\frac{1}{2} + \frac{\beta}{3}}{1 - \frac{\beta}{3}} \right)^2}} \sqrt{\frac{\partial g}{\partial\Delta\sigma_{ij}} \frac{\partial g}{\partial\Delta\sigma_{ij}}}\quad (5-31)$$

Substitute Eqs. (5-30) and (5-31) into (5-29). The  $\frac{\partial\chi}{\partial\Delta\gamma^{vp}}$  can be shown as:

$$\frac{\partial\chi}{\partial\Delta\gamma^{vp}} = -\frac{\kappa_1 \kappa_2 \exp \left( -\kappa_2 \left( \varepsilon_e^{vp,(t-\Delta t)} + \Delta\varepsilon_e^{vp,(t)} \right) \right)}{\sqrt{1+2 \left( \frac{\frac{1}{2} + \frac{\beta}{3}}{1 - \frac{\beta}{3}} \right)^2}} \sqrt{\frac{\partial g}{\partial\sigma_{ij}} \frac{\partial g}{\partial\sigma_{ij}}} - \frac{\sigma_y^0}{\Delta\gamma^{vp} N} \left( \frac{\Delta\gamma^{vp}}{\Delta t \Gamma} \right)^{\frac{1}{N}}\quad (5-32)$$

At the (k+1) iteration, the viscoplastic multiplier is calculated by:

$$(\Delta\gamma^{vp})^{k+1} = (\Delta\gamma^{vp})^k - \left[ \left( \frac{\partial\chi}{\partial\Delta\gamma^{vp}} \right)^k \right]^{-1} \chi^k \quad (5-33)$$

Because both of the nonlinear viscoelastic and viscoplastic strain increments are function of current stress, this study employs the recursive-iteration algorithm with Newton-Raphson method by minimizing the residual strain to obtain the current stress. This algorithm applies iteration at both of material and structure levels to minimize the error; otherwise, very small increments are required. The residual strain is defined as:

$$R_{ij}^t = \Delta\varepsilon_{ij}^{nve,t} + \Delta\varepsilon_{ij}^{vp,t} - \Delta\varepsilon_{ij}^t = \Delta\varepsilon_{ij}^{nve,t} + \Delta\gamma^{vp,t} \frac{\partial g}{\partial\Delta\sigma_{ij}} - \Delta\varepsilon_{ij}^t \quad (5-34)$$

In Newton-Raphson method, the stress increment at the (k+1) iteration is calculated by:

$$(\Delta\sigma_{ij}^t)^{k+1} = (\Delta\sigma_{ij}^t)^k - \left[ \left( \frac{\partial R_{ij}^t}{\partial\Delta\sigma_{kl}^t} \right)^k \right]^{-1} (R_{kl}^t)^k \quad (5-35)$$

where, the differential of  $R$  is the consistent tangent compliance and can be derived as:

$$\frac{\partial R_{ij}^t}{\partial\Delta\sigma_{kl}^t} = \frac{\partial\Delta\varepsilon_{ij}^{nve,t}}{\partial\Delta\sigma_{kl}^t} + \frac{\partial\Delta\varepsilon_{ij}^{vp,t}}{\partial\Delta\sigma_{kl}^t} \quad (5-36)$$

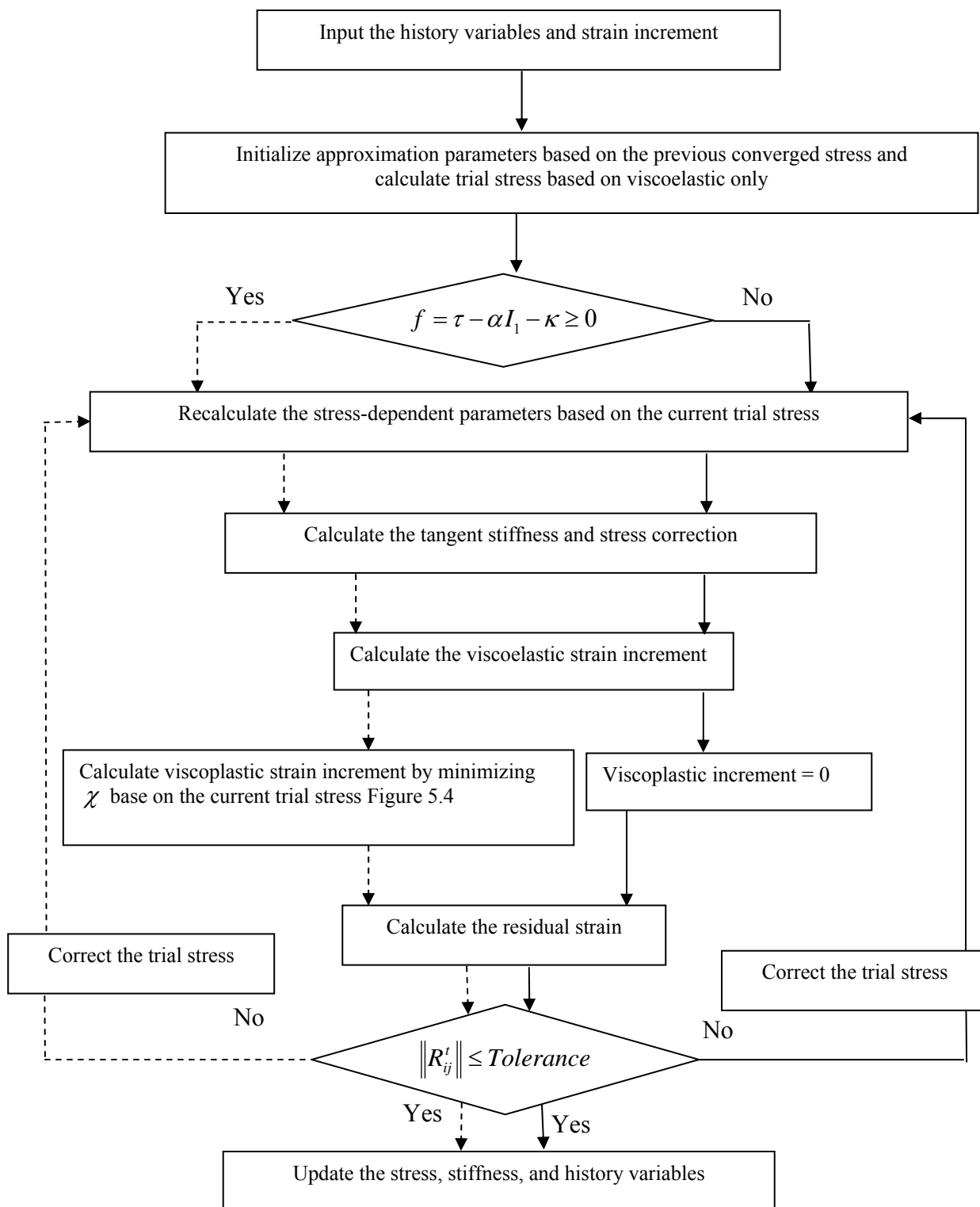
where,  $\frac{\partial\Delta\varepsilon_{ij}^{nve}}{\partial\Delta\sigma_{kl}}$  is the nonlinear viscoelastic tangent compliance which is given in Eq. (2-

19). The viscoplastic tangent compliance is derived as in Eq. (5-37).

$$\begin{aligned}
\frac{\partial \Delta \varepsilon_{ij}^{vp,t}}{\partial \Delta \sigma_{kl}} &= \frac{\partial \left( \Delta \gamma^{vp,t} \frac{\partial g}{\partial \Delta \sigma_{ij}} \right)}{\partial \Delta \sigma_{kl}} \\
&= \frac{\partial \Delta \gamma^{vp,t}}{\partial \Delta \sigma_{kl}} \frac{\partial g}{\partial \Delta \sigma_{ij}} + \Delta \gamma^{vp,t} \frac{\partial g}{\partial \Delta \sigma_{ij} \partial \Delta \sigma_{kl}} \\
&= \frac{\Delta t \Gamma N}{\sigma_y^0} \left( \frac{f}{\sigma_y^0} \right)^{N-1} \frac{\partial f}{\partial \Delta \sigma_{kl}} \frac{\partial g}{\partial \Delta \sigma_{ij}} + \Delta t \Gamma \left( \frac{f}{\sigma_y^0} \right)^N \frac{\partial g}{\partial \Delta \sigma_{ij} \partial \Delta \sigma_{kl}}
\end{aligned} \tag{5-37}$$

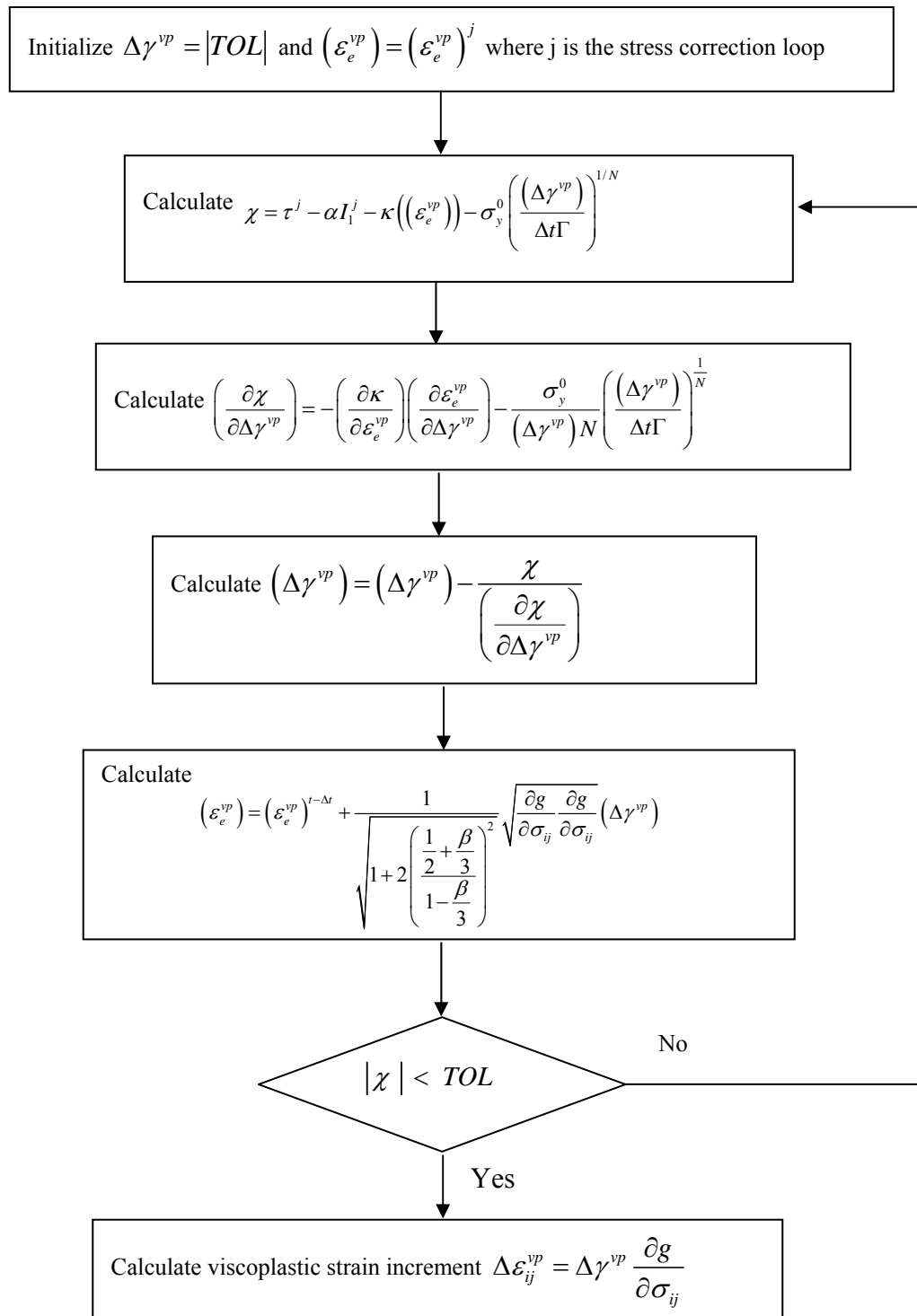
If the stress does not exceed the yield surface, the material compliance will only include the nonlinear viscoelastic compliance  $\frac{\partial \Delta \varepsilon_{ij}^{nve}}{\partial \Delta \sigma_{kl}}$ ; if it does, the material compliance will include both the nonlinear viscoelastic compliance  $\frac{\partial \Delta \varepsilon_{ij}^{nve}}{\partial \Delta \sigma_{kl}}$  and the viscoplastic compliance  $\frac{\partial \Delta \varepsilon_{ij}^{vp}}{\partial \Delta \sigma_{kl}}$ . The nonlinear viscoelastic-viscoplastic algorithm is shown as

Figure 5.3. The flowchart of viscoplastic strain increment calculation using Newton-Raphson Method is shown as Figure 5.4.



**Figure 5.3** The Flowchart of Nonlinear Viscoelastic-Viscoplastic Implementation.





**Figure 5.4** The Flowchart of Newton-Raphson Method for Viscoplastic Strain Increments.

## VERIFICATION OF FINITE ELEMENT IMPLEMENTATION

This section conducts a case with two uniaxial step loading shown in Figure 5.5 to verify the nonlinear viscoelastic-viscoplastic implementation. A closed form solution of nonlinear viscoelastic (Modified Superposition Principle (MSP)) is employed to obtain the solution of viscoelastic component. A numerical solver using Newton-Raphson method supported within the math software Mathematica™ is used to find the numerical solution of viscoplastic component. Then, the results of MSP and Mathematica™ are added and compared with the total response calculated by the FE implementation. The viscoelastic and viscoplastic material parameters are shown in Tables 5.1 and 5.2, respectively. The MSP solutions for first and second loading step are shown as:

$$\varepsilon_r = \left[ g_0^a D_0 + g_1^a g_2^a \Delta D \left( \frac{t}{a_s^a} \right) \right] \sigma^a \quad \text{For } 0 < t < t_a \quad (5-38)$$

$$\varepsilon_r = g_0^b D_0 \sigma_b + g_1^b \left[ g_2^a \sigma_a \Delta D(\psi) + (g_2^b \sigma_b - g_2^a \sigma_a) \Delta D \left( \frac{t - t_a}{a_s^b} \right) \right] \quad \text{For } t_a < t < t_b \quad (5-39)$$

In terms of viscoplastic component, for uniaxial stress with  $\beta=0$ , the viscoplastic strain can be simplified as:

$$\Delta \varepsilon_{11}^{vp,t} = \Delta \gamma^{vp,t} \frac{\partial g}{\partial \Delta \sigma_{11}} = \Delta \gamma^{vp,t} \quad (5-40)$$

The effective viscoplastic strain increment with  $\beta=0$  can also be simplified as:

$$\Delta \varepsilon_e^{vp,t} = \frac{\Delta \gamma^{vp,t}}{\sqrt{1 + 2(0.5)^2}} \sqrt{\frac{\partial g}{\partial \Delta \sigma_{ij}} \frac{\partial g}{\partial \Delta \sigma_{ij}}} = \frac{\Delta \gamma^{vp,t}}{\sqrt{1.5}} \sqrt{1.5} = \Delta \gamma^{vp,t} \quad (5-41)$$

The dynamic yield surface for uniaxial stress with  $\beta=0$  can be shown as:

$$\begin{aligned} \chi &= \tau - \alpha I_1 - \kappa_0 - \kappa_1 \left( 1 - \exp \left( -\kappa_2 \left( \varepsilon_e^{vp,(t-\Delta t)} + \Delta \varepsilon_e^{vp,(t)} \right) \right) \right) - \sigma_y^0 \left( \frac{\Delta \gamma^{vp,t}}{\Delta t \Gamma} \right)^{1/N} \\ &= \tau - \alpha I_1 - \kappa_0 - \kappa_1 \left( 1 - \exp \left( -\kappa_2 \left( \Delta \gamma^{vp,t-\Delta t} + \Delta \gamma^{vp,t} \right) \right) \right) - \sigma_y^0 \left( \frac{\Delta \gamma^{vp,t}}{\Delta t \Gamma} \right)^{1/N} \cong 0 \end{aligned} \quad (5-42)$$

Once the viscoplastic multiplier  $\Delta \gamma^{vp,t}$  is obtained by solving Eq. (5-42), the viscoplastic strain can be calculated which is equal to  $\Delta \gamma^{vp,t}$ . This study uses a numerical solver supported within Mathematica<sup>TM</sup> to solve Eq. (5-42) to obtain  $\Delta \gamma^{vp,t}$ .

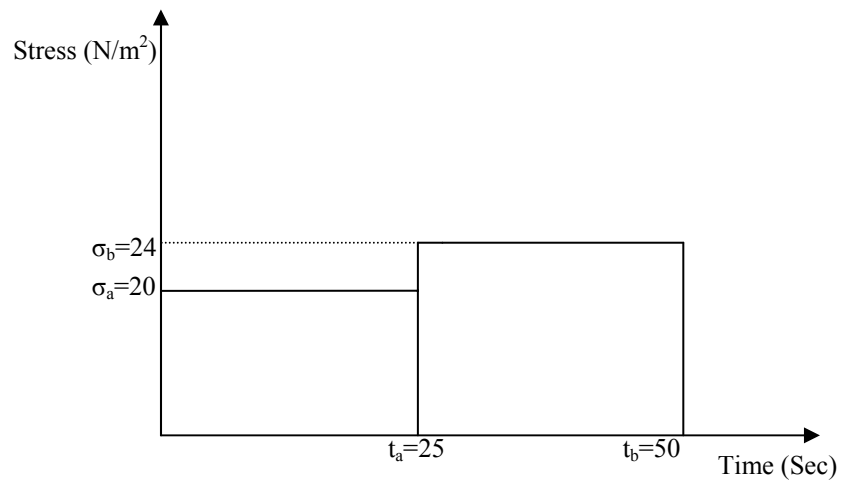
The result of comparison is shown in Figure 5.6. This figure shows that the FE can fit the results, calculated by Mathematica<sup>TM</sup> and MSP, very well. Figure 5.7 is the error between FE results and the calculated results. This figure shows that the error decreases with time. The error increases rapidly when the stress changes, because the FE needs more time increment to obtain the accuracy solution. The maximum error is around 0.4%.

**Table 5.1** Viscoelastic Material Parameters (Lai and Bakker, 1996).

n	$\lambda_n$ (Sec <sup>-1</sup> )	$D_n * 10^{-6}$ (MPa <sup>-1</sup> )
1	1	23.6358
2	10 <sup>-1</sup>	5.6602
3	10 <sup>-2</sup>	14.8405
4	10 <sup>-3</sup>	18.8848
5	10 <sup>-4</sup>	28.5848
6	10 <sup>-5</sup>	40.0569
7	10 <sup>-6</sup>	60.4235
8	10 <sup>-7</sup>	79.6477
9	10 <sup>-8</sup>	162.1790
$D_0$	270.9*10 <sup>-6</sup> (MPa <sup>-1</sup> )	

**Table 5.2** Viscoplastic Material Parameters.

Parameter	
$N$	2.18
$\alpha$	0
$\beta$	0
$\kappa_0$	20 (Pa)
$\kappa_1$	50 (Pa)
$\kappa_2$	2
$\sigma_y^0$	1 (Pa)
$d$	0.778
$\Gamma$	0.5 (Sec <sup>-1</sup> )

**Figure 5.5** The Schematic Diagram of Loading.

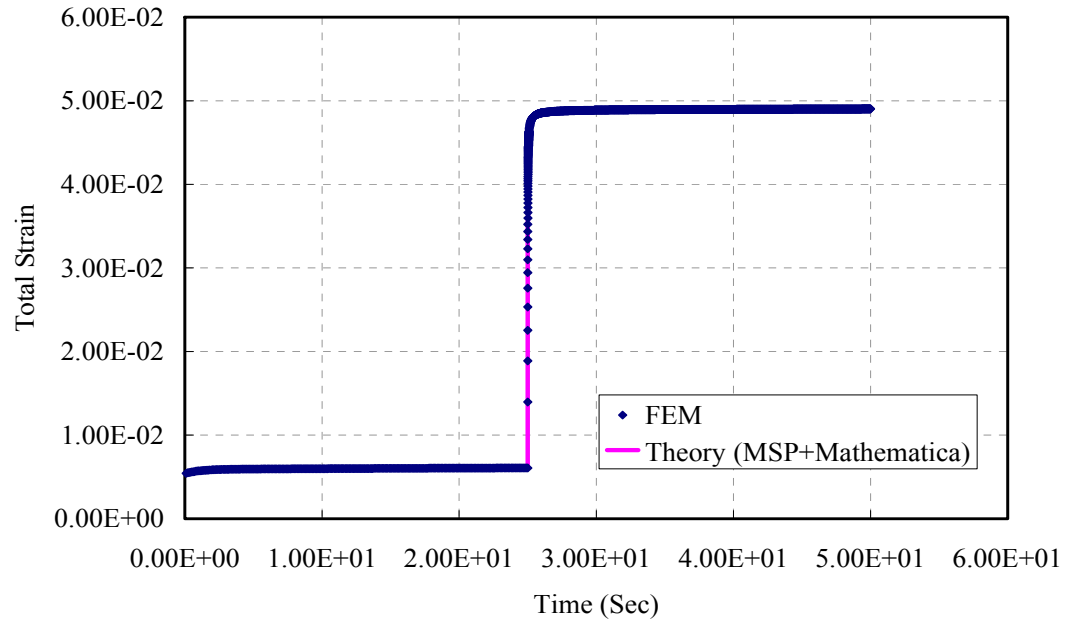


**Figure 5.6** The Total Strain Comparison Between FE Solution and Calculated Results.

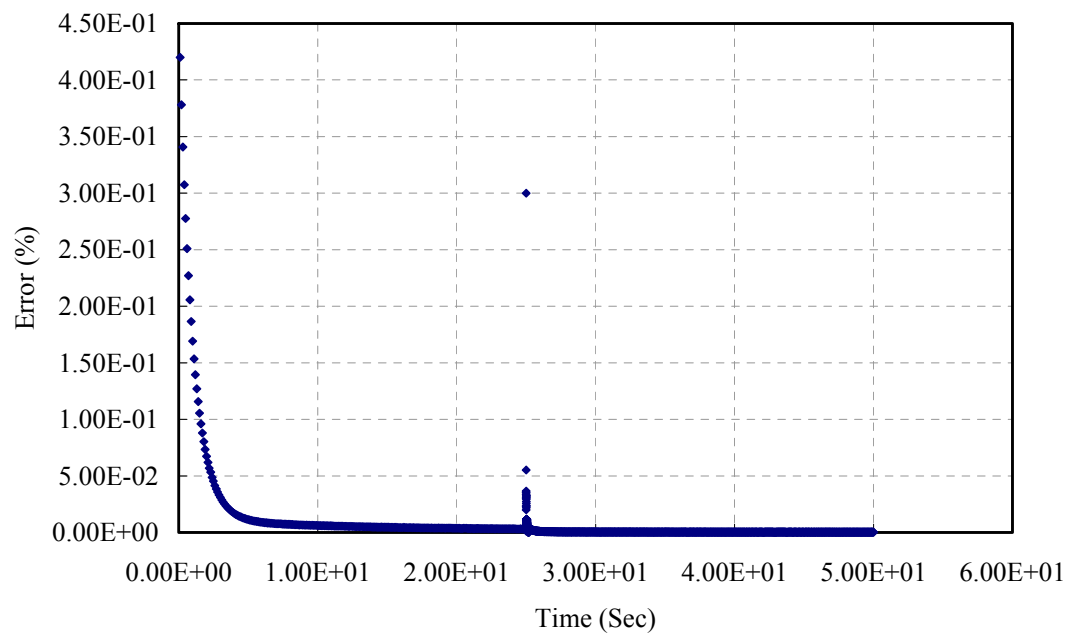


**Figure 5.7** The Error of Total Strain Between FE Solution and Calculated Results.

## PARAMETRIC ANALYSIS

A uniaxial loading condition is used to conduct parametric analysis in order to examine the influence of constitutive model parameters on the material response. The parameters that are considered here are the yield surface parameters  $\alpha$  and  $d$ ; viscoplastic potential energy parameter  $\beta$ ; flow function parameters  $\Gamma$  and  $N$ ; and hardening function parameters  $\kappa_0$ ,  $\kappa_1$ , and  $\kappa_2$ .

The yield surface parameter  $\alpha$  controls the slope of yield surface. Increasing  $\alpha$  leads to an increase in yield stress at a given confinement stress. The effect of this parameter is shown in Figure 5.8. This figure shows that decreasing  $\alpha$  will increase the strain at same stress level, because the material is easier to reach yield surface and contains more viscoplastic strain. The yield surface parameter  $d$  determines the shape of yield surface in the deviatoric plane. This parameter represents the ratio of yield stress in extension versus compression at the same confinement stress. In the compression case,  $d$  does not influence the material behavior; while the effect of  $d$  shows under tension as a decrease in  $d$  increases the yielding strain at same stress level. The effect shows in Figure 5.9.

The viscoplastic potential energy parameter  $\beta$  controls the slope of viscoplastic potential energy, which will affect the direction of viscoplastic strain increment. This parameter reflects the dilative potential and influences the portion of volumetric and deviatoric strain. Figure 5.10 shows the effect of  $\beta$ . This figure shows that at the beginning of loading, the volumetric strain of the material tends to be positive because the material behavior is viscoelastic; when the loading increases gradually, the material

contains viscoplastic strain and dilates, which makes the volumetric strain tends to be negative. This figure demonstrates that an increase in  $\beta$  causes more volumetric dilation.

The flow function parameters  $\Gamma$  controls the magnitude of viscoplastic strain increment; while  $N$  dominates the shape of overstress function. Increasing  $\Gamma$  will lead to more viscoplastic strain increment. In addition, increasing  $N$  will cause more nonlinearity of the overstress function and viscoplastic strain increment. Figure 5.11 shows the effect of  $\Gamma$  and illustrates that increasing  $\Gamma$  will induce more viscoplastic strain increment within same stress increment. Figure 5.12 shows that increasing  $N$  will cause more nonlinearity in the viscoplastic strain increment.

This study employs the exponential hardening function which is a function of effective viscoplastic strain with parameters  $\kappa_0$ ,  $\kappa_1$ , and  $\kappa_2$ .  $\kappa_0$  controls the stress which starts to have viscoplastic behavior;  $\kappa_1$  dominates the ultimate yield stress; and  $\kappa_2$  reflects the shape of hardening evolution. Figures 5.13, 5.14 and 5.15 are the effect of  $\kappa_0$ ,  $\kappa_1$ , and  $\kappa_2$ , respectively. Increasing  $\kappa_0$  will increase the yield stress, in the other words, the stress that material start to contain viscoplastic strain is higher with larger  $\kappa_0$  value. Figure 5.13 shows that the viscoplastic strain takes place at a higher stress level with larger  $\kappa_0$ , while decreasing  $\kappa_0$  leads the decreasing of the stress that induces the viscoplastic. The hardening function is related to overstress function which affects the magnitude of viscoplastic strain increment. Increasing  $\kappa_1$  will increase the hardening  $\kappa$  and then decrease the viscoplastic strain increment. Figure 5.14 also indicates that



increasing  $\kappa_1$  will decrease viscoplastic strain at same stress level. The hardening parameter  $\kappa_2$  reflects the nonlinearity of hardening and of viscoplastic strain increment. Figure 5.15 illustrates that increasing  $\kappa_2$  will increase the nonlinearity of viscoplastic strain increment, and it will also induce more nonlinearity of material behavior.

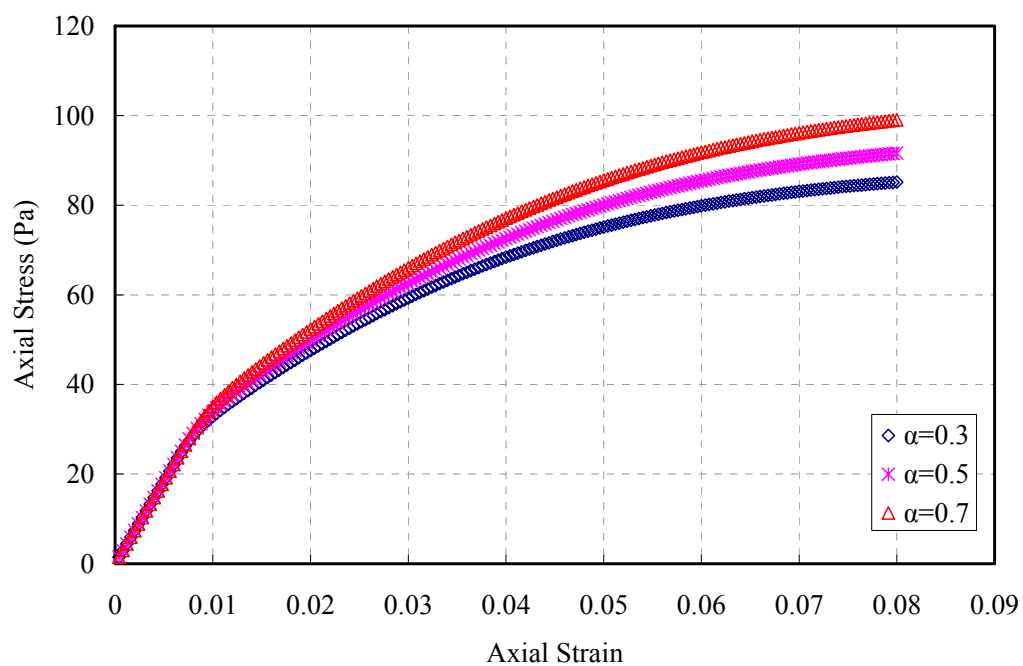
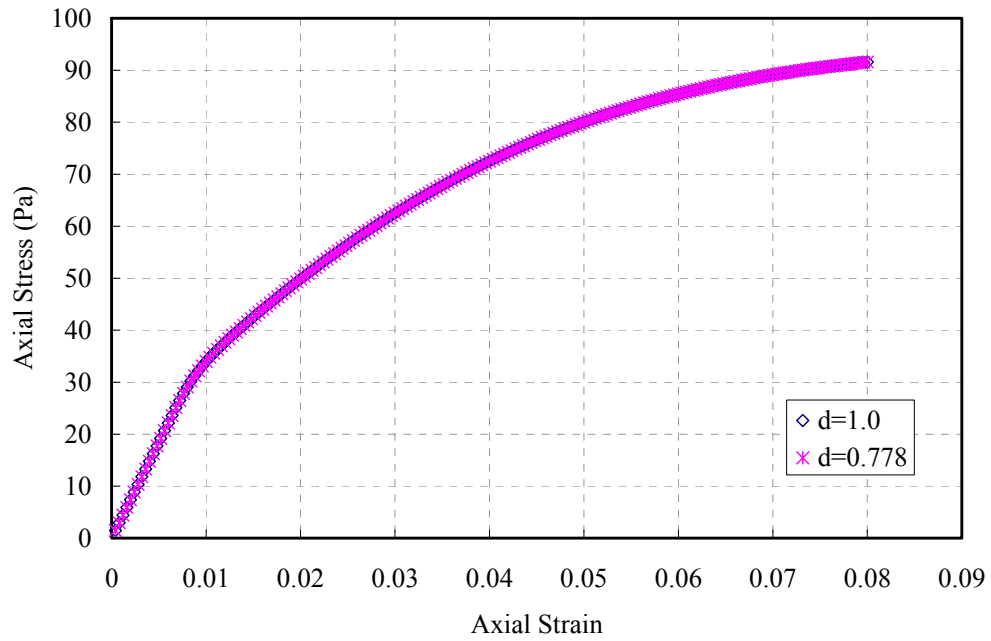
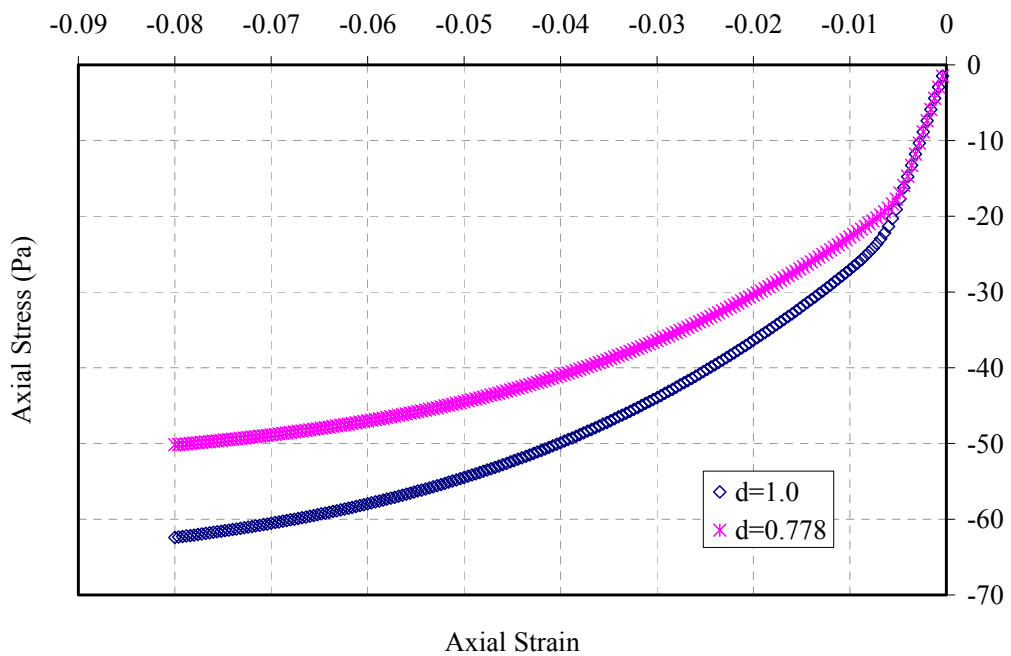


**Figure 5.8** The Effect of Yield Surface Parameter  $\alpha$  .



(a) Uniaxial Compression Case



(b) Uniaxial Tension Case

**Figure 5.9** The Effect of Yield Surface Parameter  $d$ .

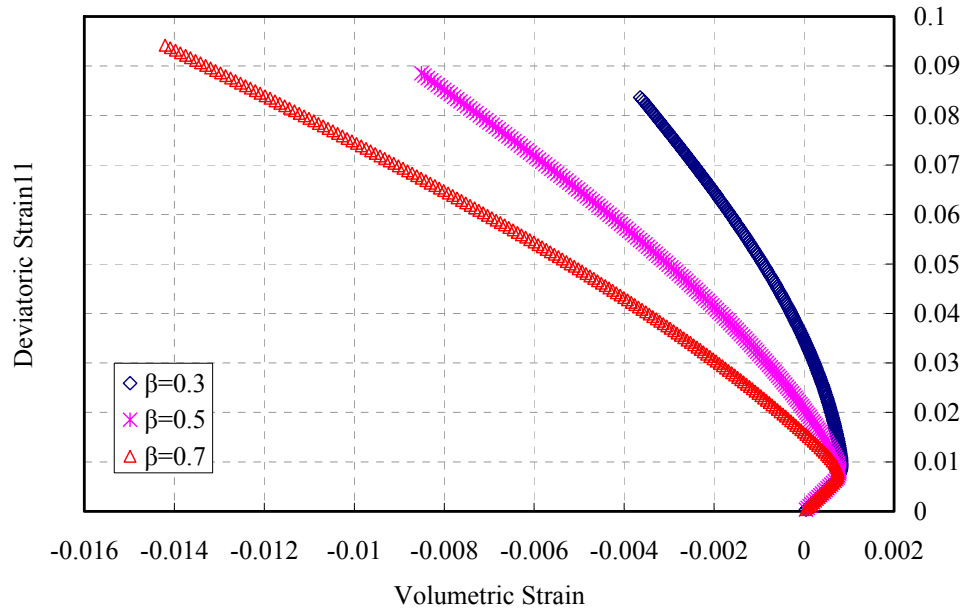


**Figure 5.10** The Effect of Viscoplastic Potential Energy Parameter  $\beta$ .

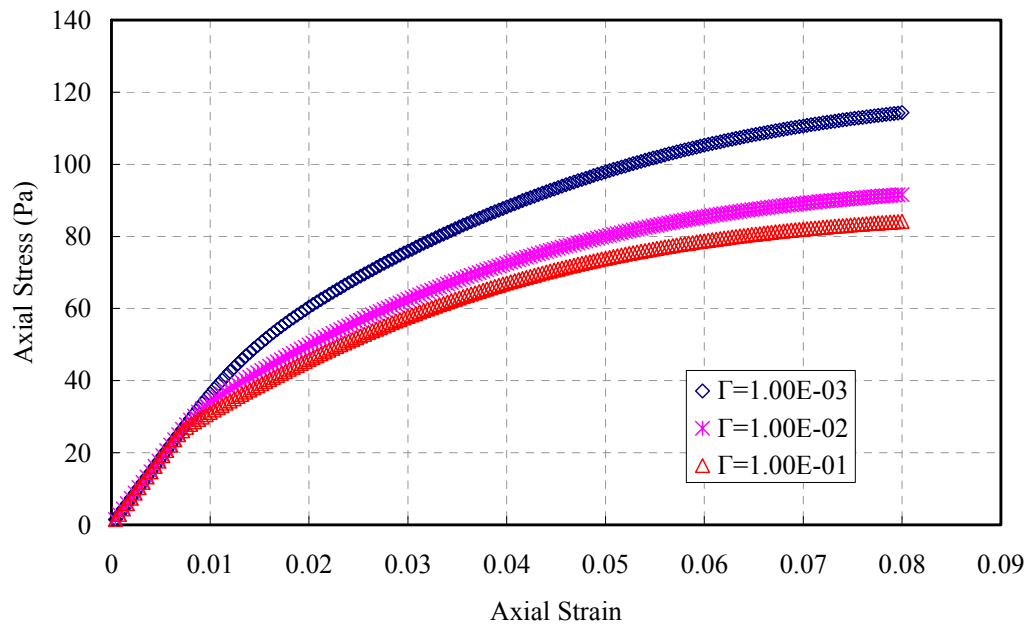


**Figure 5.11** The Effect of Flow Function Parameter  $\Gamma$ .

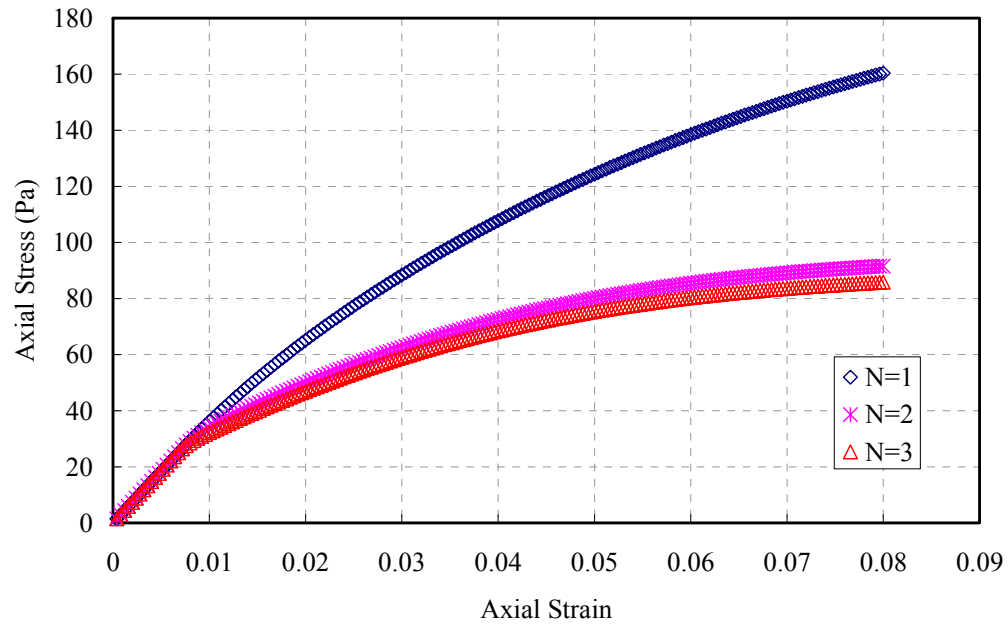


**Figure 5.12** The Effect of Flow Function Parameter  $N$ .

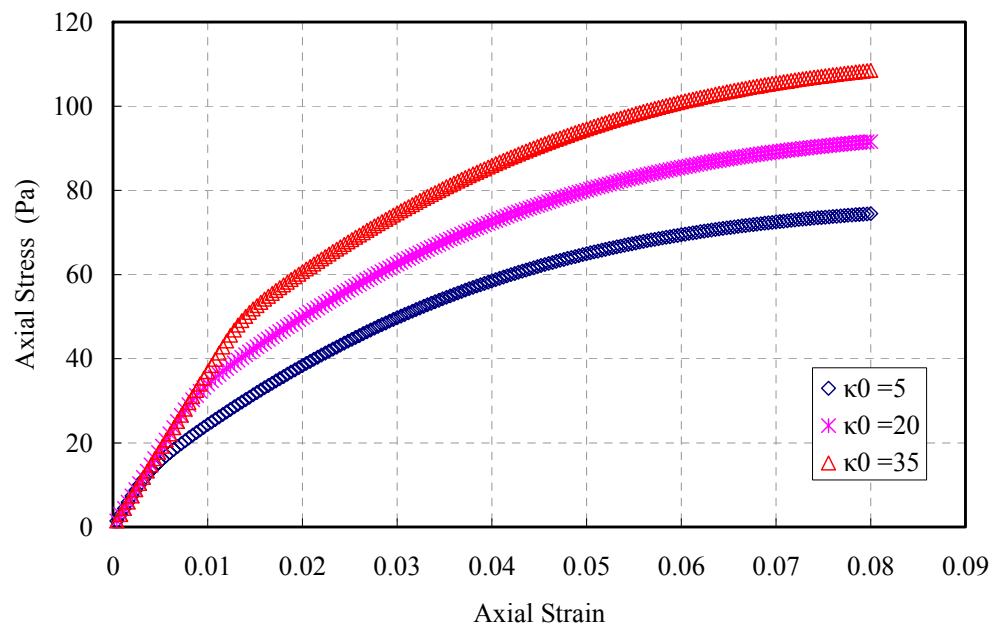


**Figure 5.13** The Effect of Hardening Function Parameters  $\kappa_0$ .

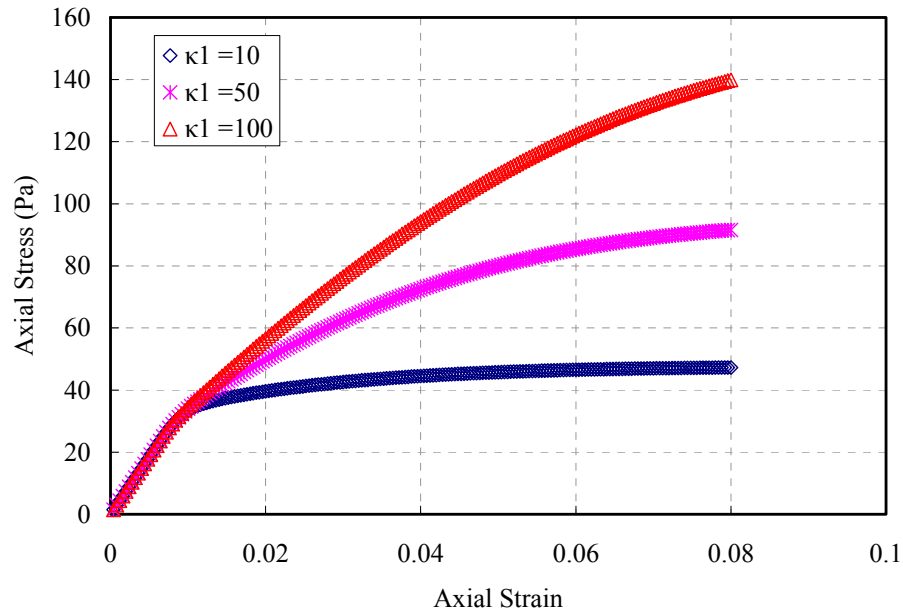


**Figure 5.14** The Effect of Hardening Function Parameters  $\kappa_1$ .

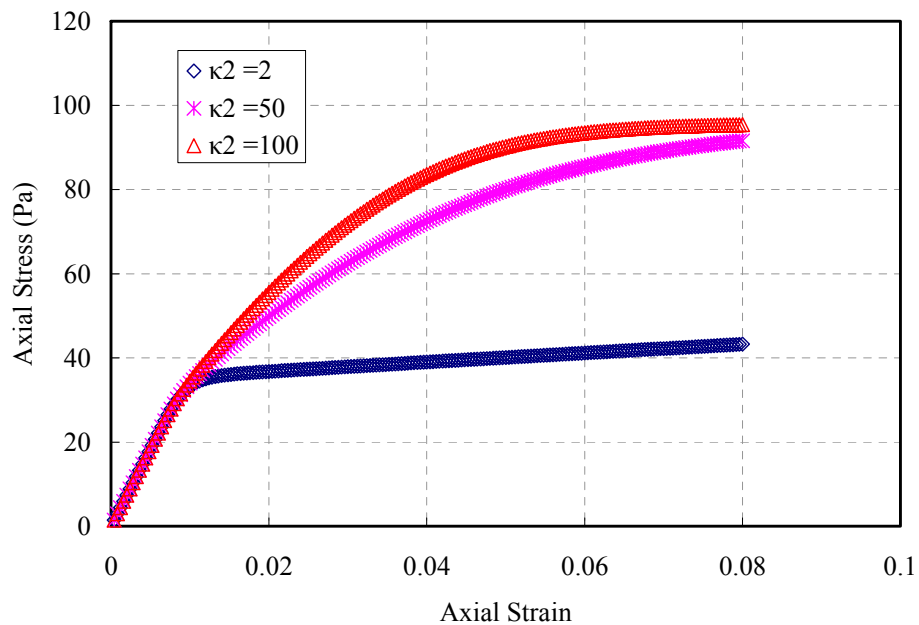


**Figure 5.15** The Effect of Hardening Function Parameters  $\kappa_2$ .

## FINITE ELEMENT SIMULATION

A finite element model of a pavement section is developed in order to demonstrate the response of asphalt pavement under loading using different constitutive model parameters. A one lane pavement section with 82 inches width is simulated. The simulated loading is a single axial loading and the distance between two wheels is 30 inches. The asphalt mix layer has a thickness of 6 inches; the base layer has a thickness of 6 inches, and the subgrade layer has 6 inches. The FE model is shown in Figure 5.16. Because the loading condition is symmetric in the wheel axis direction, the FE model includes only half of the pavement section and fixes the boundary condition of y direction on left hand side. The boundary condition on the right hand side is fixed with all degrees of freedom. The finite element domain is 42, 40, and 18 inches in width, length and depth, respectively with infinite boundary on depth and driving direction. The loading area is  $6 \times 8 \text{ in}^2$  with tire pressure 100 psi. The nonlinear viscoelastic-viscoplastic material is applied for HMA layer, while the base and subgrade layer are elastic materials. The elastic material properties for base and subgrade layer are shown in Figure 5.16.

The analysis includes conducting sensitivity analysis of finite element size in order to determine the finite element mesh with accurate solution. Three meshes with different element sizes are shown in Figure 5.17. The finite element size and total finite element number are shown in Table 5.3. The sensitivity analysis was conducted by applying a step loading 100 psi with duration time 25 sec, and compared the calculated results of each mesh. Figures 5.18 and 5.19 are the strain and Von Mises results at the

HMA layer surface located in the center of loading for different mesh sizes. It can be seen that there is a very small difference between the results at 420 and 1680 elements. Considering the calculating time shown in Table 5.3, the calculating time of 1680 elements needs around 15 times compared to the calculating time of 420 elements, but the difference between these two meshes is not significant. Hence, this study decides to conduct the analysis using a structure model with 420 elements.

**Table 5.3** The Element Size, Total FE Number and Calculating Time.

	Element Size (width*length)	Total FE number	Calculating Time (Sec)
FE Model 1	1*1	1680	38568
FE Model 2	2*2	420	2682
FE Model 3	3*4	140	653

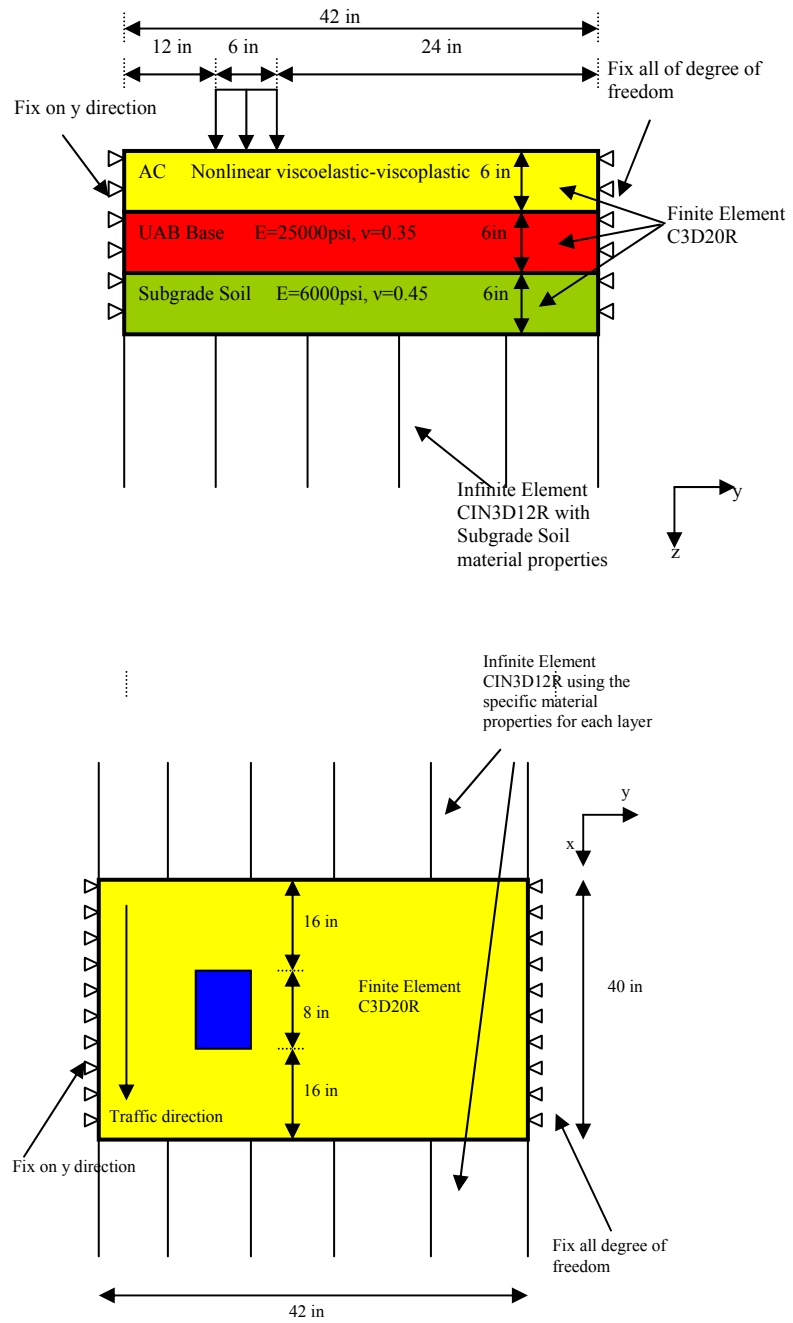


**Figure 5.16** The Sketch of Pavement Section.



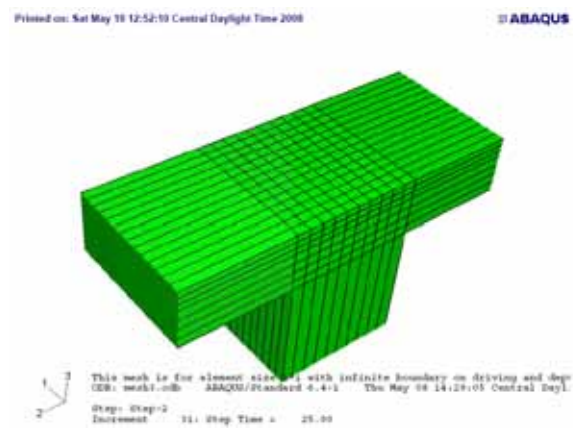
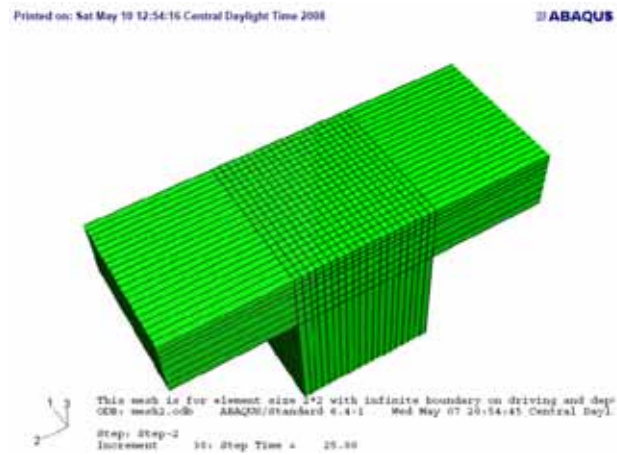
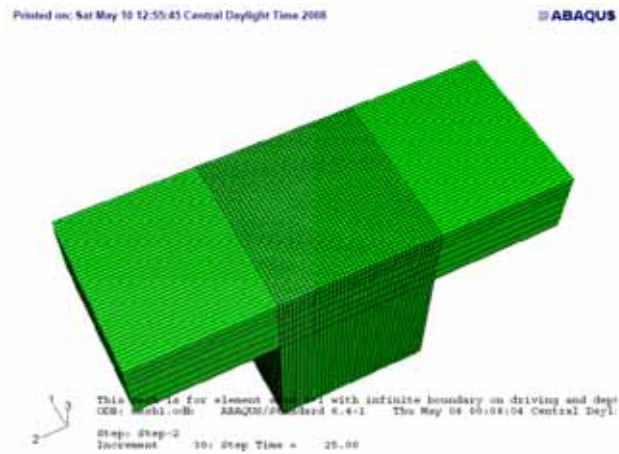


**Figure 5.17** Three Different Meshes for Conducting Sensitivity of FE Size.

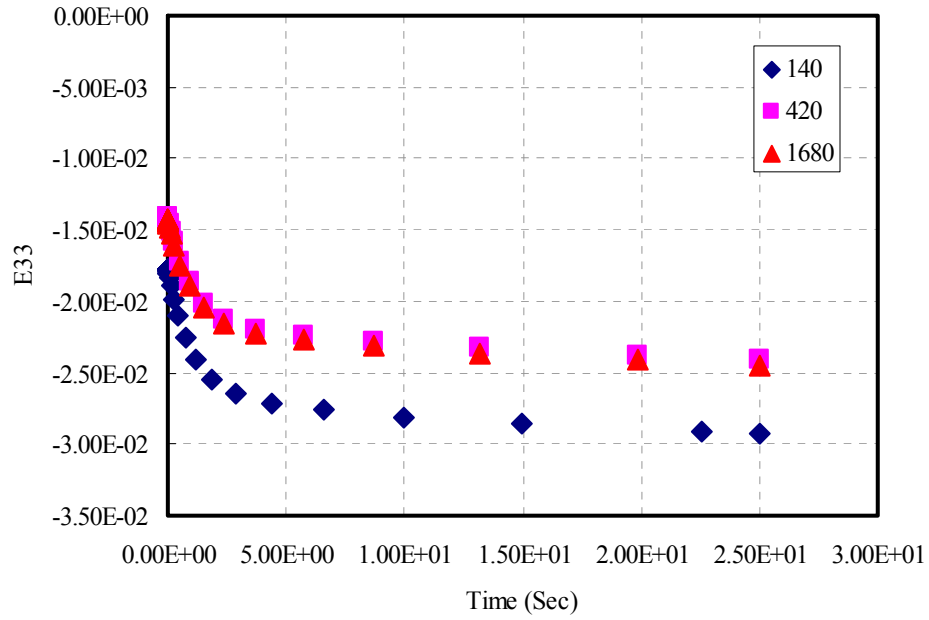


**Figure 5.18** The Strain Comparison of Three Different Meshes.

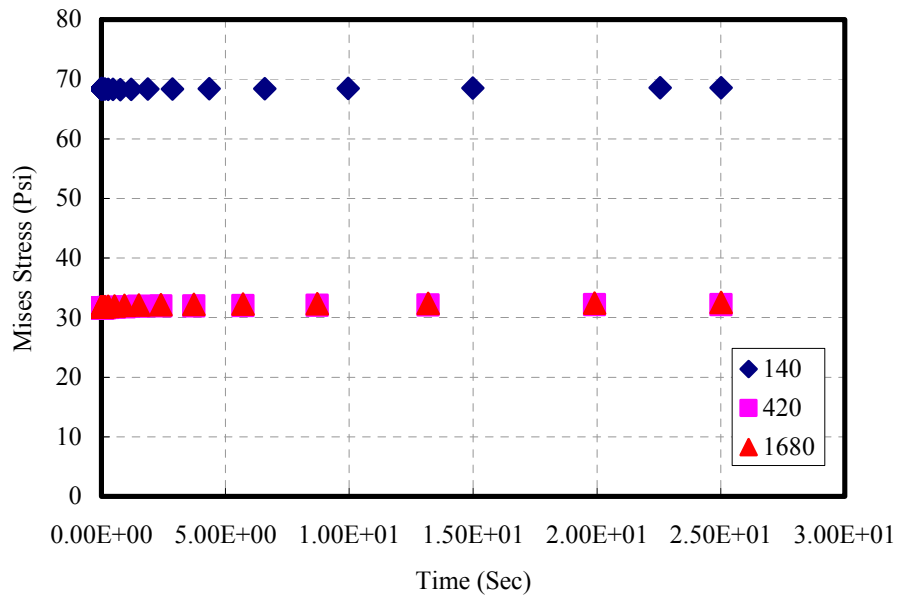


**Figure 5.19** The Von Mises Stress Comparison of Three Different Meshes.

The FE analysis considers two cases; the first case represents intermediate temperature where nonlinear viscoelastic strain is dominant, while the second case represents high temperature at which viscoplastic strain and permanent deformation are dominant. The simulation includes applying 25 loading-unloading cycles with a tire pressure of 100 psi. Within each loading-unloading cycle, the loading duration is 0.3 sec, and then removes the loading for 0.7 sec. In essence, fatigue damage is simulated by allowing the nonlinear parameters to vary as a function of number of loading cycles. This study assumes the nonlinear parameter is distributed by stress level  $g^s$  and fatigue damage  $g^f$  which is function of number of loading cycle. The relationship between  $g^s$  and  $g^f$  is assumed to be additive shown as Eq. (5-43). The exponential function is employed for  $g^s$  and  $g^f$  shown as Eqs.(5-44) and (5-45).

$$g_i = g_i^s + g_i^f \quad i = 1, 2 \quad (5-43)$$

$$g_i^s = 1 + a_i^{1s} \left\langle \exp \left[ a_i^{2s} \left( \frac{\bar{\sigma}}{\sigma_0} - 1 \right) \right] \right\rangle \quad i = 1, 2$$

$$\langle x \rangle = \begin{cases} x & , \quad \frac{\bar{\sigma}}{\sigma_0} - 1 > 0 \\ 0 & , \quad \frac{\bar{\sigma}}{\sigma_0} - 1 \leq 0 \end{cases} \quad (5-44)$$

$$g_i^{f,N} = g_i^{f,N-1} + a_i^{1f} \left\langle \exp \left[ a_i^{2f} \left( \frac{N}{N} - 1 \right) \right] \right\rangle \quad i = 1, 2$$

$$\langle x \rangle = \begin{cases} x & , \quad \frac{N}{N} - 1 > 0 \\ 0 & , \quad \frac{N}{N} - 1 \leq 0 \end{cases} \quad (5-45)$$

where,  $a_i^{1s}$ ,  $a_i^{2s}$ ,  $a_i^{1f}$  and  $a_i^{2f}$  are nonlinear parameter coefficients.  $\bar{\sigma}_0$  and  $\bar{N}$  are the limit start to have nonlinearity of stress and fatigue damage, respectively. Since the asphalt pavement under intermediate temperature contains more nonlinear viscoelastic strain and fatigue damage, while more viscoplastic strain is contained under high temperature, this study applies different material properties for intermediate and high temperature to simulate the pavement response under different temperature condition. The nonlinear parameter coefficients and viscoplastic properties for intermediate and high temperature are shown in Tables 5.4 and 5.5, respectively.

In order to show the results clearly, the following contours only demonstrate the elements around the loading area. The results of nonlinear viscoelastic and viscoplastic strain at 15<sup>th</sup> loading cycle are shown in Figure 5.20. This figure shows that the pavement section has more viscoplastic strain under high temperature, while it has more viscoelastic strain under intermediate temperature. Figure 5.21 is the comparison of the nonlinear viscoelastic parameters. The results show that the nonlinear parameters under intermediate temperature are larger than that under high temperature. The results indicate that the pavement has more fatigue damage under intermediate temperature, while the permanent deformation affects more under high temperature. Figures 5.22 and 5.23 are the results of strain and nonlinear parameters, respectively. The results also show that the effects of fatigue damage (nonlinear parameters) at intermediate temperature are more than that at high temperature. The pavement under high temperature has more permanent strain (viscoplastic strain) than it under intermediate temperature. Figures 5.24 and 5.25 are the comparison of total strain and nonlinear

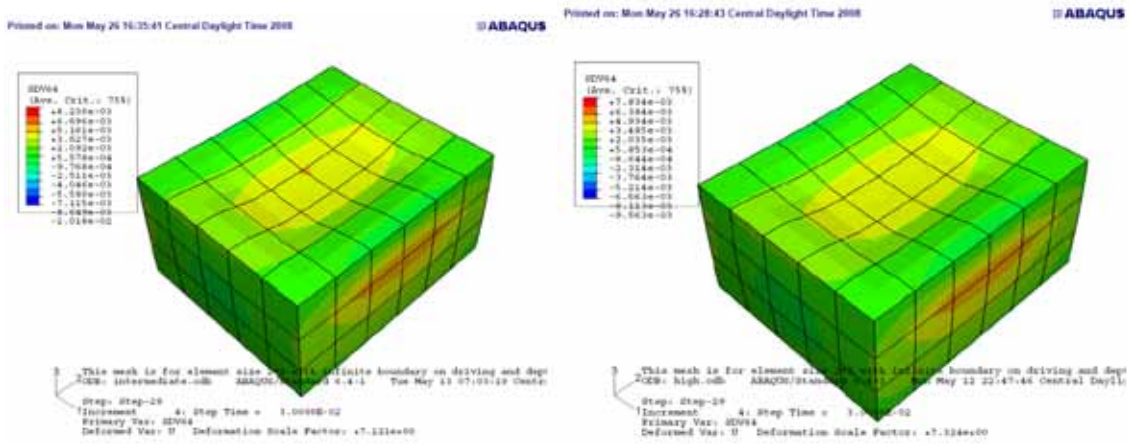
viscoelastic strain, respectively. These figures show that at 25<sup>th</sup> loading cycle, the pavement response under intermediate temperature still contains a lot of viscoelastic strain. Most of the remaining strain under high temperature is viscoplastic component. This result indicates that the remaining strain at the end of unloading can not be totally accounted to irrecoverable component, especially under intermediate temperature. Moreover, the nonlinearity of material under intermediate temperature increases with number of loading cycles. The increasing of nonlinearity under high temperature is not significant with increasing number of loading cycle. Figure 5.26 is the viscoplastic strain result. This figure shows that the viscoplastic strain under high temperature is much larger than that under intermediate temperature. Hence, the pavement under intermediate temperature has more fatigue damage (nonlinearity), while the permanent deformation is a major distress under high temperature.

**Table 5.4** The Coefficients of Nonlinear Parameter for Intermediate and High Temperature.

Intermediate Temperature				High Temperature			
$g_1$ Coefficients		$g_2$ Coefficients		$g_1$ Coefficients		$g_2$ Coefficients	
$a_1^{1s}$	1.5	$a_2^{1s}$	1.2	$a_1^{1s}$	0.5	$a_2^{1s}$	0.6
$a_1^{2s}$	0.01	$a_2^{2s}$	0.05	$a_1^{2s}$	0.005	$a_2^{2s}$	0.025
$a_1^{1f}$	0.03	$a_2^{1f}$	0.04	$a_1^{1f}$	0.015	$a_2^{1f}$	0.02
$a_1^{1f}$	0.02	$a_2^{1f}$	0.01	$a_1^{1f}$	0.01	$a_2^{1f}$	0.005

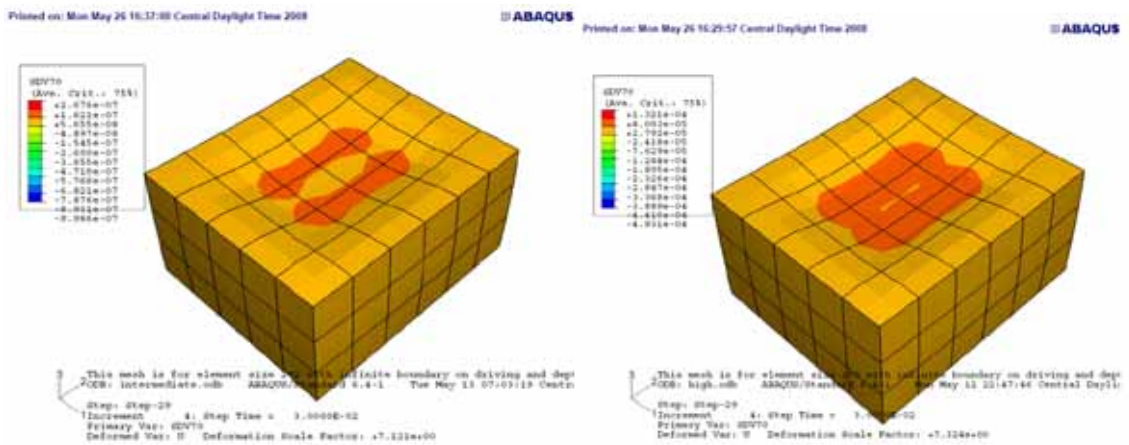
**Table 5.5** The Viscoplastic Parameters for Intermediate and High Temperature.

Intermediate Temperature		High Temperature	
$\alpha$	0.6	$\alpha$	0.5
$\beta$	0.35	$\beta$	0.35
$d$	0.778	$d$	0.778
$\Gamma$	1.0E-7	$\Gamma$	1.0E-6
$N$	1.0	$N$	2.0
$\kappa_0$	30	$\kappa_0$	20
$\kappa_1$	40	$\kappa_1$	30
$\kappa_2$	40	$\kappa_2$	30



(a) Viscoelastic Strain under Intermediate Temperature

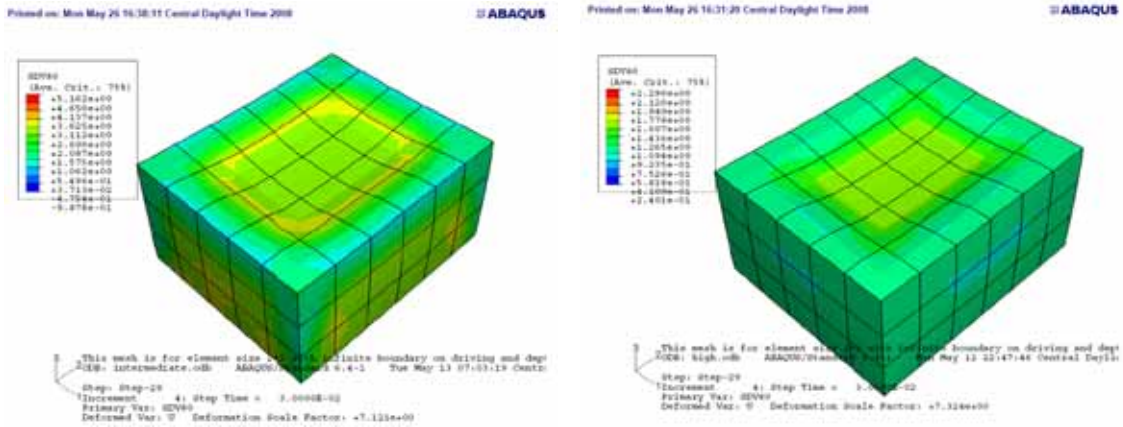
(b) Viscoelastic Strain under High Temperature



(c) Viscoplastic Strain under Intermediate Temperature

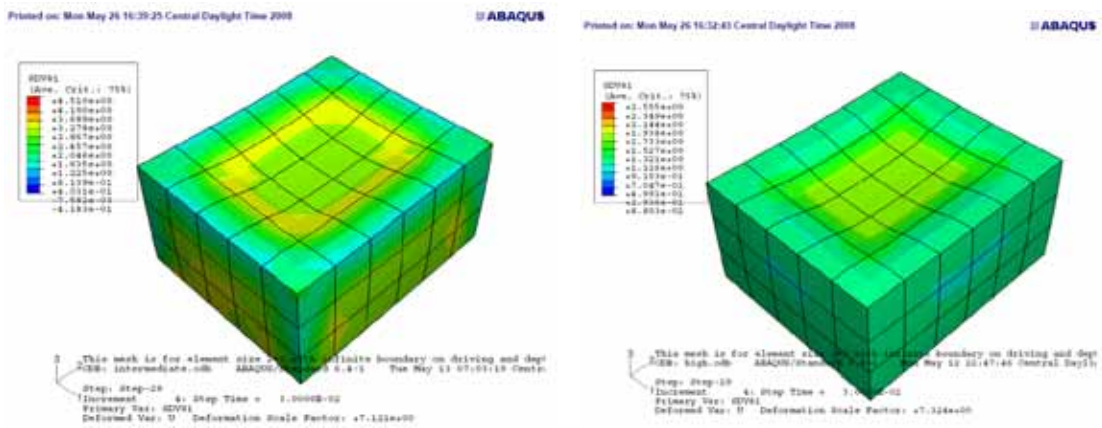
(d) Viscoplastic Strain under High Temperature

**Figure 5.20** The Viscoelastic and Viscoplastic Strain Comparison at 15<sup>th</sup> Loading Cycle.



(a) The Nonlinear Parameter  $g_1$   
under Intermediate Temperature

(b) The Nonlinear Parameter  $g_1$   
under High Temperature

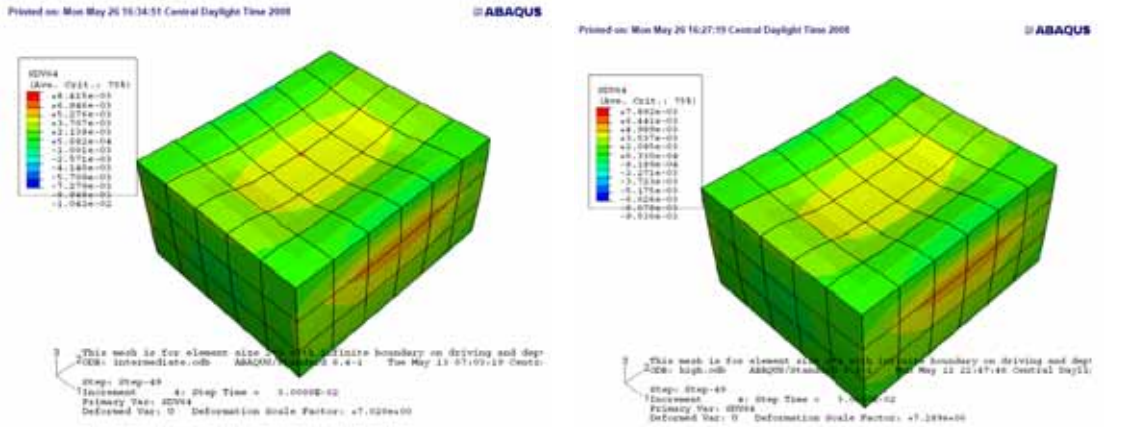


(c) The Nonlinear Parameter  $g_2$   
under Intermediate Temperature

(d) The Nonlinear Parameter  $g_2$   
under High Temperature

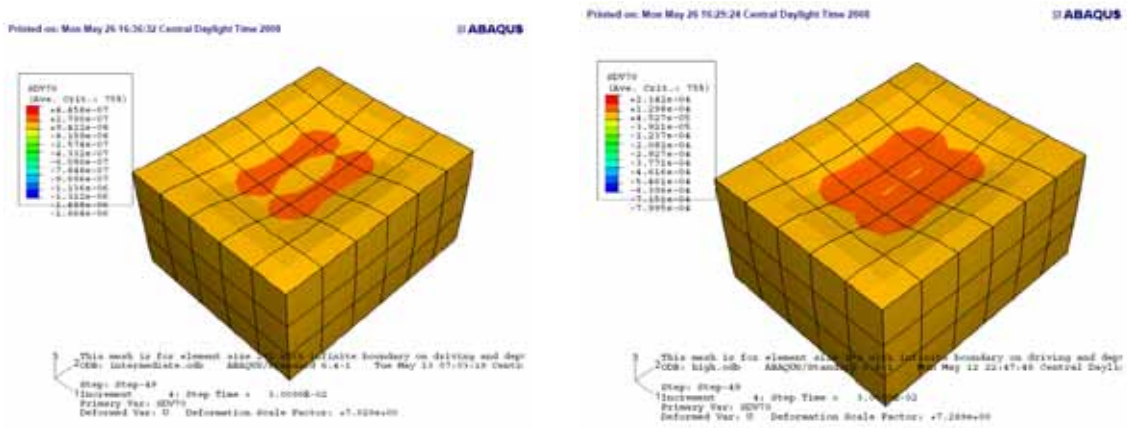
**Figure 5.21** The Nonlinear Parameters Comparison at 15<sup>th</sup> Loading Cycle.





(a) Viscoelastic Strain under Intermediate Temperature

(b) Viscoelastic Strain under High Temperature



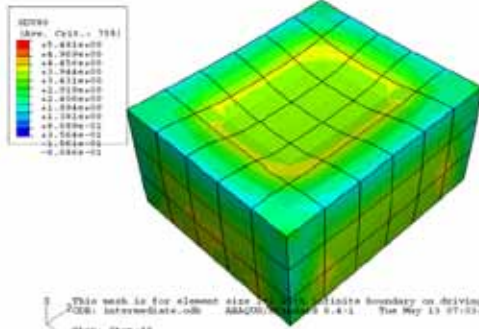
(c) Viscoplastic Strain under Intermediate Temperature

(d) Viscoplastic Strain under High Temperature

**Figure 5.22** The Viscoelastic and Viscoplastic Strain Comparison at 25<sup>th</sup> Loading Cycle.

Printed on: Mon May 26 16:37:40 Central Daylight Time 2008

ABAQUS

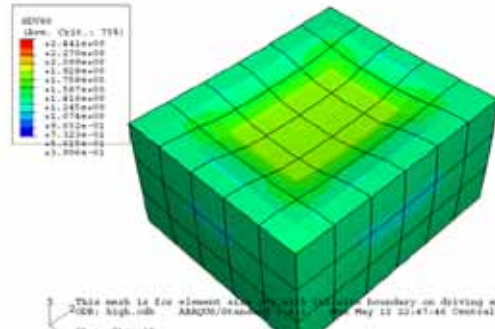


This mesh is for element size 1000.0. Finite boundary on driving end dept 2000. Intermediate.odb ABAQUS/Explicit 4.4.1 The May 13 07:02:19 Central Daylight Time  
 Step: Step-49  
 Increment: 4; Step Time = 1.0000e-02  
 Primary Var: EDV91  
 Deformed Var: U Deformation Scale Factor: \*7.025e+00

(a) The Nonlinear Parameter  $g_1$  under Intermediate Temperature

Printed on: Mon May 26 16:38:45 Central Daylight Time 2008

ABAQUS

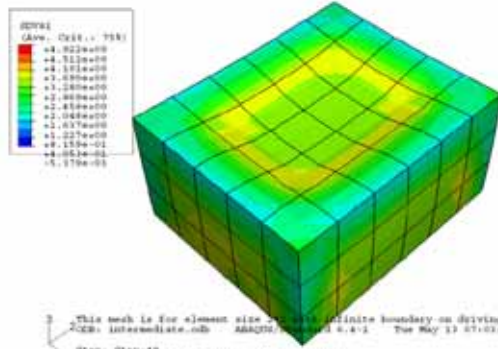


This mesh is for element size 1000.0. Finite boundary on driving end dept 2000. High.odb ABAQUS/Explicit 4.4.1 The May 13 07:07:46 Central Daylight Time  
 Step: Step-49  
 Increment: 4; Step Time = 1.0000e-02  
 Primary Var: EDV90  
 Deformed Var: U Deformation Scale Factor: \*7.189e+00

(b) The Nonlinear Parameter  $g_1$  under High Temperature

Printed on: Mon May 26 16:38:45 Central Daylight Time 2008

ABAQUS

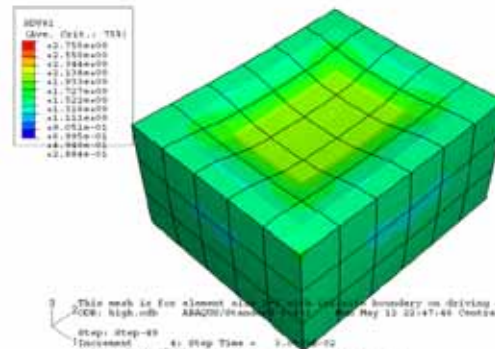


This mesh is for element size 1000.0. Finite boundary on driving end dept 2000. Intermediate.odb ABAQUS/Explicit 4.4.1 The May 13 07:02:19 Central Daylight Time  
 Step: Step-49  
 Increment: 4; Step Time = 1.0000e-02  
 Primary Var: EDV91  
 Deformed Var: U Deformation Scale Factor: \*7.025e+00

(c) The Nonlinear Parameter  $g_2$  under Intermediate Temperature

Printed on: Mon May 26 16:32:36 Central Daylight Time 2008

ABAQUS



This mesh is for element size 1000.0. Finite boundary on driving end dept 2000. High.odb ABAQUS/Explicit 4.4.1 The May 13 07:07:46 Central Daylight Time  
 Step: Step-49  
 Increment: 4; Step Time = 1.0000e-02  
 Primary Var: EDV91  
 Deformed Var: U Deformation Scale Factor: \*7.189e+00

(d) The Nonlinear Parameter  $g_2$  under High Temperature

Figure 5.23 The Nonlinear Parameters Comparison at 25<sup>th</sup> Loading Cycle.

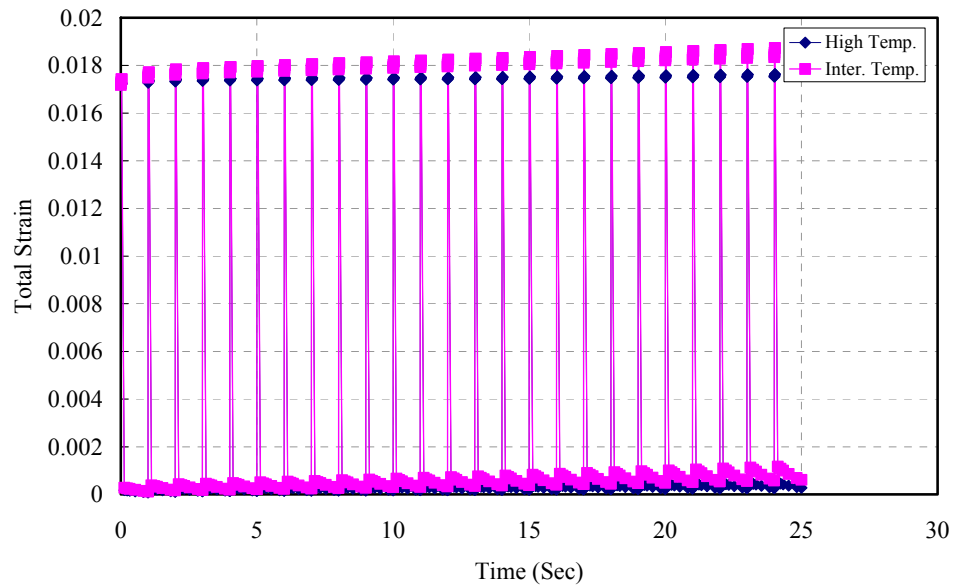


**Figure 5.24** The Comparison of Total Strain Between High and Intermediate Temperature.

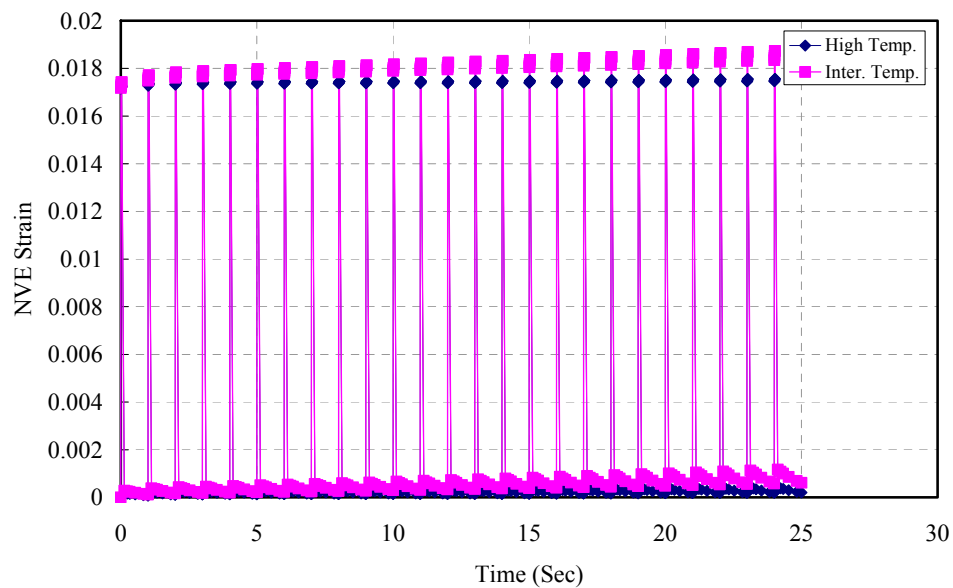
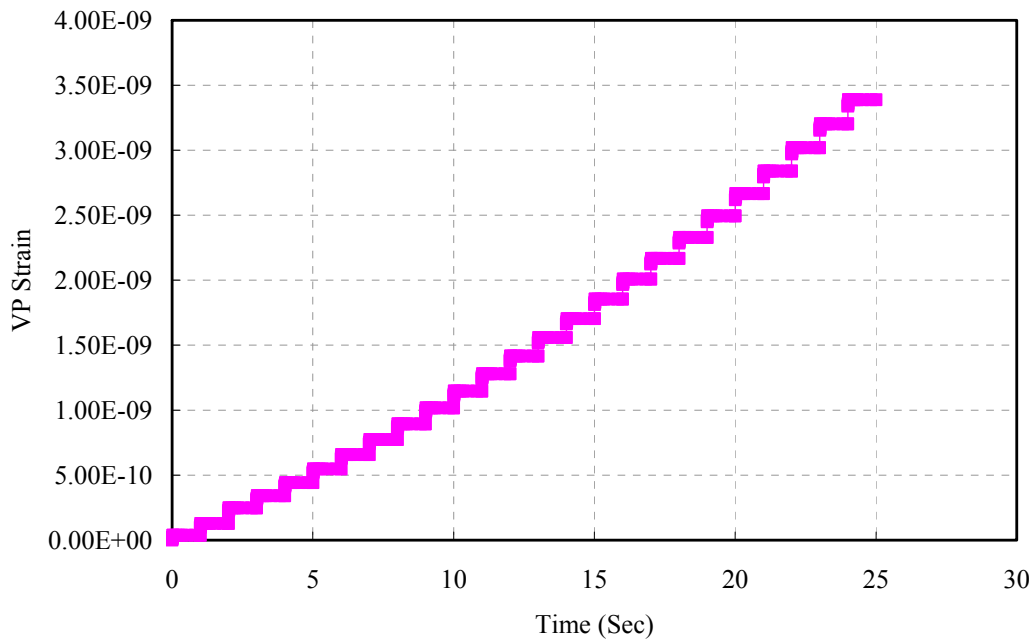
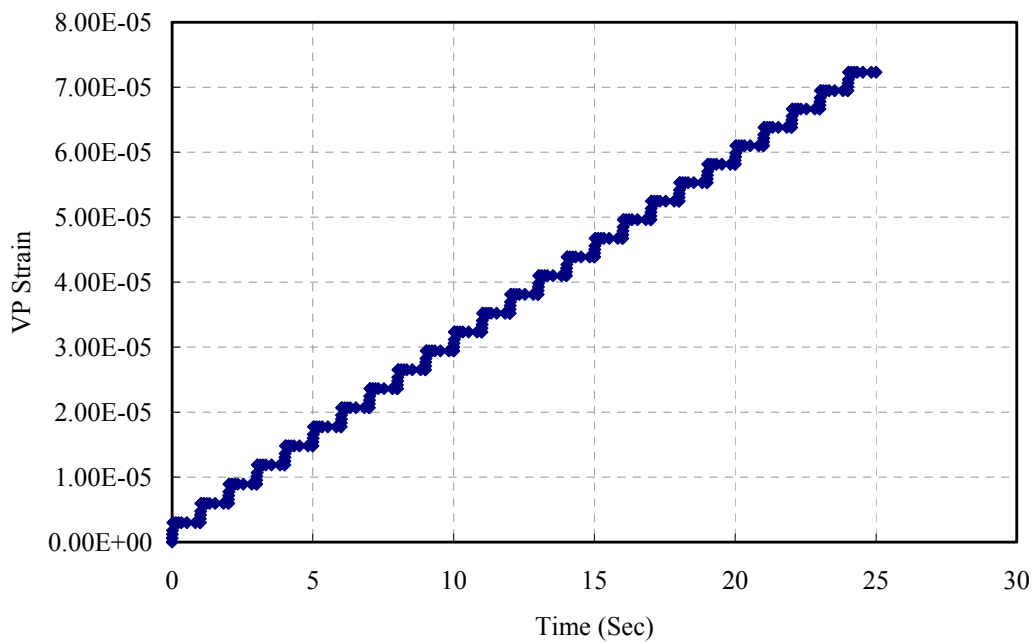


**Figure 5.25** The Comparison of Nonlinear Viscoelastic Strain Between High and Intermediate Temperature.



(a) Intermediate Temperature



(b) High Temperature

**Figure 5.26** The Viscoplastic Strain Under Intermediate and High Temperature.

## CONCLUSIONS

This chapter includes the finite element implementation of nonlinear viscoelastic-viscoplastic constitutive relationships for asphalt mixtures. Parametric analyses were conducted in order to demonstrate the effect of some of the model's parameters on mix response. All the results confirmed that the model captures the physical phenomena such as dilation, confinement dependency, and hardening associated with the behavior of asphalt mixtures.

A finite element model of a pavement structure was constructed and used to demonstrate the ability of the model to describe the response and performance of asphalt mixtures under different loading conditions. Fatigue damage is modeled by allowing the nonlinear viscoelastic parameters to vary as functions of loading cycles. Rutting is modeled by the accumulation of viscoplastic strain. The results show that the model can capture the fatigue damage under intermediate temperature and permanent distress under high temperature. This model will be extended in the future to explicitly account for the effect of temperature on the viscoelastic and viscoplastic responses.

## CHAPTER VI

### SUMMARY AND CONCLUSIONS

#### SUMMARY AND MAIN CONCLUSIONS

This study addresses a need in the asphalt pavement community in developing a constitutive relationship that can be used (1) in describing the behavior of asphalt materials (asphalt binder, asphalt mastic and mixtures) under various testing conditions, and (2) for the analysis of the performance of asphalt pavement structure. This study achieved the implementation of a nonlinear viscoelastic-viscoplastic constitutive relationship in finite element. The nonlinear viscoelastic behavior is modeled using Schapery theory; while the viscoplastic behavior is modeled by Perzyna's theory.

Chapters II, III and IV of this dissertation focused on three applications demonstrating the use of the model in the characterization of asphalt binders and mixtures subjected to various loading conditions. The main outcome of these applications demonstrates the validity of the model in describing the complex response of asphalt materials under different temperatures, loading rate, loading frequencies and temperatures. In addition, these applications demonstrate the ability of the model to extract indices for ranking asphalt materials based on performance.

In this first application reported in Chapter II, the Schapery nonlinear viscoelastic model parameters were obtained by analyzing the response of two asphalt mixes tested at different temperatures, frequencies, and strain levels. The time-strain shift factors were obtained by shifting the master curves at the different strain levels horizontally to a

reference strain level representing linear response. The nonlinear parameters were calculated by vertical shifting of the master curves at all strain levels to the same reference strain. The long-term linear viscoelastic coefficients were determined by fitting the Prony series to the data shifted horizontally at the reference strain. Inverse analysis was also conducted, and the results showed that the FE model had reasonable agreement with the experimental measurements at different combinations of temperatures and strain levels. The result of this analysis has showed that the strain horizontal shifting and nonlinear parameters can be used to predict HMA long-term nonlinear viscoelastic behavior by performing experiments at multiple strain levels within short time intervals.

In the second application, Schapery's theory was used in the analysis of nonlinear viscoelastic behavior of unaged and aged asphalt binders at different temperatures and stresses. Due to the influence of test temperatures on the stress levels that the binder can sustain prior to failure, the experimental measurements did not have a common range of stress levels that can be used in developing the master curve of nonlinear viscoelastic materials. This limitation was overcome by introducing the normalized stress concept in which the stress values of each test, at a given temperature and frequency, were normalized by the ultimate stress of that test. The results of this application has demonstrated the advantages of the analysis approach in providing a mathematical framework for describing the nonlinear response of asphalt binders, and in the possibility of describing the behavior of aged binders by using the unaged binder parameters and aging shift factors.

In this third application, the developed constitutive model was used in the analysis of asphalt binders subjected to Multiple Stress Creep Recovery test (MSCR) test. The objective of this application was to develop a new method to characterize the resistance of asphalt binders to permanent deformation. However, the challenge was in separating the nonlinear viscoelastic strain from the plastic strain that results in due to loading and unloading. Consequently, a new method was developed for separating the nonlinear viscoelastic response from the plastic response. The results show that binder varies in nonlinear viscoelastic response at common stress level. Therefore, it is necessary to use a nonlinear viscoelasticity theory to accurately determine the plastic strain.

A new index was developed based on the permanent strain (separated from the viscoelastic strain) for the characterization of resistance of asphalt binders to permanent deformations. The results showed excellent correlation between the index  $J_{nr}$  calculated using the actual permanent strain at ultimate stress level and rutting in the ALF mixtures. This new method was programmed in order to facilitate the analysis of data of testing binders using the MSCR test.



The details of the finite element implementation of nonlinear viscoelastic-viscoplastic constitutive relationships for asphalt mixtures are presented in Chapter V. Parametric analyses were conducted in order to demonstrate the effect of some of the model's parameters on mix response. The results showed that the model can reflect the physical phenomena such as dilation, confinement dependency, and hardening associated with the behavior of asphalt mixtures. A finite element model of a pavement structure was developed and used to demonstrate the ability of the model to describe the response and performance of asphalt mixtures under different conditions. The FE model was used to capture the pavement response under intermediate temperature (fatigue damage) and the pavement response under high temperature (rutting). Fatigue damage is modeled by allowing the nonlinear viscoelastic parameters to vary as functions of loading cycles; while rutting is modeled by the accumulation of viscoplastic strain. This model will be extended in the future to explicitly account for the effect of temperature on the viscoelastic and viscoplastic responses.

## **RECOMMENDATIONS**

The presented model accounts the nonlinear viscoelastic-viscoplastic behavior using Schapery nonlinear viscoelastic and Perzyna's viscoplastic model. However, HMA is a composite material which contains air voids, mastic and aggregates, and the effect of anisotropy distributed by aggregates is significant in HMA response. Hence, the material constitutive model should include the anisotropic effect in the further research. Moreover, the damage parameter should be contained in the constitute model to characterize the effect of micro-structure cracking.

The nonlinear viscoelastic analysis in this study is one dimension, but the HMA behavior is related to confinement stress. Hence, the nonlinear viscoelastic analysis should consider the effect of confinement condition.

In the future analysis, the comprehensive characterization should be conducted which includes the separation of recoverable and irrecoverable component, characterization of nonlinear viscoelastic and characterization of viscoplastic. The characterization of nonlinear viscoelastic and viscoplastic should be applied, after separation of recoverable and irrecoverable components. The characterization also should include the anisotropy and damage effect. The viscoplastic parameters used in this study are assumed. In the future, the viscoplastic parameters should be obtained by characterizing the experimental measurements. In addition, the relationship between nonlinearity of stress and number of loading cycles (fatigue damage) also should be obtained from experimental measurements.

## REFERENCES

- AASHTO: Provisional Standards (1995). American Association of State Highway Transportation Officials, Washington, DC.
- Abbas, A.R. (2004). "Simulation of the micromechanical behavior of asphalt mixtures using the discrete element method." Ph.D. dissertation, Washington State University, Pullman, WA.
- Abbas, A.R., Papagiannakis, A.T., and Masad, E. (2004). "Linear and nonlinear viscoelastic analysis of the microstructure of asphalt concretes." *Journal of Materials in Civil Engineering*, 16, 133–139.
- Abdulshafi, A., and Majidzadeh, K. (1985). "Combo viscoelastic-plastic modeling and rutting of asphalt mixtures." *Transportation Research Record* 968, Transportation Research Board, Washington, DC, 19-31.
- Airey, G.D., Rahimzadeh, B. and Collop, A. C. (2002). "Linear viscoelastic limits of bituminous binders." *Journal of Associated Asphalt Paving Technologists*, 17, 89-115.
- Airey, G.D., Rahimzadeh, B., and Collop, A.C. (2004). "Linear rheological behavior of bituminous paving material." *Journal of Materials in Civil Engineering*, 16, 212–220.
- Alfano, G., De Angelis, F., and Rosati, L. (2001). "General solution procedures in elasto/ viscoplasticity." *Computer Methods in Applied Mechanics and Engineering*, 190, 5123-5147.

- ASTM (1995): “Standard test method for indirect tension test for resilient modulus of bituminous mixtures.” Test Procedure D 4123, American Society for Testing and Materials, West Conshohocken, PA.
- Bahia, H. U., Hanson, D. L., Zeng, M., Zhai, H., Khatri, M. A., and Anderson, R. M. (2001). “Characterization of modified asphalt binders in superpave mix design.” *Report No. 459, National Cooperative Highway Research Program*, National Academy Press, Washington, DC.
- Chehab, G. R., Kim, Y.R., Schapery, R.A., Witczak, M.W., and Bonaquist, R. (2003). “Characterization of asphalt concrete in uniaxial tension using a viscoelastoplastic model.” *Journal of the Association of Asphalt Paving Technologists*, 72, 315-355.
- Chen W. F., and Han D. J. (1988). *Plasticity for structural engineers*, Springer-Verlag, New York.
- Cheung, C.Y. and Cebon, D. (1997a). “Deformation mechanisms of pure bitumen.” *Journal of Materials in Civil Engineering*, 9, 117-129.
- Cheung, C.Y. and Cebon, D. (1997b). “Thin film deformation behavior of power-law creeping materials.” *Journal of Engineering Mechanics*, 123, 1138-1152.
- Christensen, R.M. (1968). “On obtaining solutions in nonlinear viscoelasticity.” *Journal of Applied Mechanics*, 35, 129–133.
- Collop, A.C., Airey, G.D., and Khanzada, S. (2002). “Creep testing of bitumens using the dynamic shear rheometer.” *The International Journal of Pavement Engineering*, 3, 107–116.

- Collop, A.C., Scarpas, A. T., Kasbergen, C., and de Bondt, A. (2003). "Development and finite element implementation of stress-dependent elastoviscoplastic constitutive model with damage for asphalt." *Transportation Research Record 1832*, Transportation Research Board, Washington, DC, 96-104.
- Dafalias, Y. F. (1990). "The plastic spin in viscoplasticity." *International Journal of Solids and Structures*, 26, 149-163.
- D'Angelo J., R. Kluttz, R. Dongre, K. Stephens, L. Zanzotto (2007). "Revision of the superpave high temperature binder specification: the multiple stress creep recovery test." *Journal of the Association of Asphalt Paving Technologists*, 76, 293-331.
- Desai, C. S., Somasundaram, S., and Frantziskonis, G. (1986). "A hierarchical approach for constitutive modeling of geologic materials." *International Journal of Numerical and Analytical Methods in Geomechanics*, 10, 225-257.
- Dessouky, S., (2005). "Multiscale approach for modeling hot mix asphalt." Ph.D. dissertation, Texas A&M University, College Station, TX.
- Di Benedetto, H., Mondher, N., Sauzeat, C., and Olard, F., (2007). "Three-dimensional thermo-viscoplastic behavior of bituminous materials." *Road Material and Pavement Design*, 8, 285-316.
- Elseifi, M. A., Al-Qadi, I. L., and Yoo P. J. (2006). "Viscoelastic modeling and field validation of flexible pavement." *Journal of Engineering Mechanics*, 132, 172-178.
- Erkens, S., Liu, X., and Scarpas, A. (2002). "3D finite element model for asphalt concrete response simulation." *The International Journal of Geomechanics*, 2, 305-330.

- Ferry, J. D. (1961). *Viscoelastic properties of polymers*. John Wiley and Sons, Inc., New York.
- Haj-Ali, R.M., and Muliana, A.H. (2004). “Numerical finite element formulation of the Schapery non-linear viscoelastic material model.” *International Journal for Numerical Methods in Engineering*, 59, 25–45.
- Huang, C.W., Masad, E., Muliana, A., and Bahia, H. (2007). “Nonlinear viscoelastic analysis of asphalt mixes subjected to shear loading.” *Mechanics of Time Dependent Materials*, 11, 91-110.
- Kim, Y. R. (2003). “Mechanistic fatigue characterization and damage modeling of asphalt mixtures.” Ph.D. Dissertation, Texas A&M University, College Station, TX.
- Kose, S., Guler, M., Bahia, H., and Masad, E. (2000). “Distribution of strains within hot-mix asphalt binders.” *Transportation Research Record 1728*, Transportation Research Board, Washington, DC, 21–27.
- Lai, J., and Baker, A. (1996). “3-D Schapery representation for nonlinear viscoelasticity and finite element implementation.” *Computational Mechanics*, 18, 182–191.
- Li, X. and Marasteanu, M. (2005). “Cohesive modeling of fracture in asphalt mixtures at low temperatures.” *International Journal of Fracture*, 136, 285-308.
- Lou, Y.C., and Schapery, R.A. (1971). “Viscoelastic characterization of a nonlinear fiber-reinforced plastic.” *Journal of Composite Materials*, 5, 208–234.
- Lu, Y., and Wright, P. J. (1998). “Numerical approach of visco-elastoplastic analysis for asphalt mixtures.” *Journal of Computers and Structures*, 69, 139-157.

- Masad, E., and Somadevan, N. (2002). “Microstructural finite-element analysis of influence of localized strain distribution of asphalt mix properties.” *Journal of Engineering Mechanics*, 128, 1105–1114.
- Masad, E., Dessouky, S., and Little, D. (2007). “Development of an elastoviscoplastic microstructural-based continuum model to predict permanent deformation in hot mix asphalt.” *International Journal of Geomechanics*, 7, 119-130.
- Masad, E., Huang, C.W., Airey, G. and Muliana, A. (2008). “Nonlinear viscoelastic analysis of unaged and aged asphalt binders.” *Construction and Building Materials*, 22, 2170-2179.
- Muliana, A.H., and Kim, J.S. (2007). “A concurrent micromechanical model for nonlinear viscoelastic behaviors of composites reinforced with solid spherical particles.” *International Journal Solids and Structures*, 44, 6891-6913.
- Oda, M., and Nakayama, H. (1989). “Yield function for soil with anisotropic fabric.” *Journal of Engineering Mechanics*, 15, 89-105.
- Oeser, M. and Moller, B. (2004). “3D constitutive model for asphalt pavements.” *International Journal of Pavement Engineering*, 5, 153-161.
- Perl, M. Uzan, J., and Sides, A. (1983). “Visco-elasto-plastic constitutive law for bituminous mixture under repeated loading.” *Transportation Research Record 911*, Transportation Research Board, Washington, DC, 20-26.
- Poon, H., and Ahmad, F. (1999). “A finite element constitutive update scheme for anisotropic, viscoelastic solids exhibiting non-linearity of the Schapery type.” *International Journal for Numerical Methods in Engineering*, 46, 2027–2041.

- Reese, R. (1997). "Properties of aged asphalt binder related to asphalt concrete life." *Journal of the Association of Asphalt Paving Technologists*, 66, 604-632.
- Rowe, G. M., and Bouldin, M.G. (2000). "Improved techniques to evaluate fatigue resistance of asphaltic mixes." *Proceedings of the Second Enrphalt and Eurobitume Congress*, Barcelona, 754-763.
- Saadeh, S. (2005). "Characterization of asphalt concrete using anisotropic damage viscoelastic-viscoplastic model." Ph.D. dissertation, Texas A&M University, College Station, TX.
- Sadd, M.H., Parameswaran, D.Q., and Shukla, A. (2004). "Simulation of asphalt materials using finite element micromechanical model with damage mechanics." *Transportation Research Record 1832*, Transportation Research Board, Washington, DC, 86-95.
- Schapery, R.A. (1969). "On the characterization of nonlinear viscoelastic materials." *Polymer Engineering and Science*, 9, 295-310.
- Schapery, R.A. (2000). "Nonlinear viscoelastic solids." *International Journal of Solids and Structures*, 37, 359-366.
- Seibi, A. C., Sharma, M. G., Ali, G. A., and Kenis, W. J. (2001). "Constitutive relations for asphalt concrete under high rates of loading." *Transportation Research Record 1767*, Transportation Research Board, Washington, DC, 111-119.
- Shenoy, A., and Romero, P. (2002). "Standardized procedure for analysis of dynamic modulus  $|E^*|$  data to predict asphalt pavement distresses." *Transportation Research Record 1789*, Transportation Research Board, Washington, DC, 173-182.



- Shields, D.H., Zeng, M., Kwok, R. (1998). “Nonlinear viscoelastic behavior of asphalt concrete in stress relaxation.” *Journal of the Association of Asphalt Paving Technologists*, 67, 358–400.
- Sides, A., Uzan, J., and Perl, M. (1985). “A comprehensive visco-elastoplastic characterization of sand-asphalt under compression and tension cyclic loading.” *Journal of Testing and Evaluation*, 13, 49-59.
- Sousa, J. B., Weissman, S., Sackman, J., and Monismith, C. L. (1993). “A nonlinear elastic viscous with damage model to predict permanent deformation of asphalt concrete mixtures.” *Transportation Research Record*, 1384, Transportation Research Board, Washington, DC, 80-93.
- Sousa, J. B., and Weissman, S. (1994). “Modeling permanent deformation of asphalt concrete mixtures.” *Journal of the Association of Asphalt Paving Technologists*, 63, 224-257.
- Stuart, K., Mogawer, W., and Romero, P. (1999). “Validation of asphalt binder and mixture test that measured rutting susceptibility using the accelerated loading facility.” *Interim Report October 1993- October 1999*, Federal Highway Administration, McLean, VA.
- Tashman, L. (2003). “Microstructure viscoplastic continuum model for permanent deformation in asphalt pavements.” Ph.D. Dissertation, Texas A&M University, College Station, TX.

- Touati, D., and Cederbaum, G. (1997). "On the prediction of stress relaxation from known creep of nonlinear materials." *Journal of Engineering Materials and Technology*, 119, 121–124.
- Touati, D., and Cederbaum, G. (1998). "Post buckling of nonlinear viscoelastic imperfect laminated plates, Part I: Material considerations." *Composite Structures*, 42, 33–41.
- Zeinkiewicz, O., Humpheson, C., and Lewis, R. (1975). "Associated and non-associated viscoplasticity in soils mechanics." *Journal of Geotechnical Engineering*, 25, 671-689.

**VITA**

Chien-Wei Huang was born in Kaohsiung, Taiwan. He received his Bachelor of Science in civil engineering from I-Shou University in June 1999. He entered the graduate school at National Cheng-Kung University and received his Master of Science in civil engineering in June 2001. He started his Ph.D. program in civil engineering at Texas A&M University in August 2004 and received his Ph.D in December 2008. His permanent address is as follows:

No. 22, Lane 429, Chengcing Rd., Sanmin District

Kaohsiung, 807

Taiwan